Electron Interactions With SF_6

L. G. Christophorou[a] and J. K. Olthoff[b]

Electricity Division, Electronics and Electrical Engineering Laboratory, National Institute of Standards and Technology, Gaithersburg, Maryland 20899-8113

Received March 14, 2000; accepted June 6, 2000

Sulfur hexafluoride (SF_6) is commonly used as a gaseous dielectric and as a plasma etching gas. In this work, the state of knowledge on electron-interaction cross sections and electron-swarm parameters in SF_6 is comprehensively reviewed and critically assessed. Cross sections are presented and discussed for the following scattering processes: total electron scattering; differential elastic; elastic integral; elastic momentum; total vibrational; total and partial ionization; total dissociative and nondissociative electron attachment; and dissociation into neutrals. Coefficients for electron-impact ionization, effective ionization, electron attachment, electron drift, and electron diffusion are also reviewed and assessed. In addition, complementary information on the electronic and molecular structure of the SF_6 molecule and on electron detachment and ion transport in parent SF_6 gas is provided that allows a better understanding of the nature of the cross sections and swarm parameters. The assessed data are used to deduce cross sections and coefficients for which there exist no direct measurements at the present time. The present work on electron interactions with the SF_6 molecule reveals a rather simple picture which can be summarized as follows: (1) Elastic electron scattering is the most significant electron scattering process over the electron energy range from $\sim$0.01 to $\sim$1000 eV. (2) Below 15 eV the most distinct inelastic energy-loss process is vibrational excitation—direct dipole excitation involving the ν_3 mode and indirect vibrational excitation via negative ion states involving the ν_1 mode. (3) Below $\sim$0.1 eV electron attachment forming SF_6^- is the most dominant interaction (along with elastic scattering). Above this energy, the cross sections for dissociative electron attachment forming fragment anions [principally SF_x^- ($x=3$, 4, and 5) and F^-] are appreciable, with the room temperature total electron attachment cross section dominated by the formation of SF_5^- between $\sim$0.3 and 1.5 eV and by the formation of F^- beyond $\sim$2.0 eV. (4) Above $\sim$16 eV dissociative ionization becomes significant, generating principally SF_x^+ ($x=1$, 3, 4, and 5) and F^+ positive-ion fragments which, together with elastic electron scattering, makes up most of the total electron scattering cross section. (5) Electron-impact dissociation into neutral fragments SF_x ($x=1$, 2, and 3) and F occurs above $\sim$15 eV, with cross section values potentially exceeding those for ionization for electron energies near 20 eV. (6) The total electron scattering cross section exhibits distinct structure due to negative-ion resonances near 0.0, 2.5, 7.0, and 11.9 eV. The most significant data needs are for direct measurements of vibrational excitation cross sections, for cross sections for electron-impact dissociation into neutral fragments, and for the momentum transfer cross section at low energies. © *2000 American Institute of Physics.* [S0047-2689(00)00204-X]

Key words: SF_6; sulfur hexafluoride; electron interactions; scattering; ionization; attachment; dissociation; cross section; coefficients; transport; negative ions

Contents

[a]Electronic mail: loucas.christophorou@nist.gov
[b]Electronic mail: james.olthoff@nist.gov

List of Tables

List of Figures

1. Introduction

Sulfur hexafluoride (SF_6) is a man-made molecule used in many applied areas:[1,2] as an insulating medium in high-voltage transmission and distribution equipment; a high-dielectric strength gas in ultraviolet (UV) laser-triggered spark-gap closing switches; a fluorine donor in, for instance, rare gas–halide excimer lasers; a gas for plasma etching of silicon and GaAs-based semiconductors; a blanket gas for magnesium casting; a reactive gas in aluminum recycling to reduce porosity; a gas for thermal and sound insulation; and a gas for use in many other wide ranging areas including retinal detachment surgery, airplane tires, AWACS radar domes, and x-ray machines. Its general properties, especially as they relate to its use by the electric power industry, have been summarized and discussed by Christophorou *et al.*[2] Sulfur hexafluoride is also of environmental concern in that it has been shown to be a potent greenhouse gas.[3] It is an efficient absorber of infrared radiation, and because it is very stable, is largely immune to chemical and photolytic degradation. The latter accounts for its long residence lifetime in the environment. The strong infrared absorption and the long (800–3200 yr) residence lifetime[3–7] in the environment account for its high global warming potential, which for a 100 yr period is estimated to be $\sim$24 000 times greater than that of CO_2.[3]

Because of its unique structure and applied interest, the SF_6 molecule has been the subject of many experimental, theoretical, and computational studies. There have been a number of reviews of its interactions with slow electrons (e.g., Refs. 2, 8–14) and photons (e.g., Refs. 15–18).

In the present work we synthesize and critically evaluate existing knowledge on the interactions of low-energy (mostly below about 100 eV) electrons with the SF_6 molecule and recommend, suggest, or simply provide values for the various electron scattering cross sections, coefficients, and rate constants that are used to quantify these processes. These processes are identified in Table 1 along with the corresponding symbols and units.

The data assessment procedure followed in this work is the same as in the previous papers in this series.[19–25] As discussed in these earlier publications, ''recommended'' or ''suggested'' values of cross sections and coefficients are determined, where possible, for each type of cross section and coefficient for which data exist. These values are derived from fits to the most reliable data, as determined by the following criteria: (i) the data are published in peer reviewed literature; (ii) the data exhibit no evidence of unaddressed errors; (iii) the data are absolute measurements; (iv) multiple data sets exist and are consistent with one another within the combined stated uncertainties over common energy ranges; and (v) in regions where both experimentally and theoretically derived data exist, the experimental data are preferred. Data that meet these criteria are selected for each cross section or coefficient and a fit to these data is designated as our recommended data. The recommended data represent the best current estimates for the cross sections and coefficients for each of the processes. A cross section or coefficient may be designated as suggested if the available data are deemed to be reasonable but do not meet all of the criteria listed above. For example, results from a single measurement may be designated as suggested if a second, independent, confirming measurement is unavailable. In cases where no reasonable data exist, or where two or more measurements are in an unresolved contradiction, the raw data are presented for information and no recommendation is made. At the present time, we make no use of data presented on the Internet unless these have been also published in the archival literature or in a formal report of a scientific institution or conference.

No attempt is made in this article to evaluate the predic-

TABLE 1. Definition of symbols

Symbol	Definition	Common scale and units
$\sigma_{pa,t}(\lambda)$	Total photoabsorption cross section	10^{-18} cm^2; 10^{-22} m^2
$\sigma_{pi,t}(\lambda)$	Total photoionization cross section	10^{-18} cm^2; 10^{-22} m^2
$\sigma_{pi,partial}(h\nu)$	Partial photoionization cross section	10^{-18} cm^2; 10^{-22} m^2
$\sigma_{pdis,t}(\lambda)$	Total photodissociation cross section	10^{-18} cm^2; 10^{-22} m^2
$\sigma_{sc,t}(\varepsilon)$	Total electron scattering cross section	10^{-16} cm^2; 10^{-20} m^2
$\sigma_{e,diff}(\varepsilon)$	Elastic differential electron scattering cross section	10^{-20} m^2 sr^{-1}
$\sigma_{e,int}(\varepsilon)$	Elastic integral electron scattering cross section	10^{-16} cm^2; 10^{-20} m^2
$\sigma_{e,t}(\varepsilon)$	Total elastic electron scattering cross section	10^{-16} cm^2; 10^{-20} m^2
$\sigma_{m}(\varepsilon)$	Momentum transfer cross section (elastic)	10^{-16} cm^2; 10^{-20} m^2
$\sigma_{vib,diff}(\varepsilon)$	Vibrational differential scattering cross section	10^{-20} m^2 sr^{-1}
$\sigma_{vib,t}(\varepsilon)$	Total vibrational excitation cross section	10^{-16} cm^2; 10^{-20} m^2
$\sigma_{el,diff}(\varepsilon)$	Differential electronic excitation cross section	10^{-22} m^2 sr^{-1}
$\sigma_{i,t}(\varepsilon)$	Total ionization cross section	10^{-16} cm^2; 10^{-20} m^2
$\sigma_{i,partial}(\varepsilon)$	Partial ionization cross section	10^{-16} cm^2; 10^{-20} m^2
$\sigma_{dis,t}(\varepsilon)$	Total dissociation cross section	10^{-16} cm^2; 10^{-20} m^2
$\sigma_{dis,neut,t}(\varepsilon)$	Total cross section for electron impact dissociation into neutrals	10^{-16} cm^2; 10^{-20} m^2
$\sigma_{em}(\varepsilon)$	Emission cross section	10^{-19} cm^2; 10^{-23} m^2
$\sigma_{a,t}(\varepsilon)$	Total electron attachment cross section	10^{-14} cm^2; 10^{-18} m^2
$\sigma_{da,t}(\varepsilon)$	Total dissociative electron attachment cross section	10^{-17} cm^2; 10^{-21} m^2
$\sigma_{pd}(h\nu)$	Photodetachment cross section	10^{-19} cm^2; 10^{-23} m^2
$\sigma_{ic}(\mathcal{E}_{cm})$	Cross section for ion conversion	10^{-16} cm^2; 10^{-20} m^2
$\sigma_{cd}(\mathcal{E}_{cm})$	Cross section for collisional detachment	10^{-16} cm^2; 10^{-20} m^2
$\sigma_{ct}(\mathcal{E}_{cm})$	Cross section for charge transfer	10^{-16} cm^2; 10^{-20} m^2
$\alpha/N\,(E/N)$	Density-reduced ionization coefficient	10^{-18} cm^2, 10^{-22} m^2
$\eta/N\,(E/N)$	Density-reduced electron attachment coefficient	10^{-18} cm^2, 10^{-22} m^2
$(\alpha-\eta)/N\,(E/N)$	Density-reduced effective ionization coefficient	10^{-18} cm^2, 10^{-22} m^2
$k_{a,be}(n^*)$	Rate constant for bound-electron attachment	10^{-7} cm^3 s^{-1}
$k_{dis}(E/N)$	Electron-impact dissociation rate constant	10^{-9} cm^3 s^{-1}
$k_{a,t}(E/N)$	Total electron attachment rate constant	10^{-7} cm^3 s^{-1}
$(k_{a,t})_{th}$	Thermal total electron attachment rate constant	10^{-7} cm^3 s^{-1}
$w\,(E/N)$	Electron drift velocity	10^6 cm s^{-1}
$D_T/\mu\,(E/N)$	Transverse electron diffusion coefficient to electron mobility ratio	V
$D_L/\mu\,(E/N)$	Longitudinal electron diffusion coefficient to electron mobility ratio	V
$\mu_0^-\,(E/N)$	Reduced mobility of negative ions	cm^2 V^{-1} s^{-1}
$\mu_0^+\,(E/N)$	Reduced mobility of positive ions	cm^2 V^{-1} s^{-1}
$ND_L^-\,(E/N)$	Product of gas number density and negative ion diffusion coefficient	10^{18} cm^{-1} s^{-1}
$ND_L^+\,(E/N)$	Product of gas number density and positive ion diffusion coefficient	10^{18} cm^{-1} s^{-1}
$k_r(E/N)$	Ion-ion recombination rate coefficient	10^{-6} cm^3 s^{-1}
$\delta/N\,(E/N)$	Density-reduced electron detachment coefficient	10^{-19} cm^2

tions of the many Boltzmann-code and Monte Carlo-type analyses of electron transport in SF_6 (e.g., Refs. 11, 26–44) that are available in the literature. This will be the subject of a future paper.[45]

2. Electronic and Molecular Structure

The electronic structure of this highly symmetric molecule has long been a subject of much interest because of its unusual properties (e.g., unusual spectroscopy) and because of its many industrial uses. In the SF_6 molecule the sulfur atom is at the center of a regular octahedron, the corners of which are occupied by the six fluorine atoms. It has ten valence orbitals containing 48 electrons and belongs to the point group O_h.[15] Its ground-state valence electron configuration is:[46–51]

$$(\text{core})^{22}(4a_{1g})^2(3t_{1u})^6(2e_g)^4(5a_{1g})^2(4t_{1u})^6(1t_{2g})^6(3e_g)^4 \times[(1t_{2u})^6(5t_{1u})^6](1t_{1g})^6A_{1g},$$

where the first three orbitals constitute the inner-shell valence region. The four lowest empty (valence) orbitals[49,52] are: $(6a_{1g})^0(6t_{1u})^0(2t_{2g})^0(4e_g)^0$. However, there are still some questions as to the energetic sequence of the various orbitals. For instance, the $(5t_{1u})$ and $(1t_{2u})$ orbitals are nearly degenerate and their ordering is unresolved. Actually, their sequence has been interchanged by some authors (e.g., see Refs. 13 and 52, and also discussions in Refs. 16, 17, 46, 47 and 53–55). As noted by Gianturco and Jain,[56] the SF_6 molecule, being an assembly of atoms containing 70 bound electrons, is difficult to handle by *ab initio* computational methods. The rather large nuclear charges of the fluorine

atoms away from the center-of-mass, makes the single-center approach unlikely to work. Thus, computational models are by necessity approximate models.

Nonetheless, the present assessment of electron interactions with the SF_6 molecule has unveiled a rather simple picture which can be summarized as follows:

(i) Elastic electron scattering is the most significant electron scattering process over the electron energy range from ~0.01 to ~1000 eV.

(ii) From ~0.1 to 15 eV the most distinct inelastic energy-loss process is vibrational excitation—direct dipole excitation involving the ν_3 mode and indirect vibrational excitation via negative ion states involving the ν_1 mode.

(iii) Below ~0.1 eV electron attachment forming SF_6^- is the dominant inelastic interaction. Above this energy the cross sections for dissociative electron attachment forming fragment anions [principally SF_x^- ($x=3$, 4, and 5) and F^-] are appreciable, with the room temperature total electron attachment cross section dominated by the formation of SF_5^- between ~0.3 and 1.5 eV and by the formation of F^- beyond ~2.0 eV.

(iv) Above ~16 eV dissociative ionization becomes significant, generating principally SF_x^+ ($x=1$, 3, 4, and 5) and F^+ positive-ion fragments which, together with elastic electron scattering, makes up most of the total electron scattering cross section.

(v) Electron-impact dissociation into neutral fragments SF_x ($x=1$, 2, and 3) and F occurs above ~15 eV, with cross section values potentially exceeding those for ionization at electron energies near 20 eV.

(vi) The total electron scattering cross section exhibits distinct structure due to negative ion resonances at about 0.0, 2.5, 7.0, and 11.9 eV.

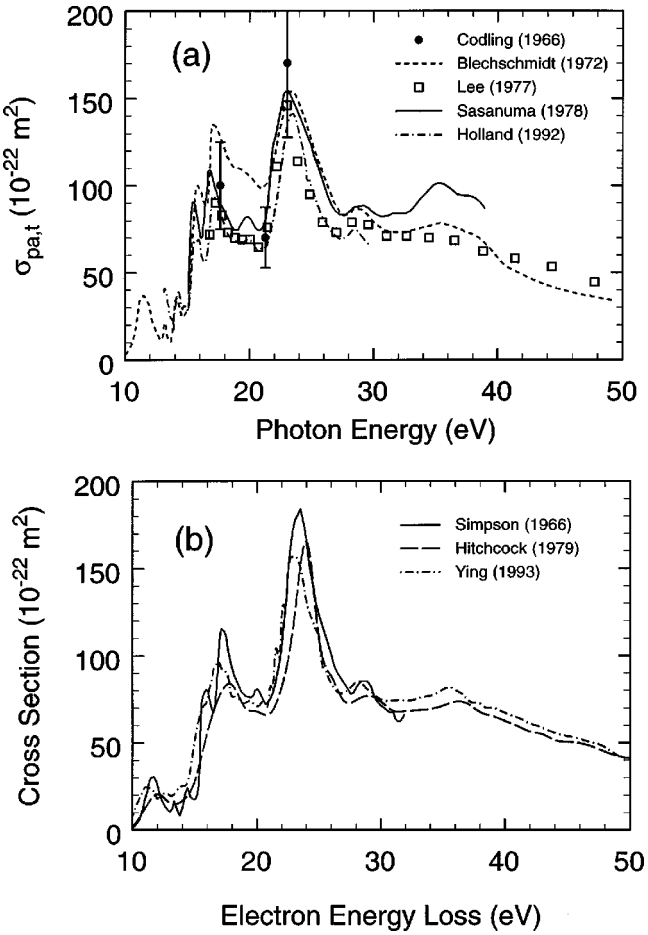

FIG. 1. (a) Total photoabsorption cross section, $\sigma_{pa,t}(\lambda)$, of SF_6 as a function of photon energy: (●) Ref. 60; (- - -) Ref. 61; (□) Ref. 53; (—) Ref. 62; (− · −) Ref. 48. (b) Total excitation (photoabsorption) cross section obtained from high-energy electron energy-loss spectra (see text): (—) Ref. 64; (– –) Ref. 59; (− · −) Ref. 65.

2.1. Total Photoabsorption Cross Section, $\sigma_{pa,t}(\lambda)$

The photoabsorption (and photoelectron) spectrum of SF_6 has been investigated extensively over broad energy ranges. It is unusual in that the most prominent features are due to intervalence transitions. Rydberg series, which often dominate molecular absorption cross sections at energies a few electron volts above the ionization threshold, are strongly suppressed in SF_6. This anomalous intensity distribution has been interpreted by Nefedov[57] and Dehmer[58] in terms of a potential barrier experienced by the outgoing electron.

Total photoabsorption cross sections, $\sigma_{pa,t}(\lambda)$, have been discussed by a number of authors (see e.g., Hitchcock and Van der Wiel,[59] Berkowitz,[16] and Holland *et al.*[48]). Also, Gallagher *et al.*[18] reviewed the data on the photoabsorption, photoionization, and ionic photofragmentation cross sections for this molecule. The reader is referred to these studies and the sources cited therein for detailed data and discussion.

In Fig. 1(a) are shown the total photoabsorption cross-section data for SF_6 of Codling,[60] Blechschmidt *et al.*,[61] Lee *et al.*,[53] Sasanuma *et al.*,[62] and Holland *et al.*[48] Collectively these measurements cover the photon energy range between ~10 and ~50 eV. There are considerable differences in these measurements. For example, the most recent cross-section measurements by Holland *et al.*[48] lie below those of Blechschmidt *et al.*,[61] in some regions of the spectrum by nearly a factor of 2. They are in closer overall agreement with the measurements of Lee *et al.*[53] and Sasanuma *et al.*[62] All the data however show that the most intense feature in the entire absorption spectrum occurs around 23 eV and is due to the $5a_{1g}\rightarrow 6t_{1u}$ and $5t_{1u}\rightarrow 2t_{2g}$ intervalence transitions which are enhanced by shape resonances.[48] For a spectral assignment see Mitsuke *et al.*,[63] Sze and Brion,[52] and Holland *et al.*[48] (see also Table 4 in Sec. 2.3).

For comparison with the photoabsorption measurements in Fig. 1(a), excitation cross sections[59,64,65] determined from high-energy electron energy-loss spectra of SF_6 are shown in Fig. 1(b). These spectra are equivalent to the total photoabsorption cross section as a function of the photon energy. The electron energy-loss spectrum of Simpson *et al.*[64] was obtained at 0° scattering angle with 400 eV incident electrons, and was normalized to the photoabsorption results of Codling[60] at 23.0 eV. The electron energy-loss spectrum of Hitchcock and Van der Wiel[59] was also obtained at 0° scat-

TABLE 2. Values of the total excitation (photoabsorption) cross section for SF_6 determined from high-energy electron energy-loss spectra of Ying *et al.* in Ref. 65. The values listed here are derived by digitally scanning the figure in Ref. 65

Energy loss (eV)	Cross section (10^{-22} m^2)	Energy loss (eV)	Cross section (10^{-22} m^2)
8	0.0	36	80.4
9	0.39	38	72.4
10	7.74	40	67.1
11	24.4	42	61.1
12	18.2	44	55.7
14	25.2	46	52.2
16	73.9	48	47.5
17	95.4	50	40.3
18	76.6	52	37.9
20	71.1	54	34.9
22	122.5	56	33.3
23	156.8	58	31.7
24	130.9	60	30.2
26	83.8	62	27.6
28	84.6	64	26.4
30	74.8	66	24.6
32	74.2	68	25.5
34	77.0	70	25.5

tering angle but with 8 keV incident electrons and was normalized to the photoabsorption data of Blechschmidt *et al.*[61] at 27 eV. Ying *et al.*[65] used a 0.5° scattering angle and 2.5 keV incident electrons. Their measurements of generalized oscillator strengths, df/dE, were put on an absolute cross section scale via the relation $\sigma_{pa,t}(10^{-18}\,\mathrm{cm}^2) = 109.75\, df/dE(\mathrm{eV}^{-1})$. These last data are listed in Table 2 since they are absolute values. They are in good agreement with the other two sets of data.

Photoabsorption cross section measurements also have been extended into the extreme UV and soft x-ray regions using synchrotron radiation by a number of investigators.[48,50,53,54,60,61,66–70]

2.2. Total Photoionization, $\sigma_{pi,t}(\lambda)$, Partial Photoionization, $\sigma_{pi,partial}(h\nu)$, and Total Photodissociation, $\sigma_{pdis,t}(\lambda)$, Cross Sections

Because the lowest ionic state of SF_6 is antibonding, the ionization process even at threshold is dissociative and results in the formation of the fragments SF_5^+ and F. No SF_6^+ ion has been observed in the preponderance of the investigations, and its abundance is estimated to be less than 10^{-4} compared to that of SF_5^+. Thus, the photoionization of SF_6 is viewed as totally dissociative, and can be attributed to any of the following processes: direct, indirect, double, or Auger. Measurements of dissociative photoionization and dissociative and nondissociative double photoionization can be found in Gallagher *et al.*[18] and Hitchcock and Van der Wiel.[59] Holland *et al.*[48] used their measurements of the absolute total photoabsorption cross section and the photoionization quantum efficiency as a function of the photon wavelength to calculate the absolute total photoionization cross section, $\sigma_{pi,t}(\lambda)$, and the absolute total photodissociation cross section, $\sigma_{pdis,t}(\lambda)$, for SF_6 shown in Fig. 2. In deducing the

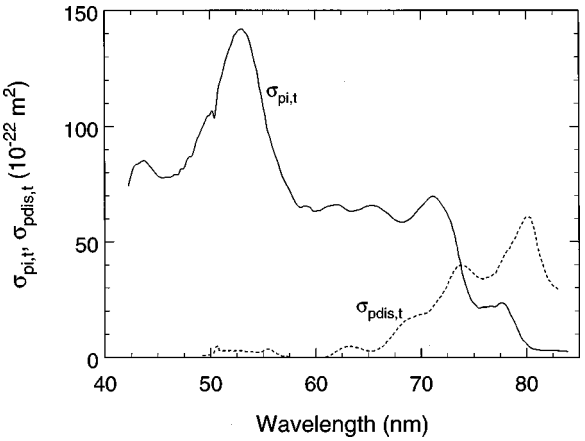

FIG. 2. Total photodissociation (- - -), $\sigma_{pdis,t}(\lambda)$, and total photoionization (—), $\sigma_{pi,t}(\lambda)$, cross sections of SF_6 as a function of photon wavelength (data of Holland *et al.* from Ref. 48).

photodissociation cross section it has been implicitly assumed that an excited SF_6 molecule can decay only by dissociation into neutral fragments or by autoionization.

In Fig. 3 are shown the partial photoionization cross sections, $\sigma_{pi,partial}(h\nu)$, of Hitchcock and Van der Wiel[59] deduced from dipole oscillator strength measurements over a range of energies up to an equivalent photon energy of 63 eV. In the same figure are also plotted the cross sections for dissociative and double photoionization of SF_6 in the energy range 75–125 eV obtained by Masuoka and Samson[71] using time-of-flight mass spectrometry and synchrotron radiation. The most abundant positive fragment ions are seen to be SF_5^+ and SF_3^+ (see also Creasey *et al.*[72] and Peterka *et al.*[73]). The relatively large cross section of the doubly charged positive ion SF_4^{++} was also observed under electron impact and was taken to indicate[74] the formation of SF_4^{++} by removal of two F^- ions. Gustafsson[54] also measured partial photoionization cross sections of SF_6 between 20 and 54 eV using synchrotron light. In general, these cross sections (not shown in Fig. 3) are rich in structure showing distinct resonance effects (e.g., see Gustafsson[54] and Dehmer[58]).

Studies employing photoelectron spectroscopy allowed detailed investigations of the photoionization process, including the relative probabilities (partial cross sections) of exciting specific electronic, vibrational, or rotational states of the molecular ion. Photoelectron–photoion coincidence experiments also allowed determination of the subsequent fate of the excited molecular ions. In addition, photoion–photoion coincidence experiments (e.g., see Refs. 75 and 76) have allowed probing of double ionization processes. These can be either direct or via an Auger decay. In the first case two highly correlated valence electrons are ejected. While in the latter case an inner-shell electron is ejected, an Auger decay occurs, and the resulting doubly charged positive molecular ion dissociates immediately into two fragment ions (plus neutrals). Using such techniques in conjunction with synchrotron radiation, Frasinski *et al.*[76] detected the two photoions from the double photoionization of SF_6. The thresholds they determined for the production of the ion pairs

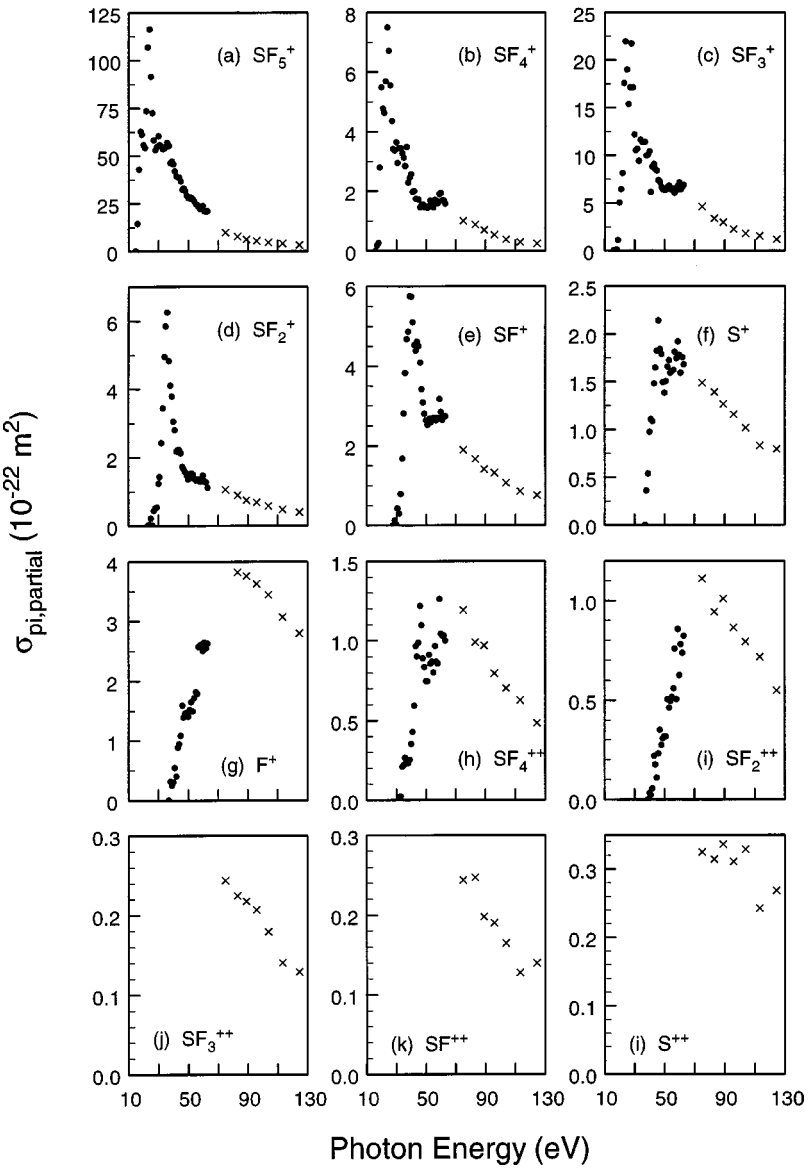

FIG. 3. Partial photoionization cross sections, $\sigma_{pi,partial}(h\nu)$, of SF_6 as a function of photon energy: (●) data of Hitchcock and Van der Wiel from Ref. 59; (×) data of Masuoka and Samson from Ref. 71 (see text).

$SF_5^+ + F^+$, $SF_3^+ + F^+$, $SF_2^+ + F^+$, $SF^+ + F_2^+$, and $SF_3^+ + F_2^+$ are listed in Table 3. According to Eland *et al.*[77] the major dissociation process of SF_6^{++} after He II ionization is $SF_6^{++} \rightarrow SF_3^+ + F^+ + F_2$. It is possible, however, that SF_6^{++} dissociation may proceed via doubly charged intermediates such as SF_4^{++}.[77] In Table 3 are listed the ionization energies of the various orbitals of the SF_6 molecule.

Ion-pair formation from photoexcitation of SF_6 is another interesting process which has revealed a great deal about the dissociation energetics and the structure of the SF_6 molecule. For instance, Mitsuke *et al.*[63] investigated the process

$$SF_6 + h\nu \rightarrow SF_6^{**} \rightarrow F^- + SF_x^+ + (5-x)F \quad [x \leqslant 5] \quad (1)$$

employing negative-ion mass spectrometry and synchrotron radiation in the 11.27–31.0 eV photon energy range. (The negative ions SF_6^- and SF_5^-, which were also observed, were attributed to the attachment of low-energy electrons generated by photoionization of the parent molecules.) Mitsuke *et al.* measured the photodissociation efficiency curve for F^- produced from SF_6 as a function of wavelength and compared the observed structure with that in the photoabsorption cross section data. The results of this study are compared with those from photoabsorption and electron energy-loss experiments in Table 4. Both the photon energy and/or energy loss and transition assignments are given in the table. For a fuller account and more detailed list of transitions see Refs. 52, 62, and 63.

2.3. Electron Energy-Loss Spectra

There have been a number of electron-impact energy-loss studies of SF_6.[52,59,64,65,83,86–88] The studies of Simpson *et al.*,[64] Hitchcock and Van der Wiel,[59] Sze and Brion,[52] and Ying *et al.*[65] are of particular interest in that their high-energy electron-impact energy-loss spectrum can be used to generate UV absorption cross sections. As discussed in the

TABLE 3. Ionization energies of various orbitals of SF_6

Type of orbital	Energy (eV)	Reference	Comments
	15.29	78[a]	Photoionization/Formation of SF_5^+
	15.3±0.2	79	Photoionization/Formation of SF_5^+
	15.32	63	Photoexcitation/Formation of SF_5^+
	15.5	80	VES[b]
$1t_{1g}$	15.67	80	VES
t_{1u}	15.69	81	PES[c]
$1t_{1g}$	15.7	55	PES
$1t_{1g}$	15.7	52	Formation of SF_5^+
	15.9±0.2	74	EI[d]; Formation of SF_5^+
	15.9±0.2	82	EI; Formation of SF_5^+
	16.0	59	Formation of SF_5^+
	16.7	80	VES
$3t_{1u}$, $1t_{2u}$	16.93	80	VES
t_{1g}	16.96	81	PES
$1t_{2u}$, $5t_{1u}$	17.0	55	PES
$1t_{2u}$, $5t_{1u}$	17.0	52	EELS[e]
	18.0	59	Formation of SF_4^+
	18.0	80	VES
$2e_g$	18.3	80	VES
e_{1g}	18.40	81	PES
$3e_g$	18.6	55	PES
$3e_g$	18.6	52	EELS
	18.7±0.2	82	EI; Formation of SF_4^+
t_{2u}	18.71	81	PES
	18.79±0.14	63	Formation of SF_3^+
	18.9±0.2	74	EI; Formation of SF_4^+
	19.1±0.5	79	Photoionization/Formation of SF_4^+
	19.0	59	Formation of SF_3^+
$1t_{2g}$	19.245 (0-0)	80	VES
	19.4±0.5	79	Photoionization/Formation of SF_3^+
t_{1u}	19.68	81	PES
$1t_{2g}$	19.8	55	PES
$1t_{2g}$	19.8	52	EELS
	20.1±0.3	74	EI; Formation of SF_3^+
	20.3±0.2	82	EI; Formation of SF_3^+
t_{2g}	22.5	81	PES
$4t_{1u}$	22.6	55	PES
$2t_{1u}$	22.7	80	VES
$4t_{1u}$	22.9	52	EELS
	26.0	59	Formation of SF_2^+
a_1	26.8	81	PES
	26.8±0.3	74	Formation of SF_2^+
$5a_{1g}$	26.85	55	PES
$5a_{1g}$	27.0	52	EELS
$2a_{1g}$	27.0	80	VES
	31.0	59	Formation of SF^+
	31.3±0.3	74	Formation of SF^+
	33	59	Formation of SF_4^{++}
	35.8±1.0	74	Formation of F^+
	37.0	59	Formation of S^+
	37.3±1.0	74	Formation of S^+
	38.0	59	Formation of F^+
$2e_g$	39.3	52	EELS
	40.0	59	Formation of SF_2^{++}
	40.6±0.5	74	Formation of SF_4^{++}
$3t_{1u}$	41.2	52	EELS
	41.1±1	76	DDP[f] producing $SF_5^+ + F^+$, $SF_3^+ + F^+$, or $SF_3^+ + F_2^+$
	45.1±1	76	DDP[f] producing $SF_2^+ + F^+$
	46.5±0.5	74	Formation of SF_2^{++}
	52.8±1	76	DDP[f] producing $SF^+ + F_2^+$

[a]The authors reported observation of a weak SF_6^+ signal using the 21 eV resonance line of helium.
[b]VES=He I induced valence electron spectra.
[c]PES=photoelectron spectra.
[d]EI=Electron impact.
[e]EELS=Electron energy-loss spectra.
[f]DDP=dissociative double photoionization.

TABLE 4. Photon energy/energy loss and transition assignments for SF_6[a]

Photon energy/Energy loss (eV)	Assignment Ref. 63[b]	Assignment Ref. 62[c]	Assignment Ref. 52[d]	Assignment Ref. 83[d]
6.494 (Ref. 52[e])				
7.93 (Ref. 84[c,f])		$5t_{1u}\rightarrow 6a_{1g}$		
9.596 (Ref. 52)			$1t_{1g}\rightarrow 6a_{1g}$[g]	
9.8 (Ref. 83[h])				$1t_{1g}\rightarrow 6a_{1g}$
10.982–12.266 (Ref. 52)	$1t_{1g}\rightarrow 6t_{1u}/5t_{1u}\rightarrow 6a_{1g}$		$1t_{1g}\rightarrow 6t_{1u}/1t_{2u}$, $5t_{1u}\rightarrow 6a_{1g}$	
11.0 (Ref. 83[h])				$1t_{2u}\rightarrow 6a_{1g}$
11.5; 11.6 (Ref. 83[i])				$5t_{1u}\rightarrow 6a_{1g}$
11.54 (Ref. 64[d,j])				
11.729 (Ref. 84[c])				
11.76 (Ref. 85[c])				
12.8 (Ref. 83[h])				$1t_{1g}\rightarrow 7a_{1g}(4s)$
13.2 (Ref. 63[k])	$1t_{1g}\rightarrow 4p$	$5t_{1u}\rightarrow 6a_{1g}$		
13.2 (Ref. 83[h])				$1t_{1g}\rightarrow 6t_{1u}(4p)$
13.143–13.309 (Ref. 52)			$1t_{1g}\rightarrow 4p$	
13.244 (Ref. 85[c])				
13.27 (Ref. 84[c])		$4t_{1u}\rightarrow 6a_{1g}$		
13.30 (Ref. 64[d,j])		$4t_{1u}\rightarrow 6a_{1g}$		
13.3 (Ref. 83[i])				$1t_{1g}\rightarrow 6t_{1u}(4p)$
14.1 (Ref. 83)				$1t_{2g}\rightarrow 6a_{1g}$
14.218 (Ref. 85[c])				
14.283 (Ref. 84[c])				
14.3 (Ref. 63[k])	$5t_{1u}\rightarrow 4s/3e_g\rightarrow 6t_{1u}$			
14.35 (Ref. 64[d,j])				
13.970–14.415 (Ref. 52)			$3e_g\rightarrow 6t_{1u}$	
14.3; 14.7 (Ref. 83[i])				$5t_{1u}\rightarrow 7a_{1g}(4s)$
14.6 (Ref. 63[k])	$1t_{1g}\rightarrow 5p$			
14.707 (Ref. 52)			$1t_{2u}$, $5t_{1u}\rightarrow 4s$	
14.90 (Ref. 64[d])				
14.9 (Ref. 83[i])				$1t_{1g}\rightarrow 7t_{1u}(5p)$
14.933 (Ref. 85[c])				
15.163 (Ref. 84[c])				
15.546 (Ref. 52)			$3e_g\rightarrow 6t_{1u}$	
15.7 (Ref. 63[k])	$5t_{1u}\rightarrow 5s/1t_{2g}\rightarrow 6t_{1u}$			
15.7 (Ref. 62[c])		$1t_{2g}\rightarrow 6t_{1u}$		
16.0; 16.1 (Ref. 83)				$3e_g\rightarrow 6t_{1u}(4p)$
17.00 (Ref. 62[c])		$1t_{2g}\rightarrow 6t_{1u}$	$1t_{2g}\rightarrow 6t_{1u}$	
17.00 (Ref. 63[k])	$4t_{1u}\rightarrow 6a_{1g}$			
17.021			$4t_{1u}\rightarrow 6a_{1g}$[g]	
19.6 (Ref. 63[k])	$4t_{1u}\rightarrow 4s$			
19.8 (Ref. 52[j])		$5t_{1u}\rightarrow 2t_{2g}$	$4t_{1u}\rightarrow 4s$	
19.8 (Ref. 62[c])		$5t_{1u}\rightarrow 2t_{2g}$		
20.9 (Ref. 52[j])			$1t_{1g}\rightarrow 2t_{2g}$[g]/$5a_{1g}\rightarrow 6a_{1g}$[g]	
21.2 (Ref. 63[k])	$4t_{1u}\rightarrow 5s$		$4t_{1u}\rightarrow 5s$	
22.1 (Ref. 63[k])	$5t_{1u}\rightarrow 2t_{2g}/4t_{1u}\rightarrow ns$ $(n\geqslant 6)$			
23.2 (Ref. 52[l])		$5a_{1g}\rightarrow 6t_{1u}$	$5a_{1g}\rightarrow 6t_{1u}/1t_{2u}$, $5t_{1u}\rightarrow 2t_{2g}$	
23.2 (Ref. 62[c])		$5a_{1g}\rightarrow 6t_{1u}$		
24.6 (Refs. 63[k] and 52[l])	$5a_{1g}\rightarrow 4p$	$5a_{1g}\rightarrow 4p$		
25.7 (Ref. 63[k])	$5a_{1g}\rightarrow 5p$			
25.8 (Ref. 52[l])		$5a_{1g}\rightarrow 5p$		
26.2 (Ref. 63[k])	$5a_{1g}\rightarrow 6p$			
28.3 (Ref. 52[l])		$4t_{1u}\rightarrow 2t_{2g}$		
28.5 (Ref. 60[c])				
28.8 (Ref. 62[c])		$1t_{2u}$, $5a_{1g}\rightarrow (6a_{1g})^2$		
31.8 (Ref. 62[c])		$3t_{1u}\rightarrow 6a_{1g}$		
35.4 (Ref. 62[c] and 60[c])		$2e_g\rightarrow 6t_{1u}$		
37.6 (Ref. 62[c])		$4t_{1u}\rightarrow 4e_g$		

[a]See Refs. 52, 62, and 63 for more details and for information on other transitions.
[b]Data from studies on ion-pair formation from photoexcitation.
[c]Data from studies on photoabsorption spectra.
[d]Data from electron energy-loss experiments.
[e]Estimated uncertainty $=\pm 0.020$ eV.
[f]The photoabsorption data show weak continuous absorption which begins at 7.93 eV (Ref. 84).
[g]Forbidden transition.
[h]Triplet
[i]Singlet
[j]Uncertainty $=\pm 0.05$ eV.
[k]Energy position of peak maximum in the F^- efficiency curve.
[l]Estimated uncertainty $=\pm 0.5$ eV.

TABLE 5. Values of the electron affinity of the SF_6 molecule reported since 1983

Electron affinity (eV)	Reference	Comments
0.0–1.49 (0.76)[a]	103	Range of 20 values listed in Ref. 103 which were reported prior to 1983.
1.05 ± 0.1	104	Energetics of electron transfer reactions
1.15 ± 0.15	105	Thermal electron attachment studies
1.07 ± 0.07[b]	106	Thermal electron attachment studies
1.19	95	Calculation
1.3–1.4	96	Calculation
1.06	107	Calculation
3.44	101	Calculation
3.46	100	Calculation
1.06		**Recommended value (see text)**

[a]Average of the values listed in Ref. 103 excluding the lowest and the highest values listed in Ref. 103.
[b]This value is a refinement of their earlier result in Ref. 105.

previous section, Simpson *et al.* obtained an energy-loss spectrum corresponding to optical electronic excitation of SF_6 using 400 eV incident energy electrons and a 0° scattering angle. Their high-energy electron-impact energy-loss spectrum was used to generate UV absorption cross sections in the 10–30 eV region by normalization to the photoabsorption results of Codling[60] at 23.0 eV [see comparison with photoabsorption data in Figs. 1(a) and 1(b)]. Hitchcock and Van der Wiel[59] also obtained electron-impact energy-loss spectra at 0° using electron-ion coincidence measurements and incident electrons with 8 keV kinetic energy. Their electron-energy loss data were also used to determine cross sections for dipole photoabsorption and photofragmentation of SF_6 in the equivalent photon energy range of 5–63 eV by normalization to the photoabsorption measurements of Blechschmidt *et al.*[61] at 27 eV. Their data are compared in Fig. 1(b) with the data of Simpson *et al.*[64]

Furthermore, Hitchcock and Van der Wiel[59] used their electron energy-loss measurements, in connection with the photoionization branching ratios they measured for the six lowest energy states of SF_6^+, to obtain partial ionization cross sections for the production of specific positive ions. These data were presented earlier in Fig. 3. Sze and Brion[52] studied inner-shell electron energy-loss spectra of SF_6 using 2.0–3.7 keV electrons and a 0° scattering angle. Their findings for valence-shell excitation spectra have been discussed earlier (Table 3). Ying *et al.*[65] performed angle-resolved electron-energy loss measurements using a coplanar electron spectrometer, and determined generalized oscillator strengths of valence shell electronic transitions in the range of 7–70 eV using electrons with initial kinetic energy of 2.5 keV. Their valence-shell electron energy-loss spectrum of SF_6 measured at 0.5° (converted to photoabsorption cross section using the relationship $\sigma_{pa,t}(10^{-18}\ \mathrm{cm}^2) = 109.75\, df/dE\ (\mathrm{eV}^{-1})$, where df/dE is the differential oscillator strength) is compared with other electron energy-loss spectra and photoabsorption data in Fig. 1(b), and values are listed in Table 2. There is general agreement among the photoabsorption data and the electron energy-loss spectra.

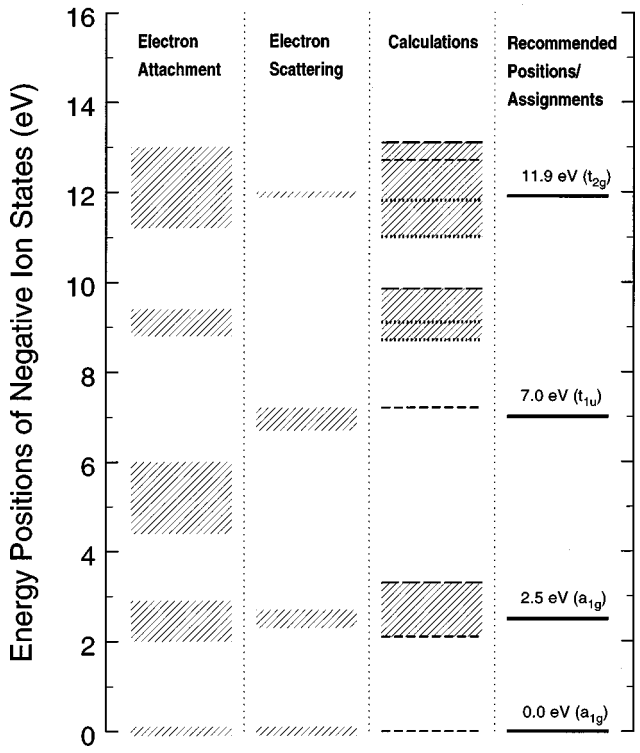

FIG. 4. Negative ion states of the SF_6 molecule as determined by electron attachment measurements, electron scattering measurements, and calculations: (- - -) Dehmer *et al.* in Ref. 112; (– –) Gianturco *et al.* in Ref. 121; (···) Gyemant *et al.* in Ref. 123. Shaded areas represent the range of measured peak energies. The last column gives the recommended average positions and assignments (see text). It should be noted that the adiabatic position of the ~0.0 eV negative ion state is at −1.06 eV [$= -|\mathrm{EA}(SF_6)|$].

Besides the above three studies, Chutjian *et al.*[86] and Trajmar and Chutjian[83] investigated the electron-impact excitation of SF_6 using 20 eV incident electrons in the energy-loss range of 7–14 eV. In their experiments the scattering angles ranged from 20° to 135°. From a comparison of their data at low energies and large scattering angles with data they obtained earlier using 400 eV electrons and a 0° scattering angle (i.e., under conditions favoring excitation of optically allowed transitions), they identified a number of spin and/or symmetry forbidden transitions in the energy range ~10–~16 eV which are listed in Table 4.

In addition to the electron energy-loss studies involving low-lying transitions, Francis *et al.*[88] recorded electron energy-loss spectra of SF_6 in the region of S $2p$, S $2s$, and F $1s$ excitation, using dipole and nondipole electron-scattering conditions. Electron-impact energies between 700 and 3200 eV and scattering angles between 0° and 30° were used. It was found that relative to dipole electron energy-loss or photoabsorption spectra, there are large intensity redistributions in both the S $2p$ and S $2s$ spectra under nondipole conditions. In contrast, the F $1s$ spectrum was found to be essentially the same in near-dipole and nondipole scattering regimes. Fomunung *et al.*[89] conducted a theoretical study of electron excitation of optically allowed transitions between 20 eV and 2.5 keV, and a number of investigations have

been conducted on the generalized oscillator strength of SF_6 (e.g., see Refs. 88 and 90).

Energy-loss spectra involving vibrational excitation of SF_6 were investigated by Trajmar and Chutjian,[83] Rohr,[91] and Randell *et al.*[92] These are discussed in Sec. 3.5.1.

2.4. The Electron Affinity and Negative Ion States of SF_6

The four lowest lying empty orbitals of SF_6 are:[49,52] $(6a_{1g})^0(6t_{1u})^0(2t_{2g})^0(4e_g)^0$. Calculations for the octahedral symmetry (O_h) of SF_6^- (see Refs. 93–96) have shown that the S–F antibonding character of the highest occupied, totally symmetric, nondegenerate $6a_{1g}$ molecular orbital of SF_6^- results in a substantial increase of the S–F bond in SF_6^- compared to neutral SF_6. Although a number of authors (e.g., Refs. 97–99) considered electron capture into degenerate molecular orbitals of lower symmetry than a_{1g}, calculations for a lower symmetry configuration (see Gutsev[100,101] and Richman and Banerjee[102]) showed the O_h octahedral structure to be the most stable.

There has been widespread unanimity that SF_6 attaches thermal and near thermal electrons with a very large cross section forming SF_6^-, and that the SF_6 molecule must thus have a positive electron affinity. However, up until recently there has been no concensus regarding the size of its electron affinity. Prior to 1983 there were at least 20 reported values for this quantity[103] that varied from near 0.0 eV to ~1.5 eV. Values reported since 1983 are listed in Table 5 along with the range of pre-1983 values listed in Ref. 103. We take the average of the two most recent and widely accepted values determined in Refs. 104 and 106 to be our presently recommended value of (1.06 ± 0.06) eV for the electron affinity of the SF_6 molecule.

In addition to the electron attachment resonance at ~0.0 eV, electron attachment and electron scattering experiments and calculations have shown the existence of several negative ion states at energies below 30 eV. The energies of these states, as determined by the positions of the maxima in the measured electron attachment cross sections, measured electron scattering cross sections, and calculated cross sections are listed in Table 6. Also listed in Table 6 are possible symmetry assignments. These experimental and the calculated values (below 15 eV) are shown in Fig. 4. The electron attachment data for each resonance exhibit a considerable spread partly because these data involve a number of different fragment negative ions. The energy range for each resonance as determined by the electron attachment studies, extends to lower energies than the respective energy range determined by the electron-scattering studies. This difference is especially large for the 7.0 eV resonance, and can be attributed to the competition between dissociation and autodetachment of SF_6^-* in the attachment studies. It is interesting to note that although electron attachment studies and theory indicate a resonance near 9 eV, none of the electron scattering investigations show any evidence of it.

The last column in Fig. 4 gives the recommended energy positions of the SF_6 negative ion resonances as determined by considering only the electron scattering data, along with their symmetry assignments. The energy positions of the lowest four negative ion states of the SF_6 molecule and their symmetries are: ~0.0 eV(a_{1g}), 2.5 eV(a_{1g}), 7.0 eV(t_{1u}), and 11.9 eV(t_{2g}). It should be noted that the adiabatic position of the ~0.0 eV negative ion state is at -1.06 eV $[= -|\mathrm{EA}(SF_6)|]$. Other negative ion states are indicated near 17 eV and higher energies (see Table 6). The resonances near 27 and 50 eV can be assigned as core-excited valence negative ion states involving the σ^* molecular orbitals.

2.5. Fundamental Vibrational Modes and Other Data

The fundamental vibrational frequencies $\nu_1 - \nu_6$ of the SF_6 molecule have a high degree of degeneracy due to the high symmetry of the molecule. Table 7 lists the vibrational assignment, energy, symmetry, infrared activity, and degeneracy of the six fundamental vibrational modes.[15,125–130] The low energies of these vibrations results in vibration excitation of these modes at relatively low temperatures above ambient. Even at room temperature the population of the $v=1$ level of ν_6 is one half of the ground-state population.

The vibrational frequencies for SF_6^- are somewhat lower than the respective frequencies for the neutral SF_6 due to the weaker bonding in the negative ion. The values (in eV) of the six fundamental frequencies of SF_6^- and their degeneracies (values in parenthesis) as listed by Chase *et al.*[129] are: 0.0868 (1), 0.0775 (2), 0.1147 (3), 0.0736 (3), 0.0620 (3), and 0.0403 (3).

In Table 8 are listed other data on SF_6 and SF_6^- which are relevant to the present discussion on electron interactions with the SF_6 molecule. The large difference between the equilibrium bond lengths of SF_6 and SF_6^- shows the large effect of electron correlation.

3. Electron Scattering by SF_6

3.1. Total Electron Scattering Cross Section, $\sigma_{sc,t}(\varepsilon)$

There have been eight sets[116–120,137–139] of experimental determinations of $\sigma_{sc,t}(\varepsilon)$. These are shown in Fig. 5. Rohr[120] determined the integrated vibrationally elastic ($\Delta\nu = 0$) electron scattering cross section for SF_6 below ~6 eV. He then obtained a value of $\sigma_{sc,t}(\varepsilon)$ by adding to this cross section the total vibrational excitation cross section he measured earlier.[91] His data on the total vibrational excitation cross section, however, need to be corrected because they were originally normalized to the data of Srivastava *et al.*,[140] which were subsequently corrected by Trajmar *et al.*[10] According to Trajmar *et al.*,[10] the vibrational cross section of Rohr[91] needs to be multiplied by a factor of 1.28 at 5 eV to correspond to the renormalized data of Srivastava *et al.* The data identified in Fig. 5 as ''Rohr (1979)'' are the original values of Rohr without this correction. The $\sigma_{sc,t}(\varepsilon)$ of Rohr is not a direct measurement and for this reason it is not

TABLE 6. Negative ion states of SF_6

Energy position (eV)	Type of study	Symmetry/Orbital	Reference
~0.0	Many electron attachment studies		
0.38	SF_5^- from SF_6		26, 108–110
0.5±0.1	SF_5^- from SF_6		111
~0.1	Excitation function of ν_1	A_{1g}	92
~0.1	Vibrational excitation by electron impact		91
~0.0	Multiple scattering calculation	a_{1g}	112
2.0	F_2^- from SF_6		26
2.2	F_2^- from SF_6		113
2.4	F_2^- from SF_6		114[a]
2.6	F^- from SF_6		26
2.8	F^- from SF_6		114
2.8	F^- from SF_6		113
~2.9	F^- from SF_6		115
2.3	Total electron scattering cross section	a_{1g}	116
2.5	Total electron scattering cross section	A_{1g}	117
2.5	Total electron scattering cross section	a_{1g}	118
2.52±0.15	Trochoidal derivative spectrum	a_{1g}	119
2.56±0.15	Total electron scattering cross section	a_{1g}	119
2.7	Angular dependence of vibrationally elastic electron scattering	a_{1g}	120
2.1	Multiple scattering calculation	a_{1g}	112
3.30	Multichannel calculation with close coupling	A_{1g}	121
4.4	F_2^- from SF_6		26
4.8	F_2^- from SF_6		114
4.8	F_2^- from SF_6		113
5.0	SF_4^- from SF_6		113
5.1	F^- from SF_6		26
5.2	F^- from SF_6		114
5.3	F^- from SF_6		113
5.4	SF_4^- from SF_6		26
5.4	SF_4^- from SF_6		114
~5.4[b]	F^-, F_2^-, and SF_4^- from SF_6		115
5.7±0.1	F^- from SF_6		111
6.0±0.1	SF_4^- from SF_6		111
6.7	Total electron scattering cross section	t_{1g}	116
7.0	Total electron scattering cross section	t_{1u}	118
7	Angular dependence of vibrationally elastic electron scattering	t_{1u}	120
7	Total electron scattering cross section	t_{1u}	117
7.01±0.16	Trochoidal derivative spectrum	t_{1u}	119
7.05±0.10	Total electron scattering cross section	t_{1u}	119
7.2	Elastic electron scattering cross section	t_{1u}	122
7.2	Multiple scattering calculation	t_{1u}	112
8.8	F^- from SF_6		26
8.9	F^- from SF_6		114
9.3±0.1	F^- from SF_6		111
9.4	F^- from SF_6		113
9.4	SF_3^- from SF_6		26
8.7; 9.1	Multiple scattering calculation	T_{1u}	123
9.85	Multichannel calculation with close-coupling	T_{1u}	121
11.2	F_2^- from SF_6		26
11.2	SF_3^- from SF_6		114
11.3	SF_3^- from SF_6		113
11.3	F^- from SF_6		26
11.5	F^- from SF_6		114
11.6	F^- from SF_6		113
11.6	F_2^- from SF_6		113
11.7	F_2^- from SF_6		26
11.8±0.1	F^- from SF_6		111
12.0	SF_2^- from SF_6		26
12.3	SF_2^- from SF_6		113

TABLE 6. Negative ion states of SF_6—Continued

Energy position (eV)	Type of study	Symmetry/Orbital	Reference
13.0	SF_2^- from SF_6		114
11.87±0.10	Total electron scattering cross section	t_{2g}	119
11.88±0.07	Trochoidal derivative spectrum	t_{2g}	119
11.9	Total electron scattering cross section	t_{2g}	118
11.9	Total electron scattering cross section	t_{2g}	116
12	Total electron scattering cross section	t_{2g}	117
12	Elastic electron scattering cross section	t_{2g}	122
12	Elastic and vibrationally inelastic electron-impact excitation		83
11	Multiple scattering calculation	T_{1u}	124
11.0; 11.8; 13.7	Multiple scattering calculation	T_{2g}	123
12.7	Multiple scattering calculation	t_{2g}	112
13.10	Multichannel calculation with close coupling	T_{2g}	121
16.8	Total electron scattering cross section		118
17	Multiple scattering calculation of total cross section for elastic electron scattering	T_{2g}	124
23–24	Angular distribution of photoelectrons		46
24	Multiple scattering calculation	E_g	124
27.0	Multiple scattering calculation	e_g	112
27.0	Multichannel calculation with close coupling	e_g	121
27.1; 28.3; 28.6	Multiple scattering calculation	E_g	123
28.84	Multichannel calculation with close coupling	E_g	121
25–55[c]	Total electron scattering cross section	e_g	119

[a]The values of Lehmann (Ref. 114) given in this table have been deduced from his figures and were reduced by 0.6 eV as discussed in the text.
[b]Main resonance.
[c]Possibly one or more resonances in this energy range.

TABLE 7. Vibrational assignment, energy, symmetry, infrared activity, and degeneracy of the fundamental frequencies of the SF_6 molecule (see Refs. 15, 125–130)[a]

Vibration	Energy (eV)	Reference	Symmetry	Infrared activity	Degeneracy
ν_1	0.0955	127	A_{1g}	No	1
	0.0959	126			
	0.0959	129			
	0.096	130			
ν_2	0.0793	127	E_g	No	2
	0.0796	126			
	0.0796	129			
	0.0798	130			
ν_3	0.1174	125	F_{1u}	Yes	3
	0.1175	127			
	0.1175	129			
	0.1175	128			
	0.1175	130			
ν_4	0.0761	127	F_{1u}	Yes	3
	0.0762	130			
	0.07625	128			
	0.0763	129			
ν_5	0.0647	127	F_{2g}	No	3
	0.0649	130			
	0.0651	126			
	0.0651	129			
ν_6	0.0430	126	F_{2u}	No	3
	0.0430	129			
	0.0432	130			
	0.0434	127			

[a]See text and Chase *et al.* (Ref. 129) for the vibrational frequencies of SF_6^-.

included in the data used to determine the recommended values of $\sigma_{sc,t}(\varepsilon)$ derived later in this section.

Another low-energy measurement of $\sigma_{sc,t}(\varepsilon)$ was made by Ferch *et al.*[137] in a transmission experiment using a time-of-

TABLE 8. Other data on SF_6 and SF_6^-[a]

Physical quantity	Value	Reference
SF_5–F bond dissociation energy[b]	3.38 eV	132[c]
	⩽(3.39±0.15) eV	133[c]
	(3.9±0.15) eV	134
	(4.1±0.13) eV	135
S–F bond length of SF_6	1.5568 Å	136
	1.564±0.01 Å	129
	1.565 Å[d]	96
	1.567 Å[d]	94
F–S–F bond angle of SF_6 and SF_6^-	90°	129
S–F bond length of SF_6^-	1.72 Å	129
	1.717 Å[d]	101
	1.710 Å[d]	94
	1.704 Å[d]	96

[a]See text for values of the vibrational frequencies of SF_6^-.
[b]Hubers and Los (Ref. 131) obtained a value of (1.0±0.1) eV for the dissociation energy of SF_5^-–F.
[c]According to Fenzlaff *et al.* (Ref. 115) this value is too low due to the low value used by these authors for the production of F^- from SF_6.
[d]Octahedral geometry.

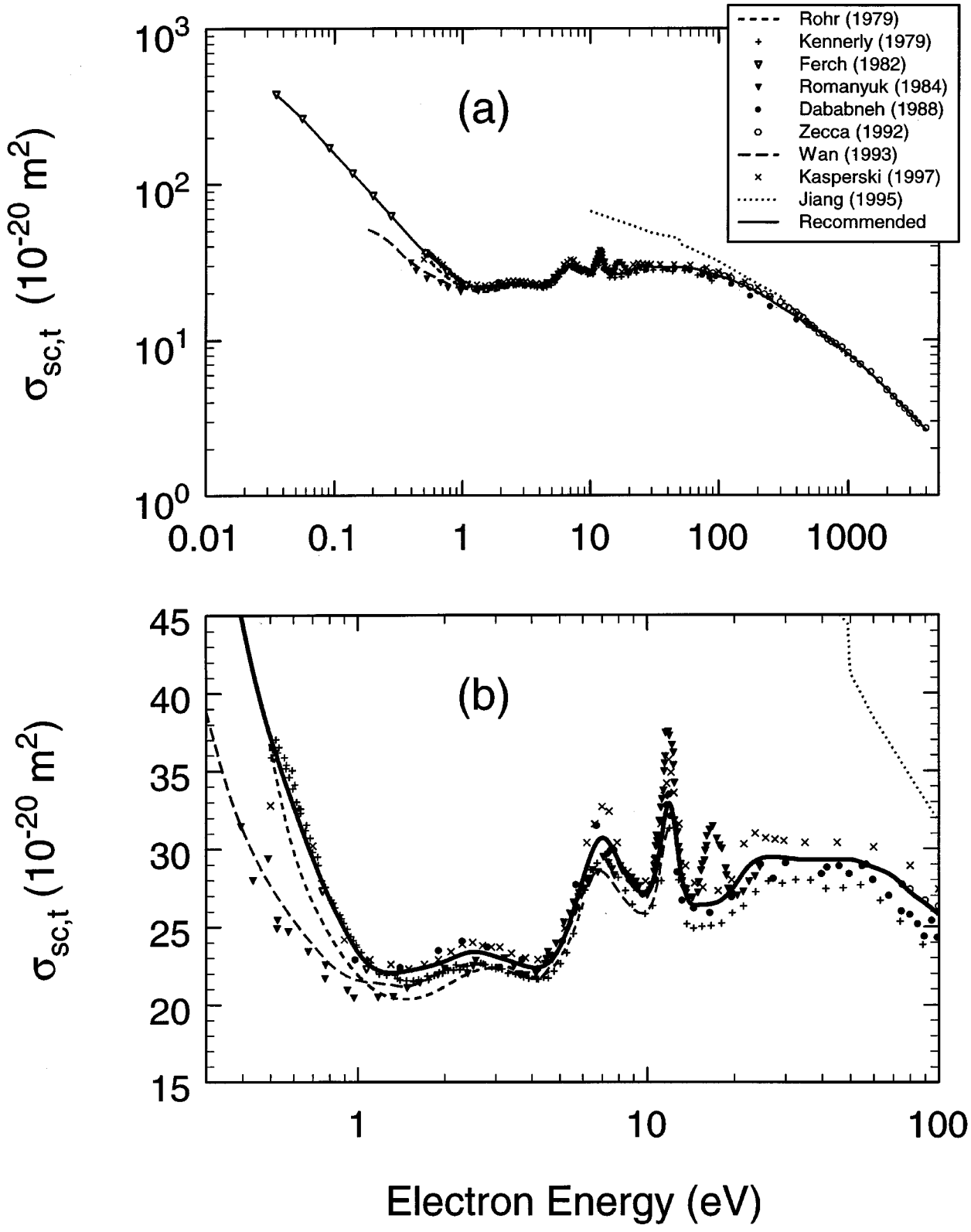

FIG. 5. (a) Total electron scattering cross section, $\sigma_{sc,t}(\varepsilon)$, of SF_6 as a function of electron energy ε: (- - -) Ref. 120; (+) Ref. 119; (▽) Ref. 137; (▼) Ref. 118; (●) Ref. 116; (○) Ref. 138; (– –) Ref. 139; (×) Ref. 117; (···) Ref. 141; (—) recommended data. (b) Expanded view.

flight spectrometer. It covered the electron energy range from 0.036 to 1.0 eV with a reported uncertainty of $\pm 7\%$ above 0.2 eV and $\pm 9\%$ below 0.2 eV. The results of Ferch *et al.* are in excellent agreement with the other available measurements of $\sigma_{sc,t}(\varepsilon)$ above 0.5 eV.

Measurements of $\sigma_{sc,t}(\varepsilon)$ extending to higher electron energies were also made using a variety of techniques. Wan *et al.*[139] measured the $\sigma_{sc,t}(\varepsilon)$ of SF_6 using an electron transmission spectrometer employing a trochoidal monochromator. The overall uncertainty of their measurements is within $\pm 15\%$ above 1 eV, but it may increase to as much as $\pm 50\%$ at energies below 0.2 eV. These data are in reasonable agreement with the other measurements above ~ 1.0 eV, but fall systematically below most of the other measurements for lower electron energies. Kennerly *et al.*[119] measured the $\sigma_{sc,t}(\varepsilon)$ of SF_6 for incident-electron energies between 0.5 and 100 eV. The uncertainty in their measurements was reported to be $\pm 5\%$ from 0.5 to 30 eV, $\pm 10\%$ from 30 to 50 eV, and $\pm 15\%$ from 50 to 100 eV. The principal source of error above 30 eV is the detection of electrons scattered inelastically in the forward direction which contribute to a higher transmission value and a lower cross section. Hence, the values above 30 eV are a lower bound.[119] Indeed, as can be seen from Fig. 5(b), the values of Kennerly *et al.* lie below those of the other groups at energies above ~ 10 eV.

Romanyuk *et al.*[118] measured $\sigma_{sc,t}(\varepsilon)$ for SF_6 from ~ 0.4 to ~ 25 eV using an electron trap method. No uncertainty is given in their paper, but their values below ~ 1.0 eV are low. In addition, the measurements of Romanyuk *et al.* show a resonance peak at 16.8 eV, which is absent from all the other data. The measurements of Dababneh *et al.*[116] extend over a larger electron energy range stretching from 1 to 500 eV and were made using an electron transmission technique. The values of $\sigma_{sc,t}(\varepsilon)$ at the resonance energies 2.3, 6.7, and 11.9 eV are, respectively, reported to be $(24.1 \pm 0.2) \times 10^{-16}$ cm^2, $(31.5 \pm 0.5) \times 10^{-16}$ cm^2, and $(33.5 \pm 0.2) \times 10^{-16}$ cm^2. Measurements of $\sigma_{sc,t}(\varepsilon)$ for SF_6 at higher energies (75–4000 eV) have been reported by Zecca *et al.*[138] and were made using a Ramsauer-type electron spectrometer. The total uncertainty in these measurements is $\sim \pm 6\%$. The data of Zecca *et al.*[138] are generally higher than those of Dababneh *et al.*[116] in the energy range from 75 to 700 eV where the two sets of data overlap. They are also higher than those of Kennerly *et al.*[119] in the range from 75 to 100 eV [see Fig. 5(b)].

Finally, a more recent measurement of the $\sigma_{sc,t}(\varepsilon)$ of SF_6 for electron energies between 0.6 and 250 eV has been made by Kasperski *et al.*[117] who employed the electron transmission method. The estimated uncertainty of these measurements is up to $\pm 7\%$ below 5 eV, less than $\pm 4\%$ between 10 and 100 eV, and approximately $\pm 5\%$ at the highest energies they investigated. These data are consistently higher than the other measurements between 20 and 100 eV, but agree well with the high-energy measurements of Zecca *et al.*[138]

In Fig. 5 are also plotted the values of $\sigma_{sc,t}(\varepsilon)$ for SF_6 calculated by Jiang *et al.*[141] who employed the additivity rule and the model complex optical potential. These calculated values of $\sigma_{sc,t}(\varepsilon)$ are not in good agreement with the measurements except at the very high energies. The additivity rule ignores molecular geometry and reduces molecular scattering to atomic scattering. Since the contribution from the interference occurring between the scattering amplitudes originating from the different constituent atoms of the molecule is not included in the additivity rule, the results of the total scattering cross section using the additivity rule show larger discrepancies in the low-energy range.

Besides the calculations by Jiang *et al.*[141] there have also been two other electron scattering calculations, one by Dehmer *et al.*[112] and another by Benedict and Gyemant.[124] However, these authors calculated cross sections for total elastic electron scattering and for this reason their results are not shown in Fig. 5 (see Sec. 3.3).

The experimental data in Fig. 5 by-and-large lie within the quoted or expected experimental uncertainties for most of the electron energy range investigated. There are however systematic differences between the various sets of experimental measurements. For instance, there exist large uncertainties in the data below ~ 1 eV and, as mentioned earlier,

TABLE 9. Recommended values for the total electron scattering cross section, $\sigma_{sc,t}(\varepsilon)$, of SF_6

Electron energy (eV)	$\sigma_{sc,t}(\varepsilon)$ (10^{-20} m^2)	Electron energy (eV)	$\sigma_{sc,t}(\varepsilon)$ (10^{-20} m^2)
0.035	379.8	13	28.9
0.040	344.7	14	26.6
0.045	315.3	15	26.4
0.050	290.1	18	26.7
0.060	249.4	20	27.6
0.070	217.6	22	28.7
0.080	192.7	25	29.4
0.090	173.1	30	29.4
0.10	157.4	35	29.3
0.15	109.5	40	29.3
0.20	84.3	45	29.3
0.25	68.7	50	29.3
0.30	58.1	60	28.8
0.35	50.4	70	28.2
0.40	44.6	80	27.2
0.45	40.3	90	26.5
0.50	37.2	100	25.8
0.60	32.8	150	22.7
0.70	29.4	200	20.2
0.80	26.8	250	18.0
0.90	24.9	300	16.3
1.0	23.4	350	15.1
1.5	22.2	400	14.1
2.0	22.8	450	13.1
2.5	23.4	500	12.4
3.0	23.1	600	11.2
3.5	22.7	700	10.2
4.0	22.4	800	9.41
4.5	22.6	900	8.73
5.0	23.7	1000	8.15
6.0	28.0	1500	6.07
7.0	30.7	2000	4.80
8.0	29.2	2500	3.94
9.0	27.6	3000	3.36
10.0	27.3	3500	2.95
11.0	29.6	4000	2.64
12.0	32.9		

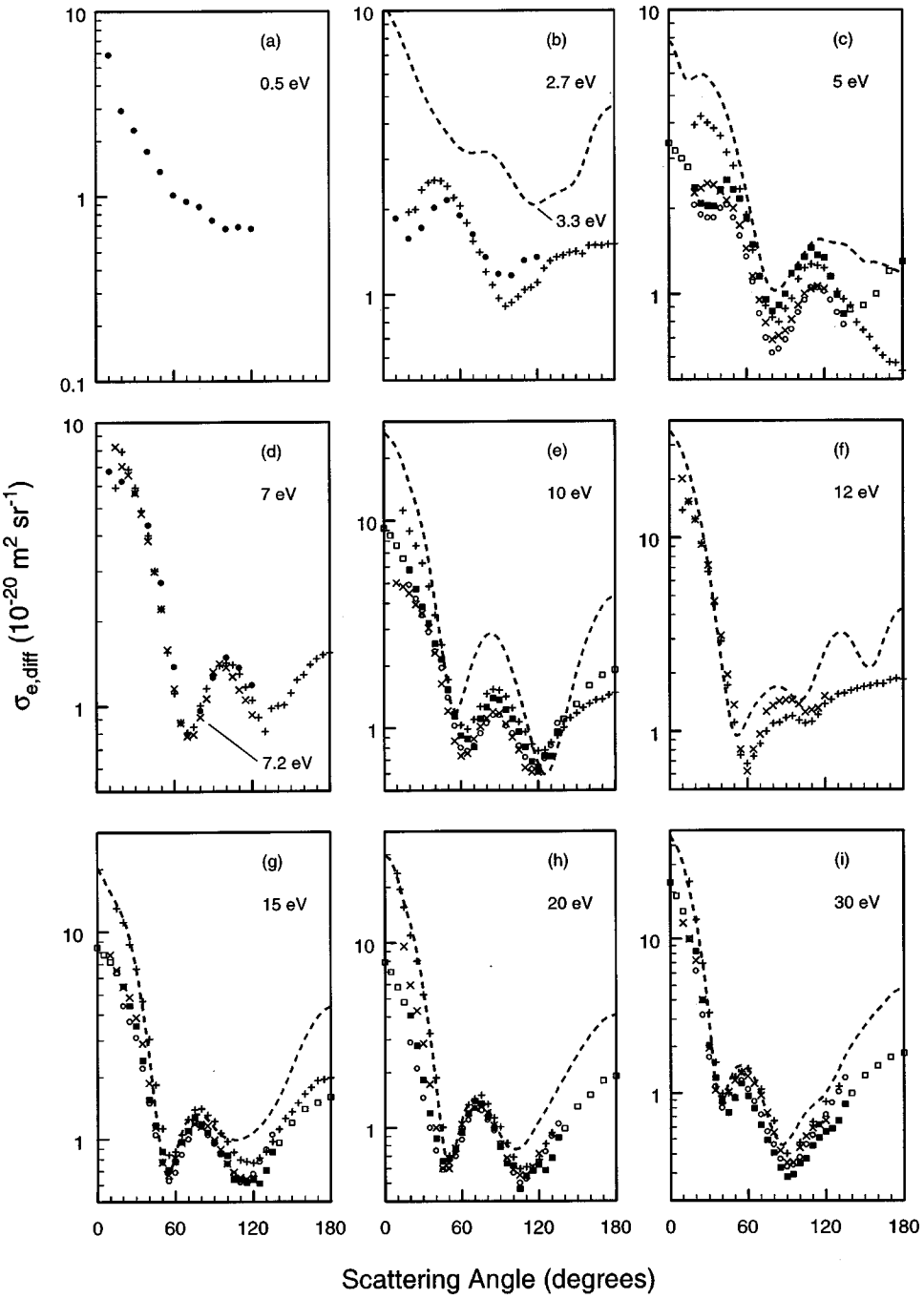

FIG. 6. Elastic differential electron scattering cross sections, $\sigma_{e,diff}(\varepsilon)$, of SF_6 as a function of electron energy ε: (○) Data of Srivastava *et al.* from Ref. 140; (■) experimental measurements from Ref. 140 as corrected by Trajmar *et al.* in Ref. 10; (□) extrapolated values of Trajmar *et al.* in Ref. 10; (●) data of Rohr from Ref. 120; (♦) data of Sakae *et al.* from Ref. 142; (×) data of Johnstone and Newell from Ref. 122; (+) data of Cho *et al.* from Refs. 143, 144; (- - -) calculations of Gianturco *et al.* from Ref. 121; (– –) calculations of Jiang *et al.* from Ref. 145.

the measurements of Romanyuk *et al.*[118] show a resonance peak at 16.8 eV which is not present in the other measurements. We thus deduced a recommended cross section $\sigma_{sc,t}(\varepsilon)$ for SF_6 by considering only the measurements of Kennerly *et al.*,[119] Ferch *et al.*,[137] Dababneh *et al.*,[116] Zecca *et al.*,[138] and Kasperski *et al.*[117] The data of Rohr were not considered because they are not direct measurements, and the data of Wan *et al.*[139] and Romanyuk *et al.*[118] were not considered because of their differences with the rest of the measurements. The recommended cross section is shown by the solid line in Fig. 5 [Fig. 5(b) is an expanded view of part of Fig. 5(a) to more clearly show the individual measurements]. Values obtained from the solid line are listed in Table 9 as our recommended values for the $\sigma_{sc,t}(\varepsilon)$ of the SF_6 molecule. It should be noted that while these values are well defined for energies above 0.5 eV, below this energy the uncertainties are potentially larger since the data rely solely on one measurement, namely, that of Ferch *et al.*[137]

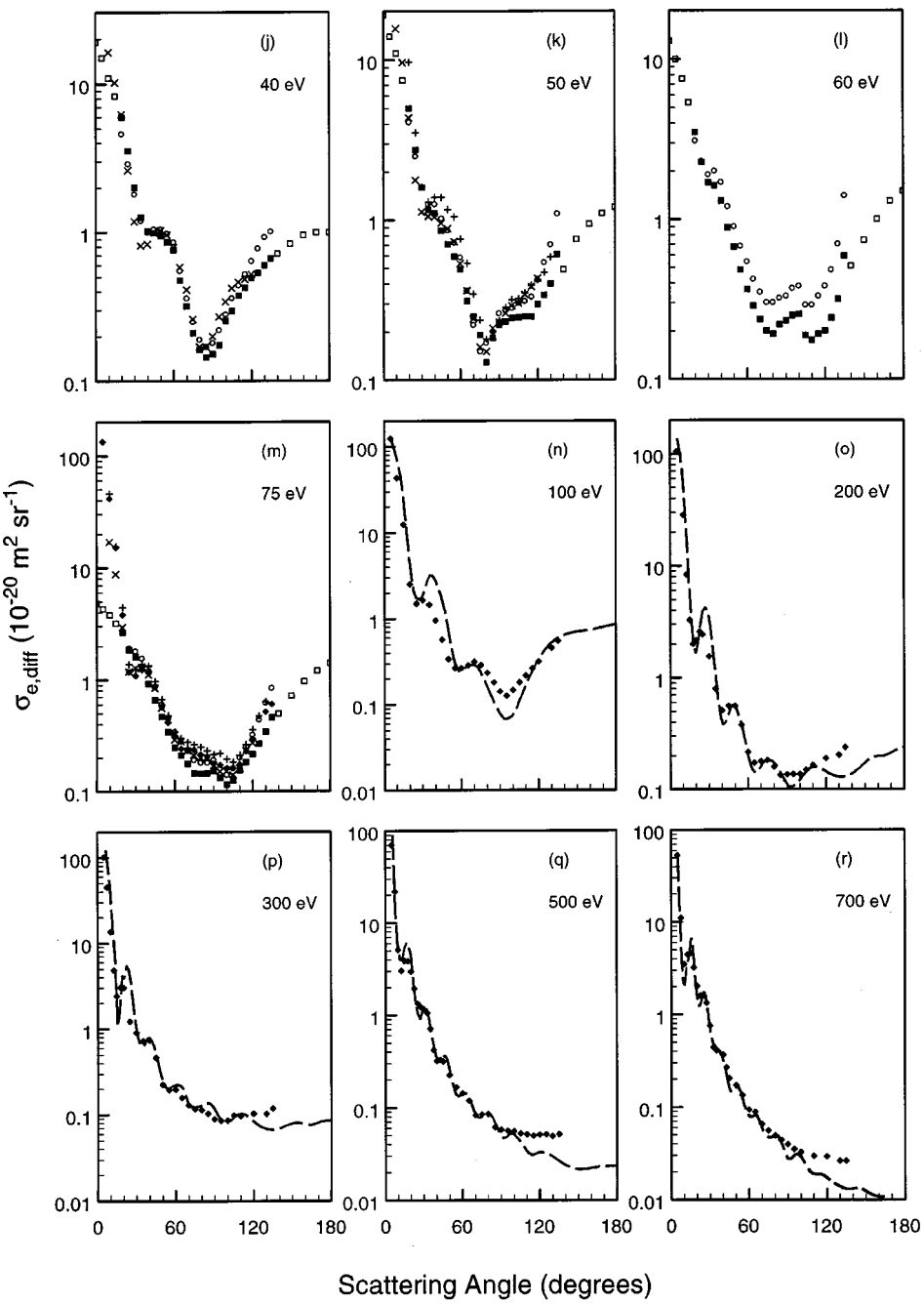

FIG. 6. Elastic differential electron scattering cross sections, $\sigma_{e,diff}(\varepsilon)$, of SF_6 as a function of electron energy ε: (○) Data of Srivastava *et al.* from Ref. 140; (■) experimental measurements from Ref. 140 as corrected by Trajmar *et al.* in Ref. 10; (□) extrapolated values of Trajmar *et al.* in Ref. 10; (●) data of Rohr from Ref. 120; (♦) data of Sakae *et al.* from Ref. 142; (×) data of Johnstone and Newell from Ref. 122; (+) data of Cho *et al.* from Refs. 143, 144; (- - -) calculations of Gianturco *et al.* from Ref. 121; (– –) calculations of Jiang *et al.* from Ref. 145—Continued

3.2. Elastic Differential Electron Scattering Cross Section, $\sigma_{e,diff}(\varepsilon)$

There have been a number of published measurements[10,120,122,140,142] and two calculations[121,145] of the elastic differential electron scattering cross section, $\sigma_{e,diff}(\varepsilon)$, of SF_6 which are plotted in Fig. 6. The early measurements of $\sigma_{e,diff}(\varepsilon)$ by Srivastava *et al.*[140] for incident electron energies between 5 and 75 eV were made relative to those for helium. It was subsequently realized[10,146] that the data of Srivastava *et al.*[140] needed to be renormalized to more accurate helium cross section values than those used in the original analysis. The data identified in Fig. 6 by the squares are the data of Srivastava *et al.*[140] for $\sigma_{e,diff}(\varepsilon)$ as recalculated by Trajmar *et al.*[10] using the improved He cross sections of Register *et al.*[147]

Another early measurement of the $\sigma_{e,diff}(\varepsilon)$ of SF_6 was made by Rohr.[120] He measured differential cross sections for vibrationally elastic ($\Delta\nu=0$) electron scattering by SF_6 up

TABLE 10. Elastic differential electron scattering cross section, $\sigma_{e,diff}(\varepsilon)$, for SF_6 in units of 10^{-20} m^2 sr^{-1}. The data are those of Rohr (Ref. 120) and were obtained by digitizing the curves in Fig. 2 in Ref. 120

	Electron energy (eV)		
Angle	0.5	2.7[a]	7.0
10°	5.82	1.85	6.75
20°	2.91	1.57	6.21
30°	2.28	1.72	5.63
40°	1.75	2.02	4.34
50°	1.36	2.15	2.73
60°	1.01	1.90	1.38
70°	0.93	1.63	0.80
80°	0.87	1.35	0.96
90°	0.74	1.18	1.26
100°	0.66	1.16	1.49
110°	0.68	1.32	1.37
120°	0.66	1.35	1.19

[a]The data shown in Fig. 2 of Ref. 120 for this energy were larger by a factor of 2 than the correct values. The values listed here are those presented in the original reference divided by 2.

to 10 eV. Absolute values of the cross section $\sigma_{e,diff}(\varepsilon)$ were obtained by comparison with data on elastic electron scattering by He and have an estimated uncertainty of about $\pm 20\%$. Interestingly, Rohr[120] found that below 1 eV the cross section appears to be determined essentially by direct scattering, while between 2 and 3 eV and around 7 eV the scattering is dominated by resonances. In Fig. 6 are shown the angular dependencies measured by Rohr for 0.5, 2.7, and 7 eV. (Note that the cross section values at 2.7 eV as presented in Fig. 2 of Ref. 120 were too large by a factor of 2. The data have been corrected as presented here in Fig. 6.) The 0.5 eV data peak sharply in the forward direction and the scattering is dominated by direct processes. The 2.7 and 7 eV measurements indicate strong resonant contributions to the scattering process. These data compare favorably with other data obtained at similar electron energies.

The measurements of $\sigma_{e,diff}(\varepsilon)$ of SF_6 by Johnstone and Newell[122] were made over a wider electron energy range (5–75 eV) using a hemispherical electron spectrometer, with an angular range of 10°–120°. The magnitude of $\sigma_{e,diff}(\varepsilon)$ was determined with reference to the respective cross sec-

TABLE 11. Elastic differential electron scattering cross section, $\sigma_{e,diff}(\varepsilon)$, for SF_6 in units of 10^{-20} m^2 sr^{-1} (data of Cho *et al.* from Refs. 143 and 144)

	Electron energy (eV)										
Angle	2.7	5	7	8.5	10	12	15	20	30	50	75
10°						13.79		23.71	55.57	49.46	45.48
12°								19.54			
15°			5.90	8.50	11.17	15.22	12.99	15.66	23.33	24.68	15.42
20°	1.95	3.94	7.90	8.82	8.89	12.41	11.13	10.98	13.26	9.67	4.41
25°	1.99	4.22	6.84	7.72	7.56	9.31	8.70	7.99	6.92	3.51	1.37
30°	2.34	4.00	5.90	6.40	6.24	6.65	6.65	5.25	3.31	1.61	1.23
35°	2.47	3.83	4.89	5.20	4.81	4.51	4.65	3.23	1.57	1.29	1.38
40°	2.52	3.60	3.99	3.89	3.51	2.91	3.05	1.87	0.99	1.38	1.33
45°	2.51	3.14	3.00	2.81	2.52	1.72	1.84	1.00	0.99	1.38	0.96
50°	2.40	2.82	2.20	2.07	1.71	1.10	1.13	0.70	1.27	1.16	0.67
55°	2.18	2.33	1.55	1.44	1.19	0.75	0.84	0.74	1.37	1.04	0.48
60°	2.05	1.89	1.11	1.09	1.03	0.68	0.87	0.98	1.43	0.76	0.34
65°	1.79	1.42	0.87	0.95	0.98	0.74	1.05	1.33		0.53	0.30
70°	1.54	1.15	0.80	0.94	1.09	0.86	1.25	1.43	1.05	0.34	0.27
75°	1.41	0.91	0.84	1.07	1.26	0.99	1.39	1.50		0.24	0.26
80°	1.20	0.82	1.00	1.26	1.46	1.09	1.40	1.34	0.66	0.18	0.25
85°	1.08	0.80	1.15	1.32	1.53	1.10	1.31	1.13		0.20	0.23
90°	0.97	0.88	1.29	1.39	1.52	1.17	1.22	1.01	0.40	0.23	0.21
95°	0.91	0.96	1.39	1.39	1.41	1.19	1.07	0.82		0.28	0.22
100°	0.94	1.12	1.42	1.35	1.24	1.13	0.97	0.69	0.47	0.32	0.19
105°	0.98	1.23	1.40	1.22	1.07	1.10	0.86	0.60		0.32	0.18
110°	1.04	1.27	1.30	1.07	0.95	1.12	0.79	0.61	0.64	0.35	0.21
115°	1.06	1.25	1.17	0.94	0.83	1.21	0.78	0.60		0.39	0.26
120°	1.10	1.23	1.05	0.82	0.77	1.38	0.77	0.67	0.87	0.42	0.36
125°	1.24	1.15	0.91	0.75	0.78	1.45	0.81	0.81		0.47	0.47
130°	1.31	1.02	0.81	0.83	0.85	1.54	0.87	0.93	1.10	0.58	0.63
135°	1.35	0.96	0.98	0.96	0.92	1.57	0.97				
140°	1.37	0.91	1.00	1.00	1.00	1.62	1.12				
145°	1.40	0.79	1.01	1.07	1.11	1.65	1.26				
150°	1.42	0.74	1.11	1.23	1.17	1.69	1.35				
155°	1.39	0.70	1.24	1.30	1.25	1.71	1.50				
160°	1.49	0.64	1.29	1.47	1.31	1.76	1.65				
165°	1.49	0.61	1.40	1.57	1.36	1.75	1.77				
170°	1.49	0.58	1.47	1.62	1.37	1.83	1.92				
175°	1.50	0.57	1.51	1.71	1.44	1.86	1.94				
180°	1.50	0.54	1.54	1.77	1.47	1.84	1.97				

TABLE 12. Elastic differential electron scattering cross section, $\sigma_{e,diff}(\varepsilon)$, for SF_6 in units of $10^{-20}\,m^2\,sr^{-1}$. The data are those of Sakae *et al.* from Ref. 142 as supplied by Professor M. Hayashi (private communication, 2000). Stated uncertainties are approximately 8%–10%

	Electron energy (eV)						
Angle	75	100	150	200	300	500	700
5.0°	133	125	117	105	102	70.3	53.2
7.5°	—	—	68.5	—	45.3	21.9	11.1
10.0°	41.3	43.2	35.7	28.4	13.6	5.11	3.48
12.5°	—	—	16.8	8.34	4.86	3.03	4.46
15.0°	15.2	12.4	6.18	3.28	2.43	3.88	4.60
17.5°	—	—	2.40	2.00	3.05	3.86	3.21
20.0°	3.80	2.53	1.64	2.17	3.04	2.95	2.03
22.5°	—	—	1.93	2.57	—	1.94	1.60
25.0°	1.17	1.51	1.96	2.44	1.22	1.34	1.60
27.5°	—	—	1.82	—	—	1.22	1.33
30.0°	1.09	1.64	1.70	1.55	0.906	1.16	0.758
32.5°	—	—	—	—	—	1.05	0.442
35.0°	1.23	1.46	1.09	0.795	0.726	0.712	0.409
40.0°	1.16	0.953	0.592	0.509	0.738	0.322	0.365
42.5°	—	—	—	—	—	0.329	0.268
45.0°	0.878	0.573	0.390	0.557	0.468	0.317	0.205
50.0°	0.575	0.338	0.372	0.559	0.227	0.227	0.171
55.0°	0.416	0.265	0.385	0.375	0.196	0.166	0.134
60.0°	0.316	0.267	0.350	0.216	0.199	0.143	0.0933
65.0°	0.241	0.286	0.243	0.172	0.159	0.119	0.0884
70.0°	0.241	0.316	0.164	0.178	0.131	0.0831	0.0652
75.0°	0.236	0.289	0.134	0.182	0.117	0.0850	0.0556
80.0°	0.214	0.234	0.139	0.159	0.114	0.0851	0.0489
85.0°	0.204	0.180	0.139	0.134	0.104	0.0616	0.0437
90.0°	0.177	0.142	0.144	0.135	0.0897	0.0577	0.0393
95.0°	0.172	0.127	0.140	0.136	0.0855	0.0561	0.0349
100.0°	0.162	0.148	0.130	0.136	0.0864	0.0557	0.0324
105.0°	0.161	0.182	0.127	0.149	0.0984	0.0524	—
110.0°	0.174	0.218	0.146	0.164	0.0974	0.0511	0.0297
115.0°	0.230	0.264	—	—	—	0.0497	—
120.0°	0.295	0.318	0.222	0.189	0.104	0.0510	0.0292
130.0°	0.514	0.456	0.345	0.202	0.103	0.0491	0.0263
135.0°	0.606	0.548	0.406	0.238	0.119	0.0516	0.0264

tions for He (calculated values by Nesbet[148] below 20 eV and measurements by Register *et al.*[147] for energies greater than 20 eV), and they have a quoted uncertainty of $\pm 12\%-\pm 14\%$. While these data are in qualitative agreement with other measurements, the degree of agreement varies with the electron energy and the scattering angle.

The measurements of Sakae *et al.*[142] were made using a crossed-beam method and extend up to 700 eV with an angular range of $5°-135°$. They were put on absolute scale by normalization to the differential electron scattering cross sections for He (data of Jansen *et al.*[149] for energies between 100 and 700 eV and data of Register *et al.*[147] for 75 eV), and have an overall uncertainty of about $\pm 10\%$.

Recent measurements of the differential elastic electron scattering cross section for SF_6 for energies ranging from 2.5 to 75 eV by Cho *et al.*[143,144] have been made in response to the discrepancies in the resultant determinations of the integral elastic scattering cross sections, $\sigma_{e,int}(\varepsilon)$, by Trajmar *et al.*,[10] Johnstone and Newell,[122] and Sakae *et al.*[142] (see discussion in Sec. 3.3.). These recent data of Cho *et al.*[143,144] are also shown in Fig. 6, and are in good agreement with the data of Sakae *et al.*[142] at 75 eV and with Rohr[120] at 2.7 and 7 eV. Cho *et al.*[143,144] directly measured the cross sections at large angles using a new magnetic deflection technique[143,150,151] that allows cross section measurements at angles up to 180°. This reduces extrapolation uncertainties when using these data to calculate the corresponding elastic integral and momentum transfer cross sections. At most energies, the measured values of $\sigma_{e,diff}(\varepsilon)$ by Cho *et al.* are seen to be higher than the corresponding measurements of Trajmar *et al.*[10] and Johnstone and Newell.[122]

In Fig. 6 are also shown the results of two calculations of $\sigma_{e,diff}(\varepsilon)$, those of Gianturco *et al.*[121] who used an *ab initio* approach and solved the multichannel scattering problem within the close-coupling methodology, and those of Jiang *et al.*[145] who calculated differential elastic scattering cross sections at six electron energies between 100 and 700 eV using the independent-atom model with partial waves. There is qualitative agreement between these calculated results and the experimental data, particularly at higher energies. The values calculated by Gianturco *et al.*[121] are generally larger than the measurements, especially at small and large scattering angles.

In Tables 10, 11, and 12 are listed, respectively, the

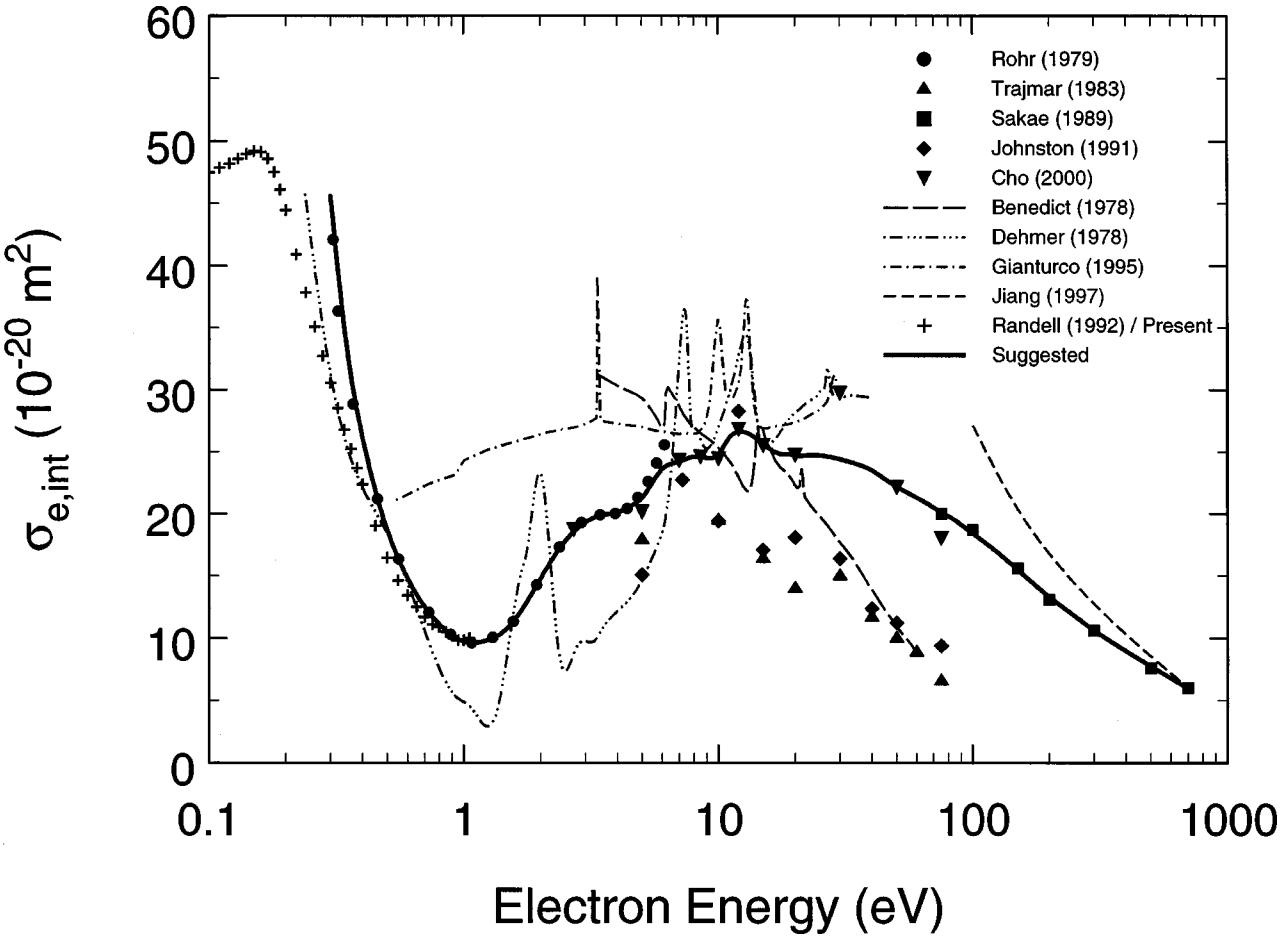

FIG. 7. Elastic integral electron scattering cross section, $\sigma_{e,int}(\varepsilon)$, of SF_6 as a function of electron energy: (●) Ref. 120; (▲) Ref. 140 as corrected by Trajmar *et al.* in Ref. 10; (■) Ref. 142; (♦) Ref. 122; (▼) Refs. 143, 144; (– –) Ref. 124; (−···−) Ref. 112; (− · −) Ref. 121; (- - -) Ref. 145; (+) deduced in present work from data in Ref. 92, see text; (—) suggested values.

$\sigma_{e,diff}(\varepsilon)$ values of Rohr[120] for low electron energies, the recently measured values of Cho *et al.*[143,144] at intermediate electron energies, and the values of Sakae *et al.*[142] at higher energies. Collectively these data provide values of the $\sigma_{e,diff}(\varepsilon)$ of SF_6 from 0.5 to 700 eV. The tabulated values of $\sigma_{e,diff}(\varepsilon)$ for Trajmar *et al.*[10] and Johnstone and Newell[122] are presented in the respective references.

3.3. Elastic Integral Electron Scattering Cross Section, $\sigma_{e,int}(\varepsilon)$

In Fig. 7 are compared the five sets of values of the elastic integral electron scattering cross section, $\sigma_{e,int}(\varepsilon)$, for SF_6 derived from the differential elastic cross section measurements of Srivastava *et al.*[140] (as corrected by Trajmar *et al.*[10]), Rohr,[120] Sakae *et al.*,[142] Johnstone and Newell,[122] and Cho *et al.*[143,144] The uncertainties for $\sigma_{e,int}(\varepsilon)$ are somewhat larger than those quoted in the preceding section for $\sigma_{e,diff}$, largely because of errors arising from the extrapolation of the elastic differential electron scattering cross section measurements to 0° and 180° scattering angles. The stated uncertainties for the $\sigma_{e,int}(\varepsilon)$ data are as follows: Srivastava *et al.*[140] (±18%); Rohr[120] (~±20%); Johnstone and Newell[122] (±17%); Sakae *et al.*[142] (~±10%); and Cho *et al.*[143] (±20%). The errors are generally larger when the differential cross sections rise steeply at small scattering angles.

The $\sigma_{e,int}(\varepsilon)$ data of Sakae *et al.*,[142] Cho *et al.*,[143] and Rohr[120] agree well within the overlapping energy ranges. The data of Trajmar *et al.*[10] and Johnson and Newell[122] are seen to fall significantly below the other data, particularly at higher electron energies. In view of the agreement between the data of Sakae *et al.*,[142] Cho *et al.*,[143] and Rohr,[120] we have chosen to fit these data in order to obtain our suggested values for this cross section. This fit is shown by the solid line in Fig. 7 and values obtained from the fit are listed in Table 13 as our suggested values for the $\sigma_{e,int}(\varepsilon)$ of the SF_6 molecule.

The cross section labeled ''Randell (1992)/Present'' in Fig. 7 was deduced by us from the relative cross section for total elastic electron scattering measured by Randell *et al.*[92] This cross section was put on an absolute scale by normalizing its value at 1 eV to the data of Rohr[120] at 1 eV. The total elastic electron scattering cross section determined this way is shown in Fig. 7 by the crosses and is seen to be in

TABLE 13. Suggested values for the elastic integral electron scattering cross section, $\sigma_{e,int}(\varepsilon)$, of SF_6

Electron energy (eV)	$\sigma_{e,int}(\varepsilon)$ $(10^{-20}\,m^2)$	Electron energy (eV)	$\sigma_{e,int}(\varepsilon)$ $(10^{-20}\,m^2)$
0.30	45.6	16	25.2
0.35	33.0	17	24.9
0.40	26.2	18	24.8
0.45	21.8	19	24.8
0.50	18.7	20	24.7
0.60	14.8	22	24.7
0.70	12.5	25	24.7
0.80	11.1	30	24.4
0.90	10.2	35	24.0
1.0	9.72	40	23.5
1.2	9.73	45	22.8
1.5	10.9	50	22.2
2.0	14.8	60	21.3
2.5	17.8	70	20.5
3.0	19.3	75	20.2
3.5	19.9	80	19.8
4.0	20.1	90	19.1
4.5	20.6	100	18.4
5.0	21.3	125	16.9
6.0	23.6	150	15.5
7.0	24.2	200	13.3
8.0	24.6	250	11.8
9.0	24.5	300	10.6
10.0	24.8	350	9.71
11.0	26.1	400	8.95
12.0	26.6	450	8.31
13.0	26.5	500	7.74
14.0	26.1	600	6.76
15.0	25.6	700	5.94

agreement with the measurements of Rohr between about 0.5 and 1 eV. Below ~ 0.5 eV the deduced values are significantly lower than the values measured by Rohr, perhaps due to the fact that the measurements of Randell *et al.* were made at only a single scattering angle (90°).

Also shown in Fig. 7 are the results of four calculations of the total elastic electron scattering cross section, $\sigma_{e,t}(\varepsilon)$, by Benedict and Gyemant,[124] Dehmer *et al.*,[112] Gianturco *et al.*,[121] and Jiang *et al.*[145] The results of the first three calculations show distinct structure due to negative ion resonances, but they agree with the experimental data only in restricted energy regions. The values of $\sigma_{e,t}(\varepsilon)$ calculated by Jiang *et al.* using the independent-atom model with partial waves are higher than the experimental data of Sakae *et al.* between 100 and 500 eV, and only merge well with the experimental data at high energies.

3.4. Momentum Transfer (Elastic) Electron Scattering Cross Section, $\sigma_m(\varepsilon)$

The momentum transfer (elastic) electron scattering cross section, $\sigma_m(\varepsilon)$, of SF_6 has been determined by Srivastava *et al.*,[140] Sakae *et al.*,[142] Johnstone and Newell,[122] and Cho *et al.*[143] from their respective differential elastic electron scattering cross section measurements extrapolated, as required, to 0° and 180° scattering angles. These determinations of $\sigma_m(\varepsilon)$ are shown in Fig. 8. The data of Srivastava *et al.*[140] shown in Fig. 8 are those that have been renormalized by Trajmar *et al.*[10] (Sec. 3.2). The quoted uncertainty in the data is $\pm 20\%$ for Srivastava *et al.*,[140] $\sim \pm 9\%$ for Sakae *et al.*,[142] $\pm 20\%$ for Johnstone and Newell,[122] and $\pm 20\%$ for Cho *et al.*[143] The uncertainty is generally larger at the higher energies due to the difficulty in accurately measuring the steeply rising differential cross section at small scattering angles.

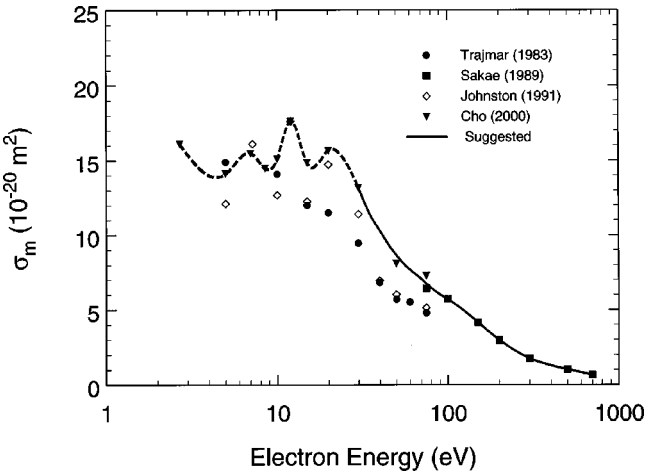

FIG. 8. Momentum transfer (elastic) electron scattering cross section, $\sigma_m(\varepsilon)$, of SF_6 as a function of electron energy: (●) Ref. 140 as corrected by Trajmar *et al.* in Ref. 10; (■) Ref. 142; (◇) Ref. 122; (▼) Refs. 143, 144; (—, - - -) suggested values. The broken line indicates an uncertainty in the significance of the structure observed at energies between 2.7 and 30 eV.

At 75 eV the data of Trajmar *et al.*[10] and Johnstone and Newell[122] lie somewhat below those of Sakae *et al.*,[142] while the data of Cho *et al.*[143] are in reasonable agreement with

TABLE 14. Suggested values for the momentum transfer (elastic) cross section, $\sigma_m(\varepsilon)$, of SF_6

Electron energy (eV)	$\sigma_m(\varepsilon)$ $(10^{-20}\,m^2)$	Electron energy (eV)	$\sigma_m(\varepsilon)$ $(10^{-20}\,m^2)$
2.75	16.0	27	14.3
3.0	15.4	30	13.2
3.5	14.5	35	11.5
4.0	14.0	40	10.3
4.5	13.9	45	9.37
5.0	14.1	50	8.65
6.0	15.1	60	7.69
7.0	15.5	70	7.06
8.0	14.8	75	6.74
9.0	14.4	80	6.46
10	15.1	90	6.03
11	16.7	100	5.70
12	17.6	125	4.92
13	17.1	150	4.16
14	15.8	200	2.98
15	14.9	250	2.23
16	14.5	300	1.76
17	14.7	350	1.47
18	15.0	400	1.28
19	15.4	450	1.13
20	15.7	500	1.02
22	15.7	600	0.82
25	15.0	700	0.66

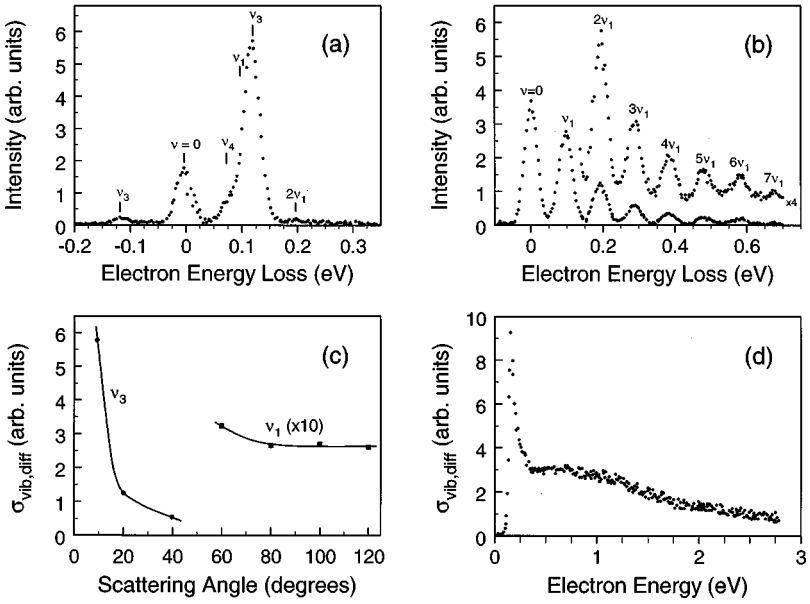

FIG. 9. Low-energy electron energy-loss spectra for SF_6 of Rohr from Ref. 91. (a) Energy-loss spectrum of SF_6 for a collision energy of 1 eV and a scattering angle of 10°. (b) Energy-loss spectrum of SF_6 at 1 eV and a scattering angle of 80°. (c) Angular dependencies of the differential cross sections for the ν_1 and ν_3 vibrational excitations (the cross section scales reflect true intensity ratios). (d) Differential cross section for excitation of the ν_1 vibrational mode of SF_6 at a scattering angle of 80°.

Sakae *et al.* Based upon this agreement, we have made a modified spline fit to the data of Cho *et al.* and of Sakae *et al.* which is shown by the line in Fig. 8. Values extracted from this fit are listed in Table 14 as our suggested data for the $\sigma_m(\varepsilon)$ of the SF_6 molecule. The data of Cho *et al.*[143] and Johnstone and Newell[122] indicate structure which can be associated with the negative ion states presented in Table 6. However, it should be noted that the variations in the measured values of $\sigma_m(\varepsilon)$ in the energy region of 2.7–30 eV are smaller than the stated uncertainties of the measurements. Thus the line designating our suggested values for $\sigma_m(\varepsilon)$ in this energy range is broken in order to highlight the potential uncertainty of the observed structure.

3.5. Inelastic Electron Scattering Cross Section, $\sigma_{inel}(\varepsilon)$

3.5.1. Vibrational Excitation

Two low-energy electron-impact vibrational-excitation studies[91,92] of SF_6 have shown that at energies below ~3 eV the energy-loss spectra of SF_6 are characterized by strong vibrational excitation and vibrationally elastic electron scattering. In this energy range these studies have also shown that the vibrationally inelastic processes are dominated by excitation of the ν_1 and ν_3 modes. This is seen from the energy-loss spectrum (collision energy of 1 eV and scattering angle of 10°) in Fig. 9(a) which is characterized by the large magnitude of the excitation of the ν_3 fundamental mode which exceeds the elastic peak by about a factor of 3. Rohr[91] estimates that at 1 eV the integral total vibrational excitation cross section is $\sim 10^{-15}\,cm^2$. The ν_3 (0.1175 eV, Table 7) vibrational mode is infrared (IR) active and is associated with vertical displacement of the apical F atoms in the octahedral structure for normal modes of vibration of SF_6, and the ν_1 (0.096 eV; Table 7) vibrational mode is the Raman active totally symmetric breathing mode.

Figure 9(b) shows the energy-loss spectrum again at a collision energy of 1 eV, but at a scattering angle of 80°. The excitation is now seen to be dominated by the ν_1 mode and its higher harmonics. No other modes or intercombination lines are seen. Rohr observed the same behavior at all angles greater than 60° for all the energies he employed.

In Fig. 9(c) are shown the angular dependencies of the differential cross sections, $\sigma_{vib,diff}$, for the ν_1 and ν_3 vibrational excitations in the angular range 10°–120° for a collision energy of 1 eV (note that the cross section scales reflect true intensity ratios and that the values of the cross section for ν_1 have been multiplied by a factor of 10). The differential cross section of the IR active ν_3 vibrational mode is peaked in the forward direction, indicating that a direct process via the dipole interaction is involved. For the Raman active totally symmetric vibration ν_1 the dipole mechanism is excluded and the angular distribution is nearly isotropic.

Figure 9(d) shows the differential cross section $\sigma_{vib,diff}(\varepsilon)$ for excitation of the ν_1 vibration at a scattering angle of 80°. The sharp peak at 0.060 eV was attributed[91] to the formation of SF_6^- negative ions and the broad maximum at near 0.7 eV to vibrational excitation via a negative ion state.

A similar crossed-beam study of SF_6 was conducted by Randell *et al.*[92] using 0.05–1 eV incident-energy electrons detected at a fixed scattering angle of 90°. Figure 10(a) shows the electron-energy loss function measured at an incident electron energy of 0.4 eV due to excitation of the ν_1, ν_3, $2\nu_1$, $\nu_1+\nu_3$, and $3\nu_1$ vibrations. The contribution to the total scattering cross section of inelastic scattering is roughly equal to the elastic scattering at this energy. The weak peak at a negative energy loss was attributed by Randell *et al.* to superelastic scattering from the thermal population of $\nu_3=1$. In agreement with Rohr,[91] Randell *et al.* have attributed the excitation of ν_3 to a direct dipole mechanism and the excitation of ν_1 to a long-lived negative ion resonance, i.e., to excitation of the symmetric breathing mode,

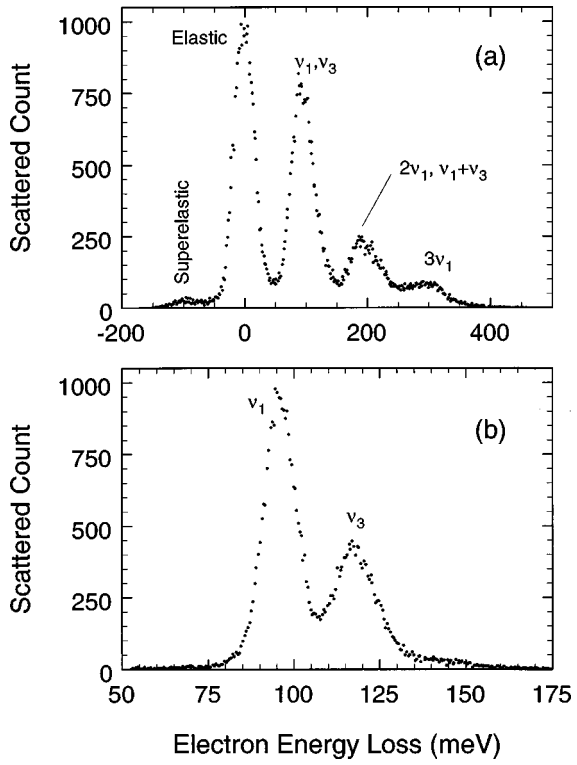

FIG. 10. Low-energy electron energy-loss spectra for SF_6 of Randell *et al.* from Ref. 92. (a) Energy-loss spectrum of SF_6 for a collision energy of 0.4 eV and a scattering angle of 90°. (b) Energy-loss spectrum of SF_6 for a collision energy of 0.18 eV and a scattering angle of 90° showing resolution of the ν_1 and ν_3 vibrational modes.

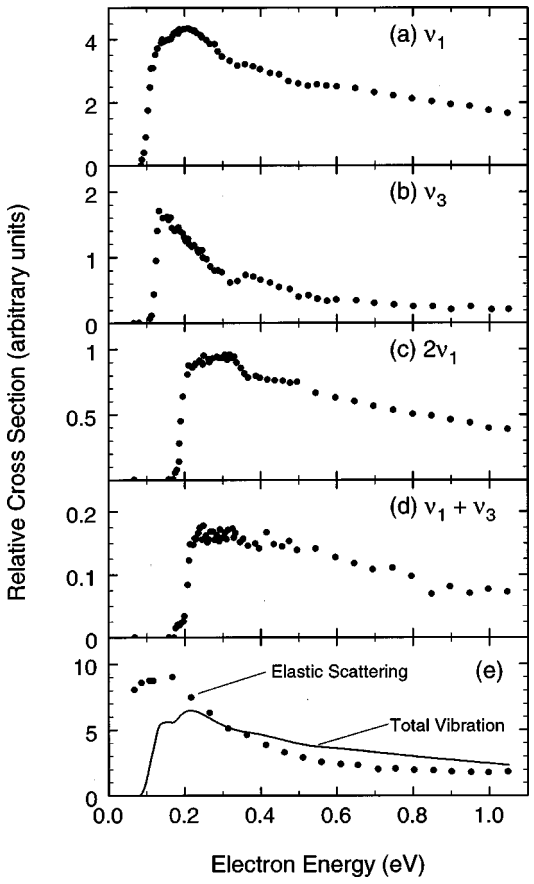

FIG. 11. Low-energy electron energy-loss spectra for SF_6 of Randell *et al.* from Ref. 92. Excitation functions for (a) ν_1, (b) ν_3, (c) $2\nu_1$, (d) $\nu_1+\nu_3$, and (e) elastic electron scattering. The solid line labeled ''Total Vibration'' in (e) is the sum of the relative excitation cross sections for ν_1, ν_3, $2\nu_1$, and $\nu_1+\nu_3$ shown in (a)–(d) (see text).

ν_1, via autoionization of SF_6^{-*}. The latter interpretation is supported by the high-resolution electron attachment studies of Klar *et al.*[152,153] which show that the attachment cross section has a pronounced cusp at 0.096 eV associated with ν_1 excitation. It is also consistent with the work of Trajmar and Chutjian[83] whose electron-energy-loss spectra using 12 eV incident electrons showed strong enhancement of vibrational excitation attributed mostly to the ν_1 mode. Figure 10(b) shows an energy-loss spectrum obtained by Randell *et al.*[92] for an electron-impact energy of 0.18 eV and a scattering angle of 90° showing resolution of electrons scattered inelastically through energies corresponding to the ν_1 and ν_3 vibrational modes. Within experimental error, the thresholds for ν_1 and ν_3 are at 0.095 and 0.117 eV, respectively, and excitation is thus at the energy threshold.

Figures 11(a), 11(b), 11(c), and 11(d) show the excitation functions, respectively, for ν_1, ν_3, $2\nu_1$, and $\nu_1+\nu_3$ as reported by Randell *et al.*[92] The scales in Fig. 11 are not in absolute units, but their vertical axes give the correct relative values of these quantities. Clearly, the excitation cross section for ν_1 is the largest, and the excitation functions for ν_1 and ν_3 are markedly different, reflecting the different mechanisms by which these vibrations are excited. The measured functional dependence of the cross section for ν_3 was found by Randell *et al.* to be in agreement with that predicted by the Born point-dipole approximation.

The relative cross sections in Figs. 11(a), 11(b), 11(c), and 11(d) have been used by us in conjunction with other assessed cross sections in this paper to deduce absolute values for the total vibrational excitation cross section, $\sigma_{\mathrm{vib,t}}(\varepsilon)$, of SF_6 for electron energies less than 1.1 eV. This was done as follows: Since the vibrational energy-loss measurements by both Rohr[91] and Randell *et al.*[92] show that the major contribution to vibrational excitation by electron impact below $\sim$3 eV comes from ν_1 (indirect excitation via the SF_6^{-*} resonances) and ν_3 (direct excitation via the dipole interaction) vibrations and their combinational excitations, we have summed the relative vibrational excitation cross sections shown in Figs. 11(a), 11(b), 11(c), and 11(d), and plotted the result in Fig. 11(e). In Fig. 11(e) is also shown the relative total elastic electron scattering cross section measured by Randell *et al.* To put the deduced total vibrational cross section of Randell *et al.* on an absolute scale, the relative vibrational values shown in Fig. 11(e) were multiplied by the same factor used to normalize the relative $\sigma_{\mathrm{e,int}}(\varepsilon)$ values of Randell *et al.* that are shown in Fig. 7 and discussed in Sec. 3.3. The values of $\sigma_{\mathrm{vib,t}}(\varepsilon)$ determined in this way are shown in Fig. 12 (closed circles).

Confirmation of these deduced values of $\sigma_{\mathrm{vib,t}}(\varepsilon)$ below

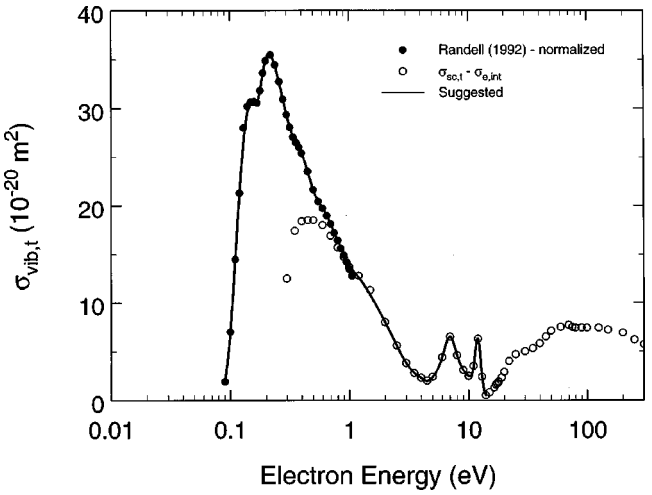

FIG. 12. Deduced total vibrational excitation cross section, $\sigma_{vib,t}(\varepsilon)$, for SF_6: (●) Ref. 92 normalized as discussed in text; (○) difference, $\sigma_{sc,t}(\varepsilon) - \sigma_{e,int}(\varepsilon)$, of the recommended values for $\sigma_{sc,t}(\varepsilon)$ and $\sigma_{e,int}(\varepsilon)$ [see text]; (—) suggested values.

TABLE 15. Deduced values of the total vibrational excitation cross section, $\sigma_{vib,t}(\varepsilon)$, of SF_6

Electron energy (eV)	$\sigma_{vib,t}(\varepsilon)$ (10^{-20} m^2)	Electron energy (eV)	$\sigma_{vib,t}(\varepsilon)$ (10^{-20} m^2)
0.09	1.9	1.2	12.6
0.10	7.0	1.5	10.8
0.12	21.3	2.0	8.0
0.15	30.6	2.5	5.6
0.17	30.6	3.0	3.8
0.20	34.9	3.5	2.8
0.22	35.5	4.0	2.3
0.25	33.6	4.5	2.0
0.28	30.9	5.0	2.4
0.30	29.4	6.0	4.4
0.35	26.8	7.0	6.5
0.40	25.4	8.0	4.6
0.45	23.5	9.0	3.1
0.50	21.6	10.0	2.5
0.60	19.7	11.0	3.5
0.70	18.1	12.0	6.3
0.80	16.4	13.0	2.4
0.90	15.1	14.0	0.5
1.0	13.9		

1.1 eV, and extension of $\sigma_{vib,t}(\varepsilon)$ to higher electron energies has been obtained by the following analysis. At energies above $\sim$1 eV and below the region of significant electronic excitation ($<$16 eV), the total electron attachment cross section of SF_6 is very much smaller than the total electron scattering cross section (see Fig. 47 in Sec. 10), so the cross section $\sigma_{vib,t}(\varepsilon)$ can be estimated by the difference $\sigma_{sc,t}(\varepsilon) - \sigma_{e,int}(\varepsilon)$, viz.,

$$\sigma_{vib,t}(\varepsilon) = \sigma_{sc,t}(\varepsilon) - \sigma_{e,int}(\varepsilon) - \sigma_{a,t}(\varepsilon) \approx \sigma_{sc,t}(\varepsilon) - \sigma_{e,int}(\varepsilon). \quad (2)$$

Using the assessed values of $\sigma_{sc,t}(\varepsilon)$ and $\sigma_{e,int}(\varepsilon)$ determined in this work, we obtained the difference $\sigma_{sc,t}(\varepsilon) - \sigma_{e,int}(\varepsilon)$, and have shown these values in Fig. 12 by the open symbols. It is encouraging to see the agreement of the two determinations of $\sigma_{vib,t}(\varepsilon)$ in the energy range from $\sim$0.5 to 1 eV, thus confirming the normalization of the data of Randell *et al.*[92] However, the two sets of values differ significantly at energies below $\sim$0.5 eV, indicating potential errors in the various cross sections employed. Nonetheless, in the absence of any direct measurements of $\sigma_{vib,t}(\varepsilon)$, we take the difference $\sigma_{sc,t}(\varepsilon) - \sigma_{e,int}(\varepsilon)$, between 1 and 14 eV, and the normalized data of Randell *et al.*[92] below 1 eV, to be a good measure of $\sigma_{vib,t}(\varepsilon)$. The solid line in Fig. 12 represents our suggested values for the total vibrational cross section, $\sigma_{vib,t}(\varepsilon)$, for SF_6 using the cross section values deduced as just described. Values of $\sigma_{vib,t}(\varepsilon)$ extracted from the solid line in Fig. 12 are listed in Table 15. In the absence of absolute experimental measurements, the values represented by the solid line in Fig. 12 can be used in combination with the relative data in Figs. 11(a), 11(b), 11(c), and 11(d) to deduce cross sections for vibrational excitation of ν_1, ν_3, $2\nu_1$, and $\nu_1 + \nu_3$ up to $\sim$4 eV. An estimate of the cross section for indirect vibrational excitation via the negative ion states near 7 and 12 eV can also be obtained from Fig. 12 and Table 15.

Above 15 eV, where $\sigma_{vib,t}(\varepsilon)$ becomes small, the difference $\sigma_{sc,t}(\varepsilon) - \sigma_{e,int}(\varepsilon)$ can be attributed to other inelastic processes (such as ionization and dissociation), and may be used to deduce a value of the total cross section for dissociation of SF_6 into neutral fragments. This will be further discussed in Sec. 5.

3.5.2. Electronic Excitation

Excitation of the SF_6 molecule by electron impact to any electronic state is generally assumed to lead to dissociation, i.e., all excited electronic states of the SF_6 molecule are antibonding. This assumption is consistent with optical emission data following electron-impact excitation of SF_6 (e.g., see Refs. 154 and 155). Electron-impact electronic excitation of SF_6 is thus an important process in controlling the rates of decomposition of this gas in electrical discharges and also indirectly the rates of electron-impact ionization and electron attachment. In spite of this, to our knowledge, there are no cross sections for electron-impact excitation functions for specific electronic transitions in SF_6. We can however direct attention to the following investigations: the electron-impact energy-loss spectra and the generalized oscillator-strength results presented in Sec. 2; the differential inelastic electron scattering cross sections, $\sigma_{el,diff}(\varepsilon = 20\,\text{eV})$, for five electronic states located at 9.8, 11.0, 11.6, 12.8, and 13.3 eV obtained by Trajmar and Chutjian[83] at one (20 eV) incident-electron energy (Fig. 13); and the Boltzmann-type calculations (e.g., Yoshizawa *et al.*[27] and Itoh *et al.*[28]) which determined an overall electronic excitation cross section function consistent with the measured ionization and attachment coefficients.

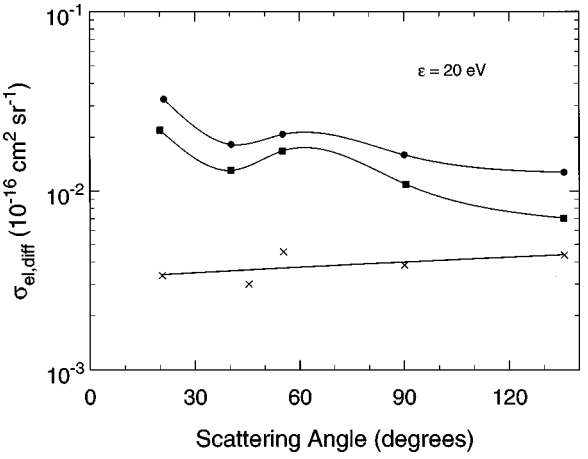

FIG. 13. Differential electronic excitation cross section, $\sigma_{el,diff}(\varepsilon)$, for excited electronic states of SF_6 at (×) 9.8 eV; (■) 11.0, 11.6, and 12.8 eV; and (●) 13.3 eV. The incident electron energy was 20 eV (data of Trajmar and Chutjian from Ref. 83).

TABLE 16. Comparison of the values of the partial ionization cross sections, $\sigma_{i,partial}(\varepsilon=100\,eV)$, of SF_6 as measured by three different groups (Refs. 157–159)

Fragment positive ion	$\sigma_{i,partial}$ (ε=100 eV) (10^{-20} m^2) Ref. 157[a]	$\sigma_{i,partial}$ (ε=100 eV) (10^{-20} m^2) Ref. 158[b]	$\sigma_{i,partial}$ (ε=100 eV) (10^{-20} m^2) Ref. 159
SF_5^+	3.38	3.42	3.52
SF_4^+	0.30	0.39	0.395
SF_3^+	0.99	1.09	0.93
SF_2^+	0.26	0.27	0.22
SF^+	0.42	0.46	0.265
S^+	0.32	0.31	0.21
F^+	0.34	0.27	0.19
SF_4^{++}	0.13	0.18	0.255
SF_3^{++}	—	—	0.03
SF_2^{++}	0.09	0.12	0.095

[a]Taken off the figures given in Ref. 157.
[b]Data for case A-type analysis in Ref. 158.

4. Electron-Impact Ionization of SF_6

4.1. Total Ionization Cross Section, $\sigma_{i,t}(\varepsilon)$

There have been five measurements[82,156–159] of the total ionization cross section, $\sigma_{i,t}(\varepsilon)$, of SF_6, which are compared in Fig. 14. Two[82,156] of these were direct measurements of the total ionization cross section. The uncertainty in the data of Rapp and Englander-Golden[156] is probably ±7%, while that of Asundi and Craggs[82] is much larger. Asundi and Craggs observed structure in their data at 14.3, 15.9, 17.5, 18.7, 20.3, and 22.2 eV. The processes at 15.9, 18.7, and 20.3 eV were attributed to the formation of SF_5^+, SF_4^+, and SF_3^+, respectively, and agree within experimental error (±0.2 eV) with the values of Dibeler and Mohler[74] which were similarly attributed to these positive ions (Table 3).

The other three experimental determinations[157–159] of $\sigma_{i,t}(\varepsilon)$ were made by summation of the respective partial ionization cross sections, $\sigma_{i,partial}(\varepsilon)$, presented in Sec. 4.2. Stanski and Adamczyk[157] measured electron-impact dissociative ionization of SF_6 as a function of electron energy to 600 eV and obtained partial ionization cross sections for the positive ion fragments SF_5^+, SF_4^+, SF_3^+, SF_2^+, SF^+, S^+, F^+, SF_4^{++}, and SF_2^{++} by normalizing their sum to the total ionization cross section of Rapp and Englander-Golden.[156]

Margreiter *et al.*[158] measured electron-impact ionization of SF_6 from threshold to 180 eV using a Nier-type ion source in combination with a double-focusing sector field mass spectrometer. They determined absolute partial ionization cross sections for the production of SF_5^+, SF_4^+, SF_3^+, SF_2^+, SF^+, S^+, F^+, SF_4^{++}, and SF_2^{++} using an improved experimental method based on ion trajectory calculations. They determined the $\sigma_{i,partial}(\varepsilon)$ using various procedures which gave cross section values at 100 eV that differed by 7%–40% for the larger ion fragments, and by as much as a factor of 3 for F^+. The cross section values at 100 eV listed in Table 16 are for the ''preferred method of analysis'' (case A) of Margreiter *et al.*, and the sum of these partial ionization cross sections at various electron energies is plotted in Fig. 14.

Rao and Srivastava[159] reported only one value (6.11×10^{-20} m^2) of the total ionization cross section at 100 eV (the sum of the partial ionization cross sections they measured at this energy, see Table 16). The stated uncertainty in their measurements is ±10%, and their value of $\sigma_{i,t}(\varepsilon)$ is also plotted in Fig. 14.

No SF_6^+ was detected by Dibeler and Mohler,[74] Rao and Srivastava,[159] Al-Nasir *et al.*,[160] or Pullen and Stockdale.[161] It is believed that the SF_6^+ ion is unstable both in its ground state and in its excited electronic states in the symmetrical configuration. Nevertheless, some authors have reported weak SF_6^+ signals. For example, Stanski and Adamczyk[157] indicated that at 100 eV the cross section for SF_6^+ is about 5×10^{-23} m^2, and Shibata *et al.*[162] reported observation of SF_6^+ in frozen-gas-target experiments where a high-energy positive-ion beam collided with SF_6 frozen on a thin Al foil held at ~15 K.

There have been a number of calculations[163–167] of the $\sigma_{i,t}(\varepsilon)$ of SF_6. Hwang *et al.*[164] and Kim and Rudd[167] calculated the total electron-impact ionization cross section using the binary-encounter-Bethe (BEB) theory, the former without and the latter with contributions from multiple ionization. Margreiter *et al.*[163] and Tarnovsky *et al.*[165,166] calculated the total single ionization cross section using the additivity rule. The results of these calculations are compared with the experimental data in Fig. 14. (See also Deutsch *et al.*[168] for a calculation of electron-impact ionization cross sections ''utilizing empirically modified collision theories.'') Surprisingly, the calculated $\sigma_{i,t}(\varepsilon)$ by Kim and collaborators for this molecule are higher than the experimental measurements, although the results of similar calculations for other molecules [see, e.g., CF_4 (Refs. 19 and 25), C_2F_6 (Refs. 22 and 25), and C_3F_8 (Ref. 23)] are in good agreement with experiment.

The experimental data shown in Fig. 14 are in reasonable agreement with each other except in some cases at low electron energies (e.g., the lowest values of Stanski and Adamczyk[157]). Overall, the data of Rapp and

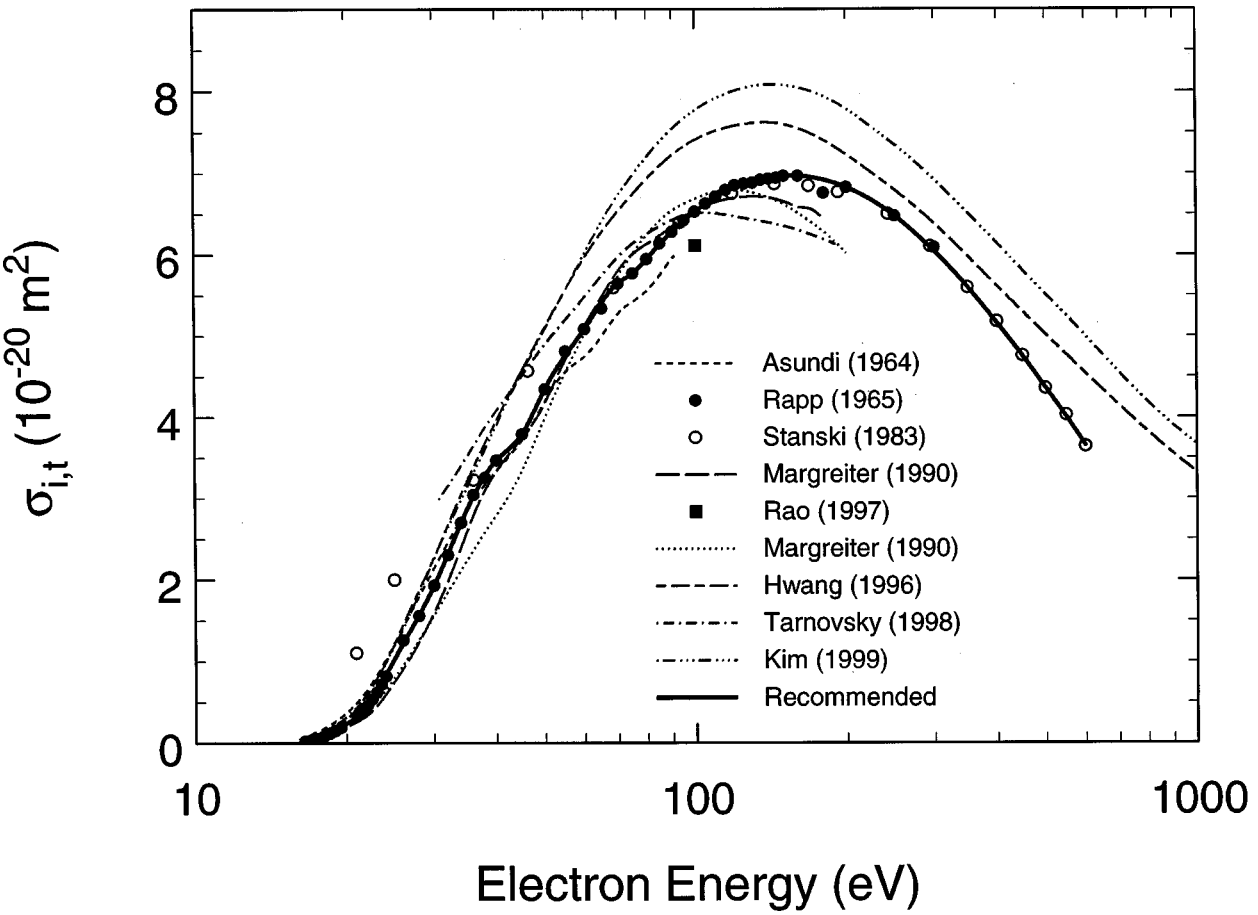

FIG. 14. Total electron-impact ionization cross section, $\sigma_{i,t}(\varepsilon)$, for SF_6 as a function of electron energy: (- - -) Ref. 82; (●) Ref. 156; (○) Ref. 157; (— —) Ref. 158; (■) Ref. 159; (···) Ref. 163; (– – –) Ref. 164; (– · –) Ref. 166; (– ···· –) Ref. 167; (—) recommended values.

Englander-Golden[156] are considered to be the most reliable, and they form the basis for our recommended data. The solid line in Fig. 14 is a fit to the data of Rapp and Englander-Golden[156] up to 300 eV, and to the data of Stanski and Adamczyk[157] for energies above 300 eV. Values derived from this fit are listed in Table 17 as our recommended values of the $\sigma_{i,t}(\varepsilon)$ of the SF_6 molecule.

The high ionization thresholds and the repulsiveness of the dissociating excited electronic states of SF_6 account for the large values of W (the energy required by energetic charged particles to produce an electron-positive ion pair in SF_6). Hilal and Christophorou[169] measured the mean energy required to produce an electron-positive ion pair in SF_6 by α particles (initial energy $\sim$5.1 MeV) and found it to be 35.45 eV per ion pair. This value is larger than that [(34.0 $\pm$0.4) eV per ion pair] measured by Lopes *et al.*[170] using ^{60}Co γ rays. The lower value for γ rays is consistent with other measurements (see Christophorou[171]) which show that for molecular gases, the energy to produce an electron-positive ion pair for α particles exceeds that for γ rays and β particles.

4.2. Partial Ionization Cross Sections, $\sigma_{i,partial}(\varepsilon)$

It was indicated in the preceding section that all electron-impact ionization processes in SF_6 are dissociative and that a number of investigators[157–159] have measured the cross sections for the production of the various positive-ion fragments following electron impact on SF_6. Thus, Stanski and Adamczyk[157] measured electron-impact dissociative ioniza-

TABLE 17. Recommended values for the total ionization cross section, $\sigma_{i,t}(\varepsilon)$, of SF_6 (derived from a fit to the data of Rapp and Englander-Golden in Ref. 156 and the data of Stanski and Adamczyk above 300 eV in Ref. 157)

Electron energy (eV)	$\sigma_{i,t}(\varepsilon)$ (10^{-20} m^2)	Electron energy (eV)	$\sigma_{i,t}(\varepsilon)$ (10^{-20} m^2)
16.5	0.020	75	5.77
17.0	0.035	80	5.95
17.5	0.055	90	6.28
18.0	0.084	100	6.53
19.0	0.155	125	6.87
20	0.240	150	6.97
22	0.457	200	6.83
25	1.04	250	6.48
30	1.93	300	6.04
35	2.87	350	5.60
40	3.47	400	5.16
45	3.79	450	4.75
50	4.35	500	4.36
60	5.09	550	4.00
70	5.65	600	3.65

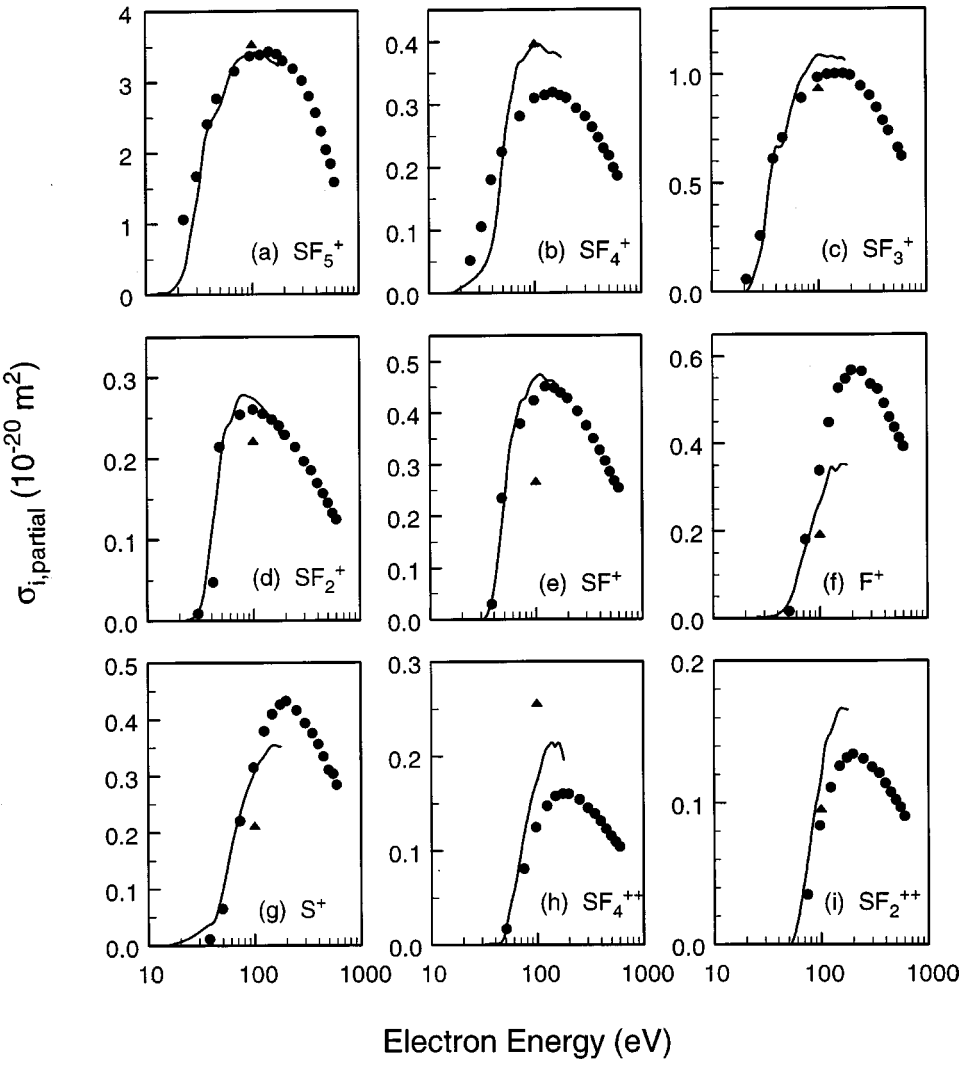

FIG. 15. Partial ionization cross sections, $\sigma_{i,partial}(\varepsilon)$, as a function of electron energy for SF_6: (●) data of Stanski and Adamczyk from Ref. 157; (—) data of Margreiter *et al.* from Ref. 158 [these data are normalized to the ''case A'' values at 100 eV (third Column, Table 16)]; (▲) data of Rao and Srivastava from Ref. 159.

tion cross sections, $\sigma_{i,partial}(\varepsilon)$, for SF_6 as a function of electron energy up to 600 eV. They reported $\sigma_{i,partial}(\varepsilon)$ for the production of the positive-ion fragments SF_5^+, SF_4^+, SF_3^+, SF_2^+, SF^+, S^+, F^+, SF_4^{++}, and SF_2^{++} from SF_6. They obtained these cross sections by normalizing the sum of the relative intensities of the fragment ions to the total ionization cross section of Rapp and Englander-Golden[156] for SF_6. Their partial ionization cross sections, $\sigma_{i,partial}(\varepsilon)$, are shown in Fig. 15. They generally maximize at or above 100 eV.

Similarly, Margreiter *et al.*[158] investigated electron-impact dissociative ionization of SF_6 and determined (see previous section for details) the $\sigma_{i,partial}(\varepsilon)$ for the same positive ion fragments as Stanski and Adamczyk.[157] The $\sigma_{i,partial}(\varepsilon)$ data for their preferred method (case A in their paper) are also plotted in Fig. 15. There is general overall agreement between the data of Stanski and Adamczyk[157] and Margreiter *et al.*[158] although for some fragments the two sets of measurements differ considerably. The difference may be due to the detection efficiency of energetic fragments, a problem which was addressed specifically in the experiment of Margreiter *et al.*[158]

The data of Rao and Srivastava[159] are for only a single incident electron energy (100 eV) and were obtained by normalization to the electron-impact ionization cross sections of the rare gases. They have a quoted uncertainty of ±10%. The data of these three groups of investigators are compared in Table 16 for the common electron energy of 100 eV. The agreement between the three sets of data varies from fragment to fragment. For some positive ion fragments (such as the energetic fragments F^+ and SF^+) the agreement between the three sets of measurements is poor and thus further measurements are indicated.

Finally, Al-Nasir *et al.*[160] employed an ejected-electron/produced-ion coincidence technique and measured relative partial doubly differential cross sections $d^2\sigma^{(n)}/dE\,d\Omega$ (partial doubly differential cross section for the production of ions in the charge state n) for the ions SF_5^+, SF_4^+, SF_3^+, SF_2^+, (SF^+, SF_4^{++}), S^+, SF_5^{++}, SF_3^{++}, and SF_2^{++} resulting from electron-impact dissociative ionization of the SF_6 molecule. They made such measurements at incident electron energies of 100 and 200 eV, ejected electron energies of 30, 50, 65, 100, and 150 eV, and ejected-electron angles ranging from 10° to 120°. Their results confirm previous observations[59,111] that the probability of production of ions of the form SF_x^+

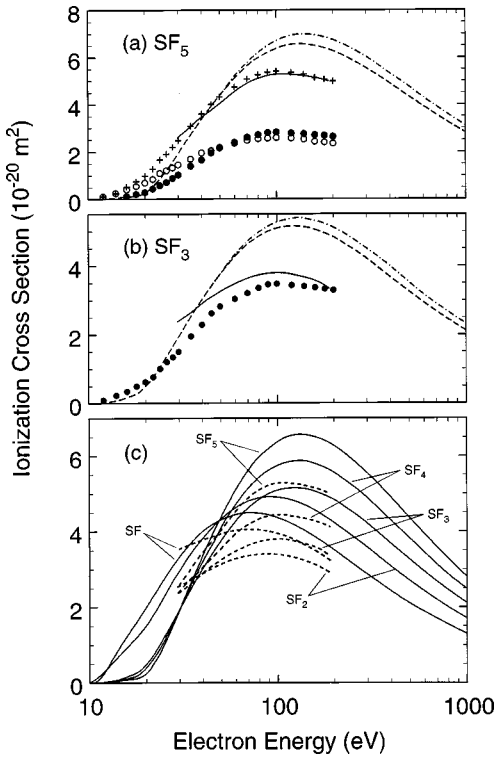

FIG. 16. Electron-impact ionization of SF_6 radicals: (a) Cross section for the formation of SF_5^+ and SF_4^+ by electron-impact on the free radical SF_5. Measurements of Tarnovsky *et al.* from Ref. 166: (○) SF_5^+; (●) SF_4^+; (+) sum of the measured cross sections for SF_5^+ and SF_4^+ generated by electron-impact on SF_5. Calculations of total electron-impact single ionization cross section of the radical SF_5: (—) data of Tarnovsky *et al.* from Ref. 166; (- - -) data of Ali *et al.* from Ref. 172 (without double ionization); (−·−) data of Ali *et al.* from Ref. 172 (with double ionization). (b) Cross section for the formation of SF_3^+ by electron-impact on the free radical SF_3: (●) measurements of Tarnovsky *et al.* from Ref. 166; (—) calculation of Tarnovsky *et al.* from Ref. 166; (- - -) calculation of Ali *et al.* from Ref. 172 (without double ionization); (−·−) calculation of Ali *et al.* from Ref. 172 (with double ionization). (c) Calculated electron-impact total single ionization cross sections as a function of the electron energy for the radicals SF_5, SF_4, SF_3, SF_2, and SF: (- - -) calculations of Tarnovsky *et al.* from Ref. 166; (—) calculations of Ali *et al.* from Ref. 172 (without double ionization).

TABLE 18. Threshold energies for appearance of positive ions from SF_6 radicals

Ion	Radical	Threshold energy (eV)	Reference
SF_5^+	SF_5	11.2 ± 1.0	166
		11.7[a]	173
		10.5 ± 0.1[b]	174
SF_4^+	SF_5	14.5 ± 1.0	166
	SF_5	15.5[a]	173
	SF_4	13.0[a]	173
	SF_4	12.03 ± 0.05[b]	174
SF_3^+	SF_5	17.0[a,c], 16.2[a,d]	173
	SF_4	14.5[a]	173
	SF_3	10.6[a], 11.4[e]	173
	SF_3	11.0 ± 1.0	166
SF_2^+	SF_5	21.8[a,f], 21.0[a,g]	173
	SF_4	19.3[a,c], 18.5[a,d]	173
	SF_3	15.4[a]	173
	SF_2	12.8[a], 11.8[e]	173
	SF_2	10.08[b]	174
SF^+	SF_5	27.8[a,h], 27.0[a,i], 26.2[a,j]	173
	SF_4	25.3[a,f], 24.5[a,g]	173
	SF_3	21.4[a,c], 20.6[a,d]	173
	SF_2	18.8[a]	173
	SF	14.7[a], 15.0[e]	173
	SF	10.09[b]	174

[a]Estimated.
[b]Listed value of the ionization threshold energy.
[c]Estimated using reactions producing two F.
[d]Estimated using reactions producing F_2.
[e]Measured.
[f]Estimated using reactions producing three F.
[g]Estimated using reactions producing F_2+F.
[h]Estimated using reactions producing four F.
[i]Estimated using reactions producing F_2+2F.
[j]Estimated using reactions producing two F.

with x odd is higher than that for similar ions with x even, and that the probability of production of ions of the form SF_x^{++} with x is even higher than that of similar ions with x odd.

All three experimental studies clearly show that SF_5^+ is by far the most abundant positive ion fragment and that the cross sections of doubly charged positive ion fragments are generally small (Fig. 15). Besides the doubly charged species SF_4^{++}, SF_3^{++}, and SF_2^{++}, Al-Nasir *et al.*[160] found a measurable signal due to SF_5^{++}, and Harland and Thynne[111] detected S^{++} from SF_6 under impact by 70 eV electrons.

4.3. Electron-Impact Ionization of SF_6 Neutral Fragments

Absolute cross sections for electron-impact ionization and dissociative ionization of the SF_5 and SF_3 free radicals have recently been measured by Tarnovsky *et al.*[166] from threshold to 200 eV using the fast-neutral-beam technique. It was found that dissociative ionization is important for SF_5, but not for SF_3. For the SF_5 radical the cross sections for formation of the parent SF_5^+ positive ion and the fragment SF_4^+ positive ion were found to be about the same, while electron-impact ionization of the SF_3 radical predominantly generates SF_3^+ parent ions. The reported uncertainties of these cross section measurements are $\pm15\%$ for the parent ionization cross sections and $\pm18\%$ for the dissociative ionization cross sections. Figure 16(a) shows the cross sections for the formation of the SF_5^+ parent ion and the SF_4^+ fragment ion from the SF_5 free radical. The two cross section curves are similar except for the shift in the appearance energy of the SF_4^+ cross section to higher energy. The sum of the two cross sections is also plotted in the figure and represents the total single ionization cross section for this radical, since Tarnovsky *et al.* put an upper limit on the contribution from all other singly charged positive ions of 0.25×10^{-16} cm^2 at 70 eV.

The cross section for the formation of the SF_3^+ parent positive ion from the SF_3 free radical is shown in Fig. 16(b). Based on the very weak signals Tarnovsky *et al.* observed for ions other than SF_3^+ from SF_3, they put an upper limit on

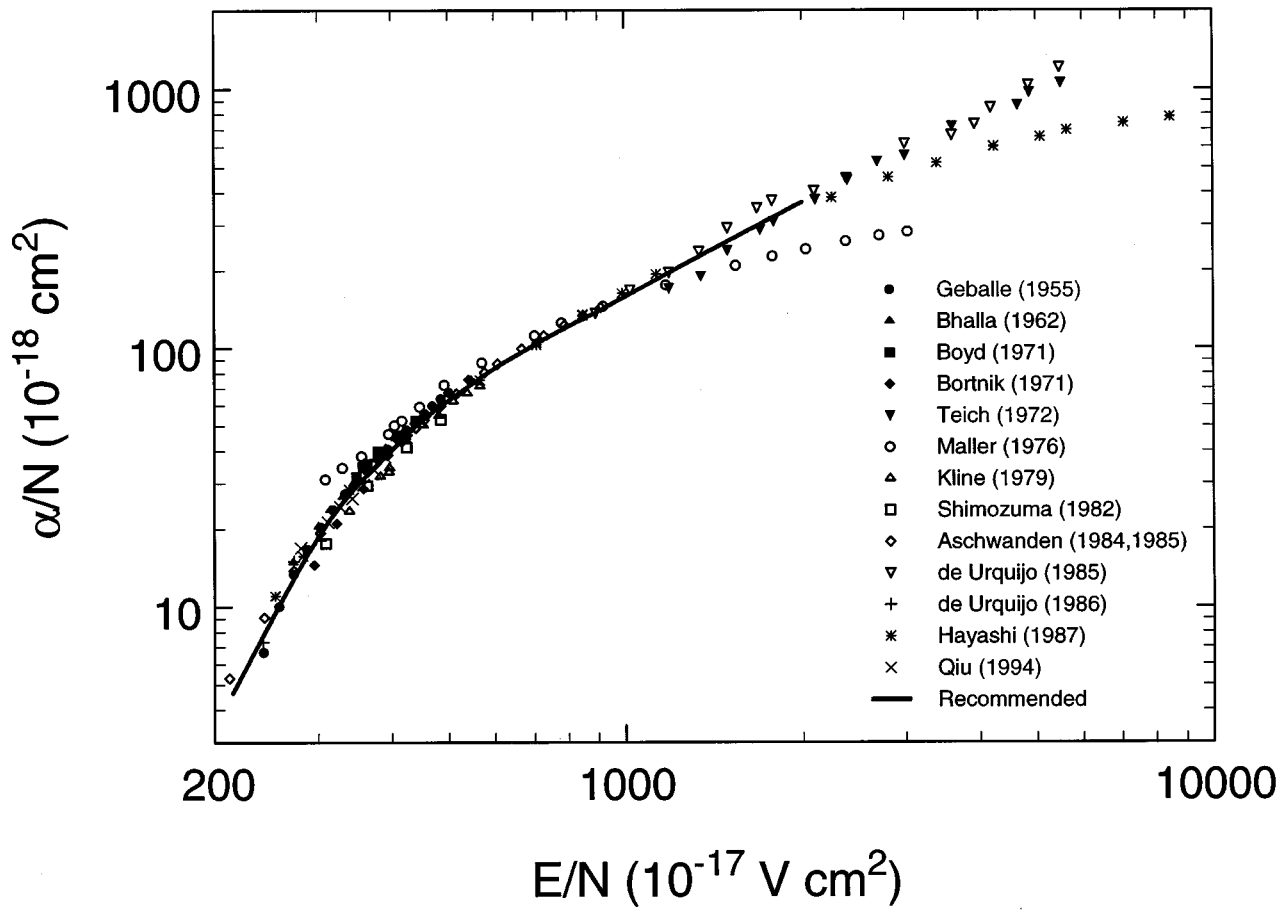

FIG. 17. Density-reduced electron-impact ionization coefficient, α/N (E/N), for SF_6 as a function of E/N $(T=293-296\,K)$: (●) Ref. 175; (▲) Ref. 177; (■) Ref. 178; (◆) Ref. 179; (▼) Ref. 184; (○) Ref. 180; (△) Ref. 26; (□) Ref. 181; (◇) Refs. 185 and 186; (▽) Ref. 187; (+) Ref. 188; (*) Ref. 182; (×) Ref. 183; (—) recommended values.

the possible contributions from all other singly charged ions of $0.2\times10^{-16}\,cm^2$ at 70 eV.

Besides the measurements in Figs. 16(a) and 16(b), there have been two calculations of the ionization cross sections of these two radicals by electron impact. The modified additivity rule calculation of the total electron-impact single ionization cross section of Tarnovsky *et al.*,[165,166] and the BEB calculation of the total electron-impact ionization cross section with and without double ionization of Ali *et al.*[172] In comparing the results of the two BEB calculations with the experimental measurements one should consider the calculated values without double ionization. The overall agreement between the experimental and calculated values is reasonable although, because the BEB cross sections are higher than the experimental data for most of the electron energy range, further scrutiny of both theory and experiment is indicated.

Besides the total electron-impact single ionization cross sections for SF_5 and SF_3, Tarnovsky *et al.*[165,166] and Ali *et al.*[172] made similar calculations for the radicals SF_4, SF_2, and SF. The calculated total electron-impact single ionization cross sections for all five radicals SF_5, SF_4, SF_3, SF_2, and SF are presented in Fig. 16(c). In all cases the BEB cross sections lie generally higher than the modified additivity rule results.

Table 18 lists values of the threshold energies for the appearance of positive ions from SF_6 radicals.

4.4. Density-Reduced Electron-Impact Ionization Coefficient, $\alpha/N(E/N)$

There have been a number of measurements of this coefficient using the steady-state Townsend method,[26,175–183] and the pulsed-Townsend method.[184–188] These measurements were made at room temperature (293–296 K) and collectively cover the E/N range from 212×10^{-17} to $8482\times10^{-17}\,V\,cm^2$. Not all of these studies quote uncertainties for the data. Bhalla and Craggs[177] and de Urquijo *et al.*[188] quote uncertainties ranging from about $\pm5\%$ to about $\pm15\%$, while Hayashi[182] estimates the uncertainty in his measurements to be about $\pm5\%$. These may be considered typical of the uncertainties in the data of the other groups.

Figure 17 shows the available data on $\alpha/N(E/N)$ for SF_6. The solid line represents a least squares fit to all the data plotted in the figure up to $2000\times10^{-17}\,V\,cm^2$, except those of Maller and Naidu[180] which clearly differ from the rest in

TABLE 19. Recommended values of the density-reduced electron-impact ionization coefficient, $\alpha/N\,(E/N)$, for SF_6

E/N (10^{-17} V cm^2)	$\alpha/N\,(E/N)$ (10^{-18} cm^2)	E/N (10^{-17} V cm^2)	$\alpha/N\,(E/N)$ (10^{-18} cm^2)
215	4.66	700	102.9
250	8.90	750	112.4
300	18.5	800	121.5
350	29.5	850	130.1
400	40.1	900	138.9
450	52.3	950	148.6
500	62.7	1000	158.2
550	73.2	1250	208.5
600	83.7	1500	259.8
650	93.3	2000	366.3

their functional dependence on E/N. Values derived from this curve are listed in Table 19 as our recommended data for the $\alpha/N(E/N)$ of SF_6. Above 2000×10^{-17} V cm^2 the data taken using the pulsed Townsend method[184,187] lie higher than those taken using the steady state Townsend technique.[182] The steady state data of Hayashi and Wang[182] for α/N above 2000×10^{-17} V cm^2 agree well with the high E/N values of $(\alpha-\eta)/N$ of Hasegawa *et al.*[189] (also obtained using the steady state Townsend method, see Sec. 6.6). However, it is possible that the values obtained by the steady state method at high E/N may be adversely affected by the low pressures and/or small drift distances used in such high E/N measurements.

Besides the above measurements, there have been a number of Monte Carlo[31] and Boltzmann[11,26–28,30,32–34,38,40,43,44] code calculations of $\alpha/N(E/N)$ for SF_6. The results of these calculations depend on the details of the calculation, especially the cross sections used and the associated energy losses (for such data and details see the individual papers).

5. Cross Sections for Electron-Impact Dissociation of SF_6 Into Neutral Fragments, $\sigma_{dis,neut}(\varepsilon)$

Relatively little work has been done on the process of electron-impact dissociation of the SF_6 molecule into neutral fragments in spite of the practical significance of this process in plasma processing and gaseous dielectrics. There have been no absolute measurements of the cross sections for total or partial dissociation of SF_6 into neutral fragments. To our knowledge the only study to date is that of Ito *et al.*[173] who used appearance mass spectrometry in a dual electron beam device and measured the energy dependence of the partial cross sections of electron-impact dissociation of SF_6 into the neutral radicals SF, SF_2, and SF_3 from threshold to 200 eV. The dissociation products SF_4 and SF_5 were below the detection limit of their system. The relative cross sections for electron-impact dissociation of SF_6 into SF, SF_2, and SF_3 reported by Ito *et al.* are shown in Fig. 18(a). The quoted relative uncertainty of these data is $\pm20\%$. Ito *et al.*[173] were unable to determine the absolute cross section scale in Fig. 18(a) because of a lack of ionization cross sections for the SF_x radicals required to normalize their relative measurements. However, such measurements have since become available (Fig. 16) and could be used to determine absolute cross sections from the relative measurements of Ito *et al.*, assuming that the other experimental variables involved are accurately known. It should be noted that the relative cross sections for the three radicals in Fig. 18 are absolute with respect to each other, and that in Table 4 of the paper by Ito *et al.*[173] the cross sections for the three fragments are listed as being in units of 10^{-20} m^2. As for the case of the CF_4 molecule,[19,25] these cross sections are expected to be much smaller than the cross sections $\sigma_{i,t}(\varepsilon)$ and $\sigma_{e,int}(\varepsilon)$ of SF_6, at electron energies above ~50 eV.

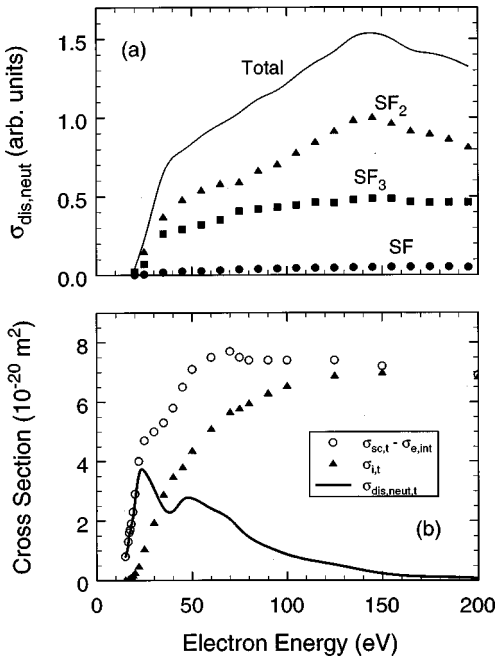

FIG. 18. (a) Relative cross sections, $\sigma_{dis,neut}(\varepsilon)$, for electron-impact dissociation of SF_6 into (■) SF_3, (▲) SF_2, and (●) SF neutral radicals from the measurements of Ito *et al.* in Ref. 173. The line (—) represents the relative sum of the cross sections for the three radicals. (b) Deduced cross section for total dissociation into neutrals, $\sigma_{dis,neut,t}(\varepsilon)$, for SF_6 from other recommended cross sections (see text).

As we have discussed in Sec. 3.5.1, at energies above ~15 eV where the cross section $\sigma_{vib,t}(\varepsilon)$ is small, the difference $\sigma_{sc,t}(\varepsilon)-\sigma_{e,int}(\varepsilon)$ can be used to deduce a value for the total cross section, $\sigma_{dis,neut,t}(\varepsilon)$, for the dissociation of SF_6 into neutral fragments via the relation

$$\sigma_{dis,neut,t}(\varepsilon)\cong[\sigma_{sc,t}(\varepsilon)-\sigma_{e,int}(\varepsilon)]-\sigma_{i,t}(\varepsilon). \qquad (3)$$

In Eq. (3) the quantity $[\sigma_{sc,t}(\varepsilon)-\sigma_{e,int}(\varepsilon)]$ is as determined in Sec. 3.5.1 (open symbols in Fig. 12 above 15 eV), and $\sigma_{i,t}(\varepsilon)$ is our recommended cross section for the total ionization cross section (Table 17). These two quantities, along with their difference, $\sigma_{dis,neut,t}(\varepsilon)$, are shown in Fig. 18(b). The cross section $\sigma_{dis,neut,t}(\varepsilon)$ deduced this way is seen to have a different energy dependence than the sum of the relative cross sections for dissociation of SF_6 into the neutral

TABLE 20. Deduced values of the total cross section, $\sigma_{dis,neut,t}(\varepsilon)$, for electron-impact dissociation of SF_6 into neutral fragments

Electron energy (eV)	$\sigma_{dis,neut,t}(\varepsilon)$ (10^{-20} m^2)	Electron energy (eV)	$\sigma_{dis,neut,t}(\varepsilon)$ (10^{-20} m^2)
15	0.8	45	2.7
16	1.2	50	2.8
17	1.6	60	2.4
18	1.8	70	2.1
19	2.2	75	1.7
20	2.7	80	1.5
22	3.5	90	1.1
25	3.7	100	0.87
30	3.1	125	0.53
35	2.4	150	0.23
40	2.3	200	0.07

fragments SF_3, SF_2, and SF reported by Ito *et al.*[173] [Fig. 18(a)]. This discrepancy is consistent with previous observations[25] of possible inaccuracies in magnitude and energy dependence in the cross sections for dissociation into neutrals measured by Sugai and co-workers for CF_4 and CHF_3. Ito *et al.* obtained the relative cross sections in Fig. 18(a) under the assumption that the total ionization cross section for each of the SF_6 radicals is similar in shape to that of SF_6.[190]

In the absence of any absolute data on the $\sigma_{dis,neut,t}(\varepsilon)$ of SF_6, we list in Table 20 the values of $\sigma_{dis,neut,t}(\varepsilon)$ deduced as described above as our presently suggested data. It should be realized that these data are approximate and require experimental confirmation.

Table 21 lists the expected or measured threshold energies for dissociation of SF_6 into SF_5, SF_4, SF_3, SF_2, SF, F_2, and F as given by Ito *et al.*[173]

There have been a few other studies[154,155,191,192] dealing with electron-impact dissociation of SF_6 into excited neutral fragments. These provide complementary information on the dissociation mechanisms of this molecule. Thus, Corr *et al.*[191] studied the dissociation of the SF_6 molecule into neutral metastable fragments as a function of the incident electron energy from threshold to 300 eV. They identified a number of dissociation channels involving both partial and total fragmentation of the SF_6 molecule by electron impact. In Table 22 are listed the threshold energies they determined for the production of the various excited fragments. The work of Corr *et al.*[191] shows that dissociation leading to total fragmentation of SF_6 is responsible for the formation of the S fragments and also the dominant process for the formation of F atoms. The finding that the F atoms are predominantly produced by complete dissociation of the SF_6 molecule is also consistent with the results of three other studies by Becker and collaborators[154,155,192] on the optical emission from excited atomic fragments generated by electron-impact dissociation of SF_6. Thus, Blanks *et al.*,[155] using a crossed electron beam–gas beam apparatus, measured absolute emission cross sections and appearance potentials for the most intense $3p \rightarrow 3s$ atomic fluorine lines in the visible range of the optical spectrum between 620 and 780 nm. According to Blanks *et al.* these lines are emitted by atomic fluorine fragments that are formed in the various excited states associated with the $1s^2\,2s^2\,2p^4\,3p$ electron configuration. Figure 19 shows the absolute emission cross section, $\sigma_{em}(\varepsilon)$, of the integrated FI $3p^4D^0 \rightarrow 3s^4P$ multiplet as a function of the incident electron energy, and Table 23 lists the absolute emission cross sections, σ_{em} (100 eV), measured for various visible FI emission lines for an incident-electron energy of 100 eV.

The threshold energies for excited neutral fragments produced by electron impact on SF_6 as obtained by these workers are also listed in Table 22. Blanks *et al.*[155] determined a

TABLE 21. Expected or measured threshold energies given by Ito *et al.* in Ref. 173 for electron-impact dissociation of SF_6 into neutrals

Reaction	Expected threshold energy (eV)	Measured[a] threshold energy (eV)
$SF_6+e \rightarrow SF_5+F+e$	9.6	—
$SF_6+e \rightarrow SF_4+2F+e$	12.1	—
$SF_6+e \rightarrow SF_4+F_2+e$	11.3	—
$SF_6+e \rightarrow SF_3+3F+e$	16.0	16.0[b]
$SF_6+e \rightarrow SF_3+F+F_2+e$	15.2	
$SF_6+e \rightarrow SF_2+4F+e$	18.6	19.5[b]
$SF_6+e \rightarrow SF_2+2F+F_2+e$	17.8	
$SF_6+e \rightarrow SF_2+2F_2+e$	17.0	
$SF_6+e \rightarrow SF+5F+e$	22.7	22.0[b]
$SF_6+e \rightarrow SF+3F+F_2+e$	21.9	
$SF_6+e \rightarrow SF+F+2F_2+e$	21.1	

[a]Estimated uncertainty: ± 0.5 eV.
[b]The experimental value is affected by contributions from all respective processes given in the first column of the table.

TABLE 22. Threshold energies of excited neutral fragments upon electron impact on SF_6

Fragment	Threshold energy (eV)	Reference	Species detected
F_2^R	18.7 ± 1.0	191	Rydbergs
	17.9 ± 1.0	191	Photons/total
	18.0 ± 1.0	161	F_2^+
Metastable fragments	27	191	Low-energy fragments
	30.0 ± 1.0	191	Neutrals/total
	26.8 ± 0.3	74	SF_2^+
	27.0 ± 0.3	161	SF_2^+
F^R	36.0 ± 1.0	191	Rydbergs
	35.0 ± 1.0	191	Photons/total
	35.8 ± 1.0	191	Neutrals/total
	35.8 ± 1.0	74	F^+
	37.5 ± 1.0	161	F^+
	35.8 ± 1.5	154	F*
F^R, S^R	44.3 ± 1.0	191	Rydbergs
	44.5 ± 1.0	191	Photons/total
	44.9 ± 1.0	191	Neutrals/total
	42.0 ± 1.5	154	F*
	41.6 ± 1.5	155	F*
	40 ± 2	192	F*
	43.6 ± 1.5	154	S*

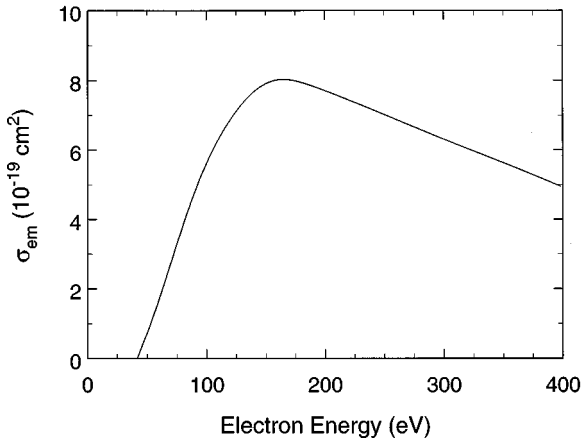

FIG. 19. Emission cross section for the integrated FI $3p^4D^0 \rightarrow 3s^4P$ multiplet as a function of the energy of the incident electrons impacting on SF_6 (data of Blanks *et al.* from Ref. 155).

value of 41.6 ± 1.5 eV for the threshold energy of the strongest line emission at 685.6 nm. This relatively high onset indicates that total fragmentation of the molecule plays a leading role in the electron-impact-induced dissociation of SF_6.

Becker and collaborators[154,192] also investigated light emission resulting from electron impact on SF_6 in other (shorter) wavelength regions. Blanks and Becker[192] investigated the wavelength range from 200 to 600 nm, and Forand *et al.*[154] studied the wavelength range from 45–185 nm using 200 eV incident electrons. Blanks and Becker[192] found that the $^{2,4}D \rightarrow {}^4P$ multiplet at 366.8 nm has the largest emission cross section with a cross section of $(4.4 \pm 1.2) \times 10^{-20}$ cm^2 at 100 eV. Figure 20 shows the emissions produced by 200 eV electrons on SF_6. The spectrum consists of a broad structure from 200 to 320 nm and several line emissions. The strongest line emissions originate from excited fluorine fragments in the $^{2,4}S^0$, $^{2,4}P^0$, and $^{2,4}D^0$ states associated with the $2p^4 4p$ electron configuration. These states lie approximately 16 eV above the ground state atom and decay into the $2p^4 3s^{2,4}P$ states emitting several multiplets in the wavelength region between 350 and 400 nm. The threshold energy of the strongest line was found by Blanks and Becker to be (40 ± 2) eV (Table 22). Interestingly, no emission from ionic fluorine was observed by Becker and collaborators. A later study by Field and Eland[193] using wavelengths of 58.4, 30.4, and 25.6 nm to excite SF_6 is consistent with the electron-impact result in that no detectable ionic emission from either parent or fragment ions was observed. However, according to Forand *et al.*,[154] at shorter wavelengths (45–185 nm), the observed lines following electron impact of 200 eV electrons on SF_6 could be identified with singly ionized S atoms, besides neutral S and F atomic transitions.

From the work of Becker and collaborators,[154,192] it can be concluded that electron impact on SF_6 results in the formation of neutral and ionized excited atomic fragments with significant probabilities, and that light observed following electron impact on SF_6 is due to de-excitation of these excited fragments. These results would indicate that the weak light emission observed by some investigators from the motion of electron swarms in SF_6 at high E/N or from SF_6 discharges may be due to such excited fragments, although another possible source of these weak emissions may be impurities. It has, for instance, been shown that small amounts of N_2 in SF_6 greatly enhance light emission as the nitrogen

TABLE 23. Absolute emission cross sections, σ_{em} (100 eV), for various visible FI emission lines for 100 eV incident electrons impacting on SF_6 (data of Blanks *et al.* from Ref. 155)

Transition	Line (nm)	σ_{em} (100 eV)[a] (10^{-19} cm^2)
$^4S^0 \rightarrow {}^4P$	624.0	0.6
	634.9	0.4
	641.3	0.3
$^4D^0 \rightarrow {}^4P$	677.4	0.4
	679.5	<0.1
	683.4	0.6
	685.6	2.5
	687.0	0.4
	690.2	1.4
	691.0	0.4
$^2P^0 \rightarrow {}^2P$	703.7	0.6
	712.8	0.3
	720.2	0.2
$^2S^0 \rightarrow {}^2P$	731.1	1.4
$^4P^0 \rightarrow {}^4P$	733.2	
	739.9	2.1
	746.5	0.3
	755.2	
	757.3	1.1
$^2D^0 \rightarrow {}^2P$	760.7	
	775.5	2.0
	788.0	1.1

[a]The uncertainty is $\pm 20\%$ for σ_{em} (100 eV) values larger than 10^{-19} cm^2, $\pm 25\%$ for σ_{em} (100 eV) values smaller than 10^{-19} cm^2, and about $\pm 40\%$ for the σ_{em} (100 eV) of emissions at wavelengths longer than 750.0 nm.

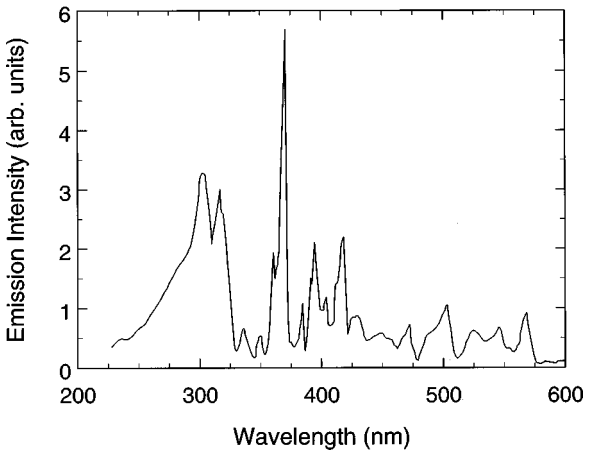

FIG. 20. Emission spectrum of SF_6 between about 200 and 600 nm generated by collisions with 200 eV incident electrons (data uncorrected for the wavelength dependence of the detector efficiency) from Blanks and Becker in Ref. 192.

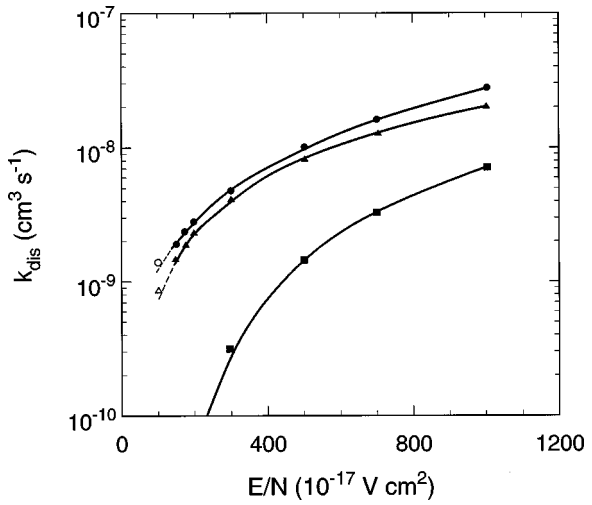

FIG. 21. Calculated electron-impact dissociation rate, $k_{dis}(E/N)$, as a function of E/N for (●) total dissociation, (▲) total electronic excitation, and (■) total dissociative ionization (results of Phelps and Van Brunt from Ref. 40). The open points (○), (△) are calculated results by Masek *et al.* in Ref. 195 at $E/N=100\times10^{-17}$ V cm^2. The dashed lines are extrapolations by Phelps and Van Brunt of their calculations to lower E/N.

molecule has a large excitation coefficient for the second positive group radiation ($C\,^3\Pi_u \rightarrow B\,^3\Pi_g$) and quenching of the C states of N_2 by SF_6 is not very strong.[194]

Finally, in the absence of any measurements of the electron-impact dissociation rate for SF_6, we show in Fig. 21 the results[40] of a Boltzmann calculation of the electron-impact induced dissociation rate, $k_{dis}(E/N)$, of SF_6 (also see Ref. 196). It should be realized that these data are model-specific.

6. Electron Attachment to SF_6

6.1. Cross Sections for the Formation of Negative Ions

It has long been established that SF_6 is an electronegative gas. Electron attachment to SF_6 leads to the formation of both parent (SF_6^-) and fragment (SF_5^-, SF_4^-, SF_3^-, SF_2^-, F_2^-, and F^-) negative ions. The experimental data on the cross sections for the formation of each of these negative ions are presented and discussed in this section. The measured cross sections for the various negative ions formed by electron impact on SF_6 show that the parent negative ion SF_6^- is formed only at extremely low electron energies (below $\sim$0.2 eV), and that the fragment negative ions are formed via a number of negative ion states located between 0 and $\sim$15 eV.

6.1.1. SF_6^-

The stable parent negative ion SF_6^- produced at zero and near-zero electron energy is initially formed as a metastable SF_6^-* ion which subsequent to its formation is stabilized by collision or radiation. Its autodetachment lifetime, τ_a, under collision-free conditions has been found to be between 10 and 68 μs[197–202] using time-of-flight (TOF) mass spectrometric measurements. Similar measurements using ion cyclotron resonance (ICR) techniques found the lifetime of SF_6^-* to be much longer, in the ms range.[203–205] This is not surprising, since a number of studies[201,202,206] have shown that the autodetachment lifetime of many polyatomic long-lived transient negative ions depends on the experimental conditions (kinetic energy of the captured electron, internal energy of the electron capturing molecule, and hence the gas temperature), and the electron energies in ICR experiments are normally much lower than in TOF experiments. While no effect of the attaching electron's energy on the τ_a of SF_6^-* has been reported, such energy dependence has been found for other transient anions.[201,207–211] Furthermore, Delmore and Appelhans[212] observed an increase of $\sim$33% in the τ_a of metastable SF_6^-* when the temperature of the ion source was decreased from $\sim$475 to $\sim$375 K. This was attributed to the contribution of various excited states to the autodetachment process. It has also been shown[204] that the τ_a of SF_6^-* in the ICR spectrometer varies with the observation time of the experiment, thus accounting for radiative and collisional cooling of SF_6^-*.[204,213]

Besides the formation of SF_6^- by direct attachment of low-energy electrons, SF_6^- can also be formed indirectly by relatively higher energy electrons when these electrons lose ''all'' of their energy to inelastic electron scattering and are then attached efficiently as ''zero-energy'' electrons to SF_6 molecules. Indeed, this is the basis of the so-called ''SF_6^- threshold-electron-excitation technique'' used to locate negative-ion states and excited electronic states, especially optically forbidden states, of neutral molecules.[214–217]

Many early studies[82,114,198,214,215,218–222] showed that SF_6^- is formed near 0.0 eV with a very large cross section. These studies also indicated that the shape of the measured cross section for the formation of SF_6^- was instrumental, i.e., the SF_6^- resonance is narrower than the energy spread of the electron pulse or beam used to measure it. This narrowness of the SF_6^- resonance is largely responsible for the large uncertainty and spread in the early published values of the attachment cross section, $\sigma_{a,SF_6^-}(\varepsilon)$, for formation of SF_6^- at thermal and near-thermal energies. There have been a number of subsequent (room temperature) studies using both conventional electron beam[26,139,223] and electron swarm[108,109,224–228] techniques. Additionally, newer very-high resolution and very-low energy electron beam techniques have been used to provide accurate values of the absolute cross section for the attachment of free electrons to SF_6 to form SF_6^- from $\sim$1 eV down to the μeV range.[152,153,229–236] Besides these methods, information on $\sigma_{a,SF_6^-}(\varepsilon)$ has been provided in the thermal and subthermal electron energy range by another new technique using ''bound-electron'' capture in collisions of SF_6 with high-Rydberg atoms.[234,237–253] The results obtained by these methods are complementary to those obtained by direct ''free'' electron-impact methods.

The cross section data for total electron attachment determined by these methods are plotted in Fig. 22 over an energy

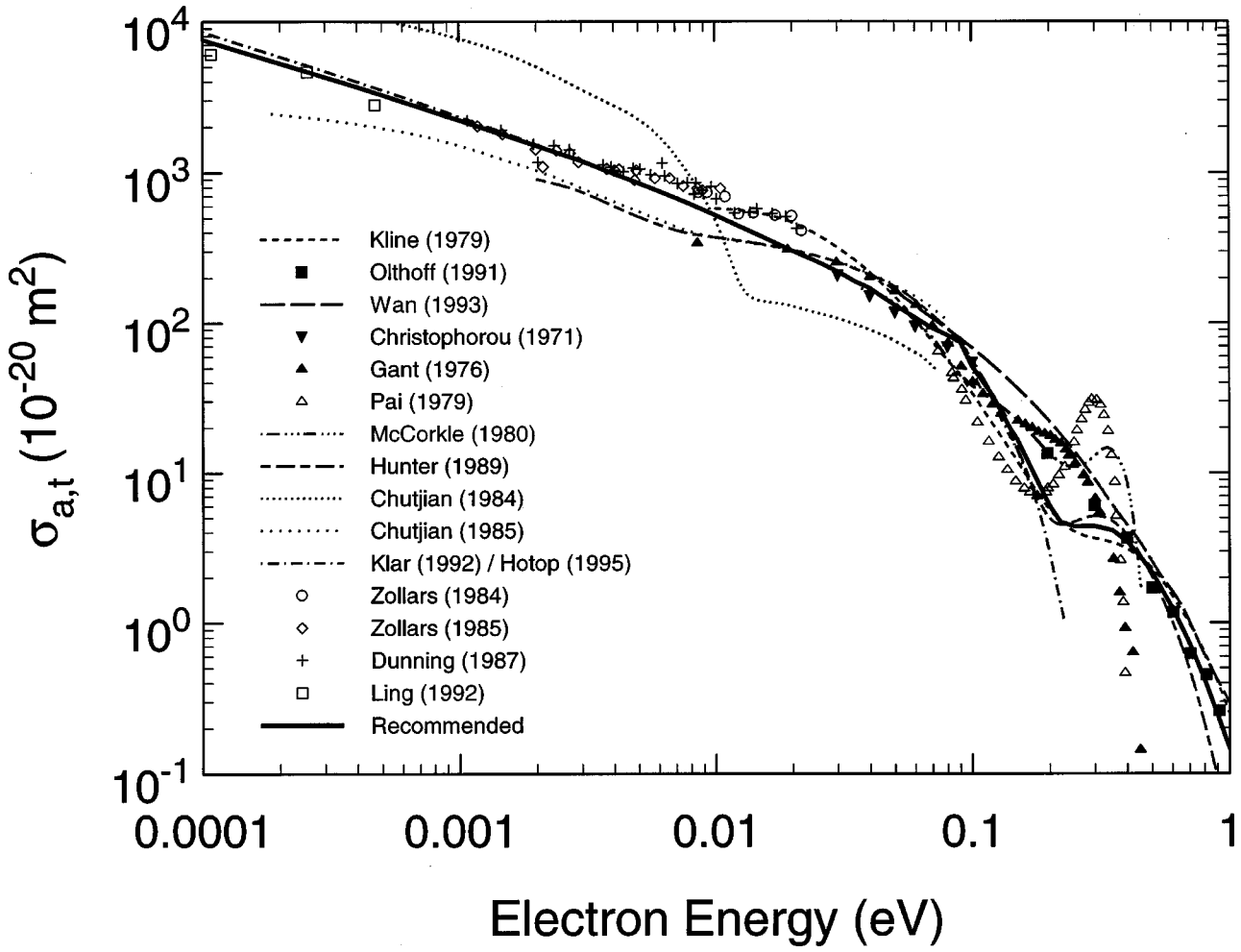

FIG. 22. Measured total electron attachment cross section, $\sigma_{a,t}(\varepsilon)$, for SF_6 as a function of the electron energy, for free electrons and for electrons bound in high-Rydberg states of atoms (see text). Below ~0.1 eV this cross section is about equal to $\sigma_{a,SF_6^-}(\varepsilon)$ for the production of SF_6^-. Conventional electron-beam data: (- - -) Ref. 26; (■) Ref. 223; (– –) Ref. 139. Swarm-unfolded data: (▼) Ref. 108; (▲) Ref. 225; (△) Ref. 226; (−···−) Ref. 227; (— - —) Ref. 228. TPSA technique: (···) data from Ref. 232 normalized to the thermal electron attachment rate constant value of Crompton and Haddad in Ref. 254; (· · ·) data of Ref. 233 normalized to the swarm-unfolded cross section of McCorkle *et al.* in Ref. 227. LPA technique: (− · −) Refs. 152, 255, 261. High-Rydberg data: (○) Xe* (nf), Ref. 240; (◇) Rb* (ns,nd), Ref. 241; (+) Rb* (ns,nd), K*(nd), Xe*(nf), Ref. 243; (□) K*(np), Ref. 248. (—) Recommended values.

range of 0.0001–~0.2 eV, and are briefly discussed below.

Data obtained by conventional electron-swarm and electron-beam techniques—The swarm data[108,109,224–228] plotted in Fig. 22 have been unfolded from the total electron attachment rate-constant measurements made in mixtures of SF_6 with N_2 buffer gas. They are therefore total electron attachment cross sections. However, since SF_6^- is the predominant negative ion in the energy region below ~0.1 eV, these cross sections give the value of $\sigma_{a,SF_6^-}(\varepsilon)$. It is difficult to assess the uncertainty of these cross section data. Although the rate constant measurements are expected to have an uncertainty around ±10%, the cross section values have a larger uncertainty. Similarly, the electron beam data have a large uncertainty at low energies. Kline *et al.*[26] used the retarding potential difference method in their experiments and their energy resolution was typically between 80 and 100 meV. Their cross section below ~0.1 eV is therefore instrumental. The measurements of Olthoff *et al.*[223] and Wan *et al.*[139] are for the total electron attachment cross section and were made using a trochoidal monochromator (T = 328 K). They have a quoted uncertainty of ±15% above 1 eV and a larger uncertainty below this energy, which perhaps increases to ±50% at 0.2 eV.

Data obtained from very-high resolution, very-low energy electron-beam techniques—Two such techniques have been developed, one by Chutjian and collaborators[229,230,232,233] and the other by Hotop and collaborators.[152,153,234–236] The two techniques are similar in principle. The technique of the former group uses vacuum uv photoionization of rare-gas atoms mixed with SF_6 to generate *in situ* photoelectrons of well defined and variable energy. It is referred to as the threshold-photoelectron-spectroscopy-by-electron-attachment (TPSA) technique and provides relative cross sections for electron energies in the range from a few meV to 150 meV with electron-energy resolution between 6 and 8 meV (full-width at half-maximum).[232] The energy depen-

dence of the cross section is obtained using convolution techniques and the absolute value is determined by normalization to electron swarm data. The data of Chutjian *et al.*[232] were normalized to the thermal electron attachment rate constant ($2.27\times10^{-7}\,\mathrm{cm^3\,s^{-1}}$) of Crompton and Haddad,[254] while the data of Chutjian and Alajajian[233] were normalized to the electron swarm-unfolded cross section data of McCorkle *et al.*[227] The technique of Hotop and collaborators is referred to as the laser-photoelectron-attachment (LPA) method and is based on the controlled production of variable-energy photoelectrons using lasers to photoionize a well-collimated beam of metastable Ar* ($4s^3P_2$) atoms ''from a differentially pumped dc discharge source in a field-free region.'' The resulting negative ions are then detected by application of pulsed electric fields.[152] This technique has permitted the energy dependence of the electron attachment cross section to be measured directly with sub-meV resolution. The values measured by Hotop and collaborators[152,255] for the $\sigma_{a,SF_6^-}(\varepsilon)$ in the range 0.0001–0.250 eV are shown in Fig. 22. These cross-section values were obtained by normalization to the thermal ($T=300\,\mathrm{K}$) rate constant measurement of Crompton *et al.*[254,256] It should be emphasized that the cross section of Hotop *et al.* in Fig. 22 is only for the formation of SF_6^-, while the rest of the data above 0.1 eV are total electron attachment cross sections.

Data obtained from high-Rydberg atom bound-electron capture methods—A number of investigators, foremost the group at Rice University, have used beams of atoms excited in high-Rydberg states, $A^{**}(nl)$, to measure the rate constant for the reaction

$$A^{**}(nl)+SF_6\rightarrow A^+ + SF_6^- \qquad (4)$$

down to ~4 μeV.[253] In almost all such investigations, $A^{**}(nl)$ is a rare-gas or an alkali-metal atom in a Rydberg state with principal quantum number n and angular momentum quantum number l. In these studies the rate constant $k_{a,be}$ for the formation of SF_6^- is measured as a function of the principal quantum number n, or as a function of the effective principal quantum number n^* ($n^*=n-\delta_l$, where δ_l is the l-dependent quantum defect). An example of the $k_{a,be}(n^*)$ measurements is shown in Fig. 23. From data such as in Fig. 23, the cross section for bound-electron capture, $\sigma_{a,be}(v)$, is determined via the relation

$$\sigma_{a,be}(v)=k_{a,be}(n^*)/v_{rms}, \qquad (5)$$

where v_{rms} is the root-mean-square velocity of the Rydberg electron. While a number of authors (e.g., see Refs. 251 and 253) have shown Eq. (5) to be inappropriate for Rydberg states with l small compared to n, and while postattachment electrostatic attraction between the products (A^+, SF_6^-) may have significant effects on the size of the measured cross section (e.g., see Ref. 253), a number of studies (e.g., Refs. 241, 248, 252, and 253) have shown that the cross sections for bound-electron capture are consistent with the ''free'' electron model *for sufficiently large values* (>30) *of the principal quantum number n*. In such cases, then, the excited electron and the core can be considered independent particles, the electron in the Rydberg atom essentially being equivalent to a free electron having the same kinetic energy as the binding energy of the Rydberg electron. These studies, as well as those of Chutjian and collaborators and Hotop and collaborators (referred to earlier in this section) have shown that at very low energies ($\lesssim1$ meV[152,236]) the attachment cross section for the formation of SF_6^- varies inversely with the electron velocity in accordance with the Wigner threshold law for s-wave electron attachment.[257]

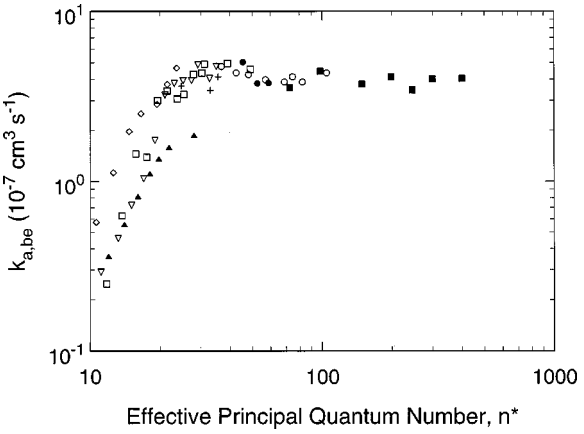

FIG. 23. Rate constant, $k_{a,be}(n^*)$, for bound-electron capture as a function of the effective principal quantum number n^* in collisions of Rydberg atoms with SF_6 (from Ling *et al.* in Ref. 248): (■) K*(np), Ref. 248; (○) Rb*(nd), Ref. 241; (●) Rb*(ns), Ref. 241; (□) K*(nd), Ref. 243; (▽) Na*(np), Ref. 244; (◇) Ne*(ns), Ref. 234; (▲) Ne*(nd), Ref. 234.

Reaction (4) has been studied using a number of Rydberg atoms: $He^*(n=14,{}^1P)$;[250] $Ne^*(ns,nd)$;[234] $Xe^*(nf)$;[237,238,240,243] $K^*(nd)$;[242,243,245] $K^*(np)$;[248] $Na^*(np)$;[244] $Rb^*(ns,nd)$;[241,243] and $Cs^*(ns,np,nd)$.[246] The results of these high-Rydberg-atom studies on $\sigma_{a,be}(v)$ are plotted in Fig. 22.

The wide spread in the data shown in Fig. 22 and the many factors that can affect them (many of which are often not clearly discerned) makes the deduction of a recommended total attachment cross section, $\sigma_{a,t}(\varepsilon)$, for SF_6 difficult. However, since at energies below ~1.5 eV, SF_6^- and SF_5^- are the only negative ions produced by electron attachment to SF_6 with significant intensity, we determined the recommended value of $\sigma_{a,t}(\varepsilon)$ for SF_6 shown by the solid line in Fig. 22, by summing our recommended cross sections for SF_6^- and SF_5^- formation, which are determined separately below.

The determination of the recommended cross section, $\sigma_{a,SF_6^-}(\varepsilon)$, for the formation of SF_6^- was made by considering the data in Fig. 24(a). The dot-dash line ($-\cdot-$) represents the measurements of Hotop and collaborators[152,255] obtained using the LPA technique (much of this curve from ~0.003 to 0.2 eV is overlaid by the solid recommended line discussed later). The broken lines ($-\ -$) and ($-\ -\ -$) are the cross sections for the production of only SF_6^- as obtained, respectively, from electron-swarm-based measurements by Hunter *et al.*[228] and from electron-beam-based measurements by Kline *et al.*[26] The symbols shown in the figure are the

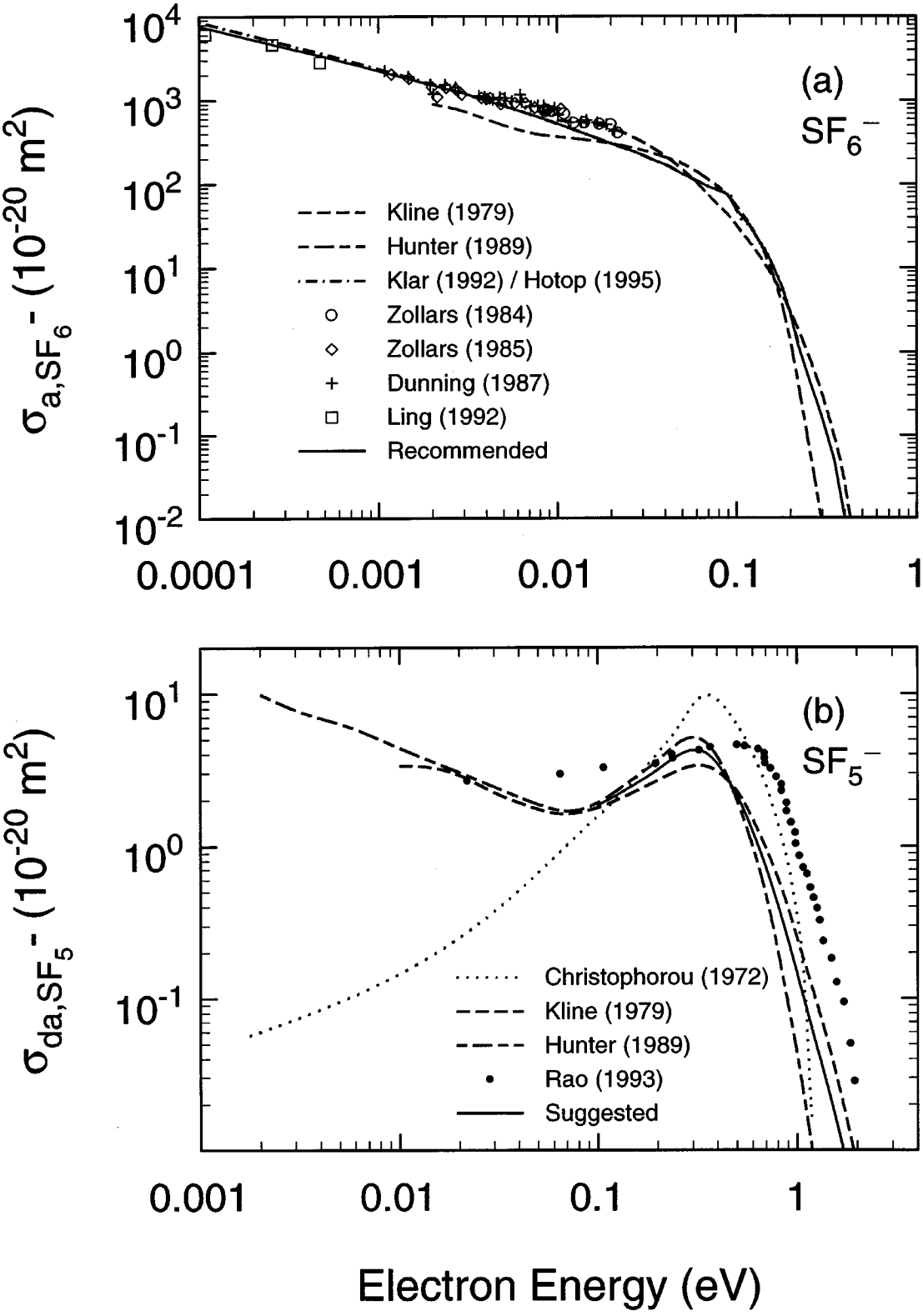

FIG. 24. (a) Selected measurements of the electron attachment cross section, $\sigma_{a,SF_6^-}(\varepsilon)$, for the formation of SF_6^- from SF_6 as a function of the electron energy: (- - -) Ref. 26; (– – –) Ref. 228; (– · –) Refs. 152, 255, 261; (○) Ref. 240; (◇) Ref. 241; (+) Ref. 243; (□) Ref. 248; (—) recommended values. (b) Selected measurements on the dissociative electron attachment cross section, $\sigma_{a,SF_5^-}(\varepsilon)$, for the formation of SF_5^- from SF_6 as a function of the electron energy: (···) Refs. 108, 109; (- - -) Ref. 26; (– – –) Ref. 228; (●) Ref. 113; (—) suggested data.

TABLE 24. Recommended values of the electron attachment cross section, $\sigma_{a,SF_6^-}(\varepsilon)$, for the formation of SF_6^- by electron impact on SF_6 in the electron energy range 0.0001–0.40 eV

Electron energy (eV)	$\sigma_{a,SF_6^-}(\varepsilon)$ (10^{-20} m^2)	Electron energy (eV)	$\sigma_{a,SF_6^-}(\varepsilon)$ (10^{-20} m^2)
0.0001	7617	0.030	221
0.0002	5283	0.035	190
0.0003	4284	0.040	171
0.0004	3692	0.045	149
0.0005	3280	0.050	132
0.0006	2968	0.060	109
0.0007	2724	0.070	92.7
0.0008	2529	0.080	82.9
0.0009	2369	0.090	74.3
0.001	2237	0.10	49.5
0.002	1511	0.12	30.8
0.003	1202	0.14	17.8
0.004	993	0.15	14.2
0.005	859	0.16	10.5
0.006	760	0.18	5.85
0.007	683	0.20	2.86
0.008	621	0.22	1.24
0.009	569	0.25	0.52
0.010	526	0.28	0.25
0.015	383	0.30	0.16
0.020	304	0.35	0.05
0.025	257	0.40	0.01

TABLE 25. Suggested values for the dissociative electron attachment cross section, $\sigma_{da,SF_5^-}(\varepsilon)$, for the formation of SF_5^- by electron attachment to SF_6 as a function of the electron energy

Electron energy (eV)	$\sigma_{da,SF_5^-}(\varepsilon)$ (10^{-20} m^2)	Electron energy (eV)	$\sigma_{da,SF_5^-}(\varepsilon)$ (10^{-20} m^2)
0.10	1.85	0.40	3.45
0.12	2.09	0.45	2.75
0.14	2.36	0.50	2.15
0.15	2.48	0.60	1.25
0.16	2.61	0.70	0.72
0.18	2.87	0.80	0.42
0.20	3.15	0.90	0.25
0.22	3.45	1.0	0.15
0.25	3.86	1.2	0.060
0.28	4.15	1.5	0.020
0.30	4.24	1.9	0.005
0.35	4.07		

bound-electron attachment cross sections of Refs. 240, 241, 243, and 248. At the lowest energies (<0.005 eV), the cross section values of Hotop and collaborators are in excellent agreement with the bound-electron attachment measurements for $n>30$. At higher energies, the cross section of Hotop and collaborators drops off abruptly at the onsets of the ν_1, ν_3, and $2\nu_1$ vibrational excitations (see discussions in Refs. 152 and 255), and is in overall agreement with the data of Hunter *et al.* and Kline *et al.* considering the precipitous decline in the magnitude of the cross section with increasing electron energy in this energy range. The measurements of Hotop and collaborators[152,255] from 0.0001 to 0.23 eV, the bound-electron attachment data below 0.005 eV, and the data of Hunter *et al.* and Kline *et al.* above 0.2 eV were fit to yield the solid line in Fig. 24(a). This line represents our recommended values for $\sigma_{a,SF_6^-}(\varepsilon)$ in the energy range 0.0001–0.4 eV, and values extracted from the line are listed in Table 24.

The other free-electron data for $\sigma_{a,SF_6^-}(\varepsilon)$ shown in Fig. 22 were not considered for various reasons: (1) The data of Chutjian and collaborators are indirect measurements both in absolute magnitude and energy dependence. Also, according to Chutjian[258] part of the disagreement between the data they obtained using the TPSA technique and the data obtained using the LPA and bound-electron attachment methods are due to the effects of stray fields on the TPSA measurements. (2) The electron beam data of Olthoff *et al.*[223] and Wan *et al.*[139] do not show the enhancement at ~ 0.4 eV due to SF_5^- borne out by all other electron beam and electron swarm studies, and no means exists to differentiate between the SF_6^- and SF_5^- contributions. (3) From the various swarm-based cross sections we considered only the more recent data of Hunter *et al.*[228] since these measurements were more accurate and more extensive than the previous ones, and since more recent cross sections were employed in the determination of the electron energy distribution functions used to obtain the swarm-based cross sections from the measured rate constants.

6.1.2. SF_5^-

A number of electron-beam studies[26,108–111,113,115,259] have shown that at energies below ~ 2 eV, SF_5^- is produced via the dissociative electron attachment reaction

$$e + SF_6 \rightarrow SF_5^- + F \tag{6}$$

with maxima at ~ 0.0 and 0.38 eV. It has been shown by Chen and Chantry[110] that the first peak at ~ 0.0 eV is very sensitive to gas temperature (Sec. 6.4.1) and that the second peak at 0.38 eV is rather independent of temperature. Interestingly, Matejcik *et al.*[259] have recently found that the first peak at 0.0 eV disappears at temperatures below ambient.

In Fig. 24(b) are compared the published values of the cross section, $\sigma_{da,SF_5^-}(\varepsilon)$, for the formation of SF_5^- by low-energy electron-impact on SF_6 as a function of electron energy for swarm-normalized data[108,109,228] and electron-beam data.[26,113] None of these studies quoted uncertainties. As can be seen from Fig. 24(b) there are large differences in the cross section data for the production of SF_5^- from SF_6. The large discrepancies below 0.1 eV may be partly due to the varied effects of temperature on the formation of SF_5^- at the low energies (e.g., see Refs. 152, 260, and 261) which are still unresolved. For this reason, we suggest data for the cross section, $\sigma_{da,SF_5^-}(\varepsilon)$, for the formation of SF_5^- by electron attachment to SF_6 down to only 0.1 eV. These suggested data are shown in Fig. 24(b) by the solid line which was obtained by a least squares fit to the data of Kline *et al.*[26] and Hunter *et al.*[228] Values derived from the line are listed in Table 25. The data of Rao and Srivastava[113] were excluded from the fit since they exhibit a large energy uncertainty due

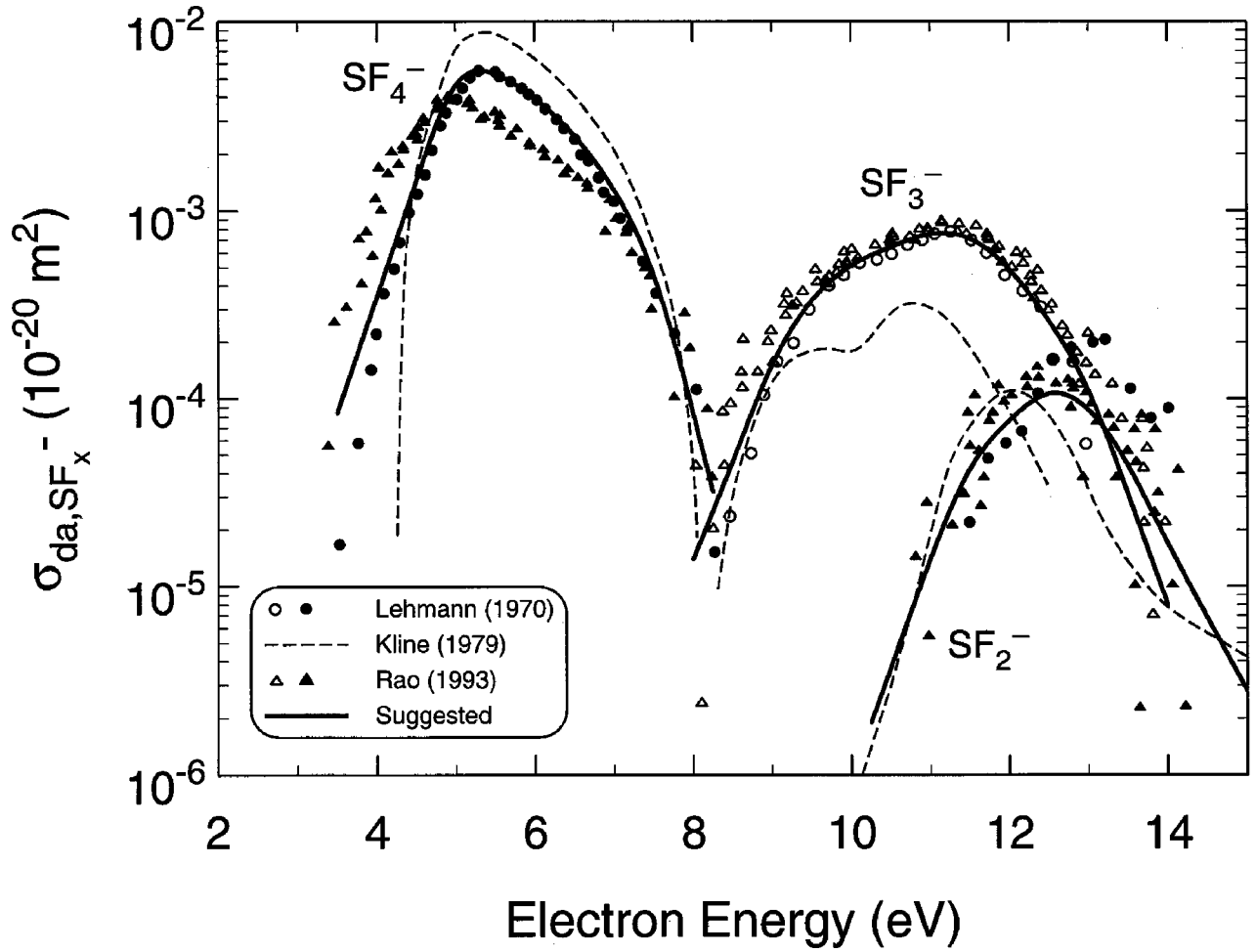

FIG. 25. Cross sections for the formation of SF_4^-, SF_3^-, and SF_2^- by dissociative electron attachment to SF_6 as a function of the electron energy: (○), (●) Ref. 114; (- - -) Ref. 26; (△), (▲) Ref. 113; (—) suggested values.

to the difficulty of obtaining accurate values from the sharp SF_5^- peak shown in the figure in their paper. It should be noted, that at room temperature the contribution of SF_5^- to the total electron attachment cross section below ~ 0.1 eV is small compared to SF_6^- production.

6.1.3. SF_4^-, SF_3^-, and SF_2^-

The smaller SF_x^- $(x=2,3,4)$ ions are generated mostly through negative-ion states located at progressively higher electron energies (see Table 26). The SF_4^- fragment is generated from a broad resonance between 4 and 8 eV. Harland and Thynne[111] attributed the production of this ion to the reaction

$$SF_6 + e \rightarrow SF_4^- + 2F \tag{7}$$

and reported the cross section maximum for this ion to be at (6.0 ± 0.1) eV. In contrast, Fenzlaff *et al.*,[115] although not excluding reaction (7) for the formation of SF_4^-, attributed its formation ''at least on the high energy side of the resonance,'' to the reaction

$$e + SF_6 \rightarrow SF_6^-{}^*(5.4\,\text{eV}) \rightarrow SF_4^- + F_2 \tag{8}$$

with a threshold at (2.8 ± 0.1) eV and a peak at 5.4 eV.

Cross sections for all three fragment negative ions were measured at room temperature by Lehmann,[114] Kline *et al.*,[26] and Rao and Srivastava,[113] and are shown in Fig. 25. Kline

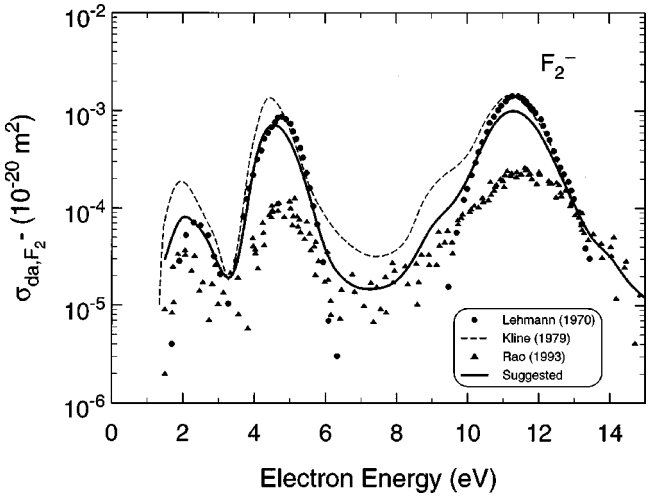

FIG. 26. Cross section for the formation of F_2^- by dissociative electron attachment to SF_6 as a function of the electron energy: (●) Ref. 114; (- - -) Ref. 26; (▲) Ref. 113; (—) suggested data.

TABLE 26. Energy positions of cross section maxima in the formation of negative ions by low-energy electron impact on SF_6

Negative ion	Energy position of cross section maximum (eV)	Reference(s)	Suggested reaction
SF_6^-	~0.0	Many (see text)	$e+SF_6 \rightarrow SF_6^{-*}$
SF_5^-	0.50±0.1	111	$e+SF_6 \rightarrow SF_5^- + F$
	0.38	108, 109	
	~0.0; 0.38	110, 26	
	~0.0[a]; 0.38	115	
	~0.0	113[b]	
SF_4^-	6.0±0.1	111	$e+SF_6 \rightarrow SF_4^- + 2F$
	5.4	114[b,c]	
	5.4	26[b]	
	5.4	115	$e+SF_6 \rightarrow SF_4^- + F_2$ and $(SF_4^- + 2F)$
	5.0	113[b]	
SF_3^-	11.2	114[b,c]	
	9.4; 10.9	26[b]	
	11.3	113[b]	
SF_2^-	13.0	114[b,c]	
	12.0	26[b]	
	12.3	113[b]	
F_2^-	2.4; 4.8; 11.7	114[b,c]	
	2.0; 4.4; 11.2	26[b]	
	5.4	115	$e+SF_6 \rightarrow SF_6^{-*}$ (5.4 eV) $\rightarrow SF_4 + F_2^-$
	2.2; 4.8; 11.6	113[b]	
F^-	5.7±0.1	111	$e+SF_6 \rightarrow SF_6^{-*} \rightarrow SF_4 + F + F^-$
	9.3±0.1	111	$e+SF_6 \rightarrow SF_6^{-*} \rightarrow SF_3 + 2F + F^-$
	11.8±0.1	111	$e+SF_6 \rightarrow SF_6^{-*} \rightarrow SF_2 + 3F + F^-$
	2.8; 5.2; 8.9; 11.5	114[b,c]	
	2.6; 5.1; 8.8; 11.3	26[b]	
	~2.9	115	$e+SF_6 \rightarrow SF_6^{-*} \rightarrow SF_5 + F^-$
	5.4	115	$e+SF_6 \rightarrow SF_6^{-*} \rightarrow SF_4 + F + F^-$
	2.8; 5.3; 9.4; 11.6	113[b]	

[a]The zero-energy peak was found to ''disappear'' at temperatures below ambient (Ref. 259).
[b]Determined from the respective figures of each of these references.
[c]All energy values determined from the figures given in Ref. 114 were reduced by 0.6 eV (see text).

et al. established the magnitudes of the cross sections by measuring the various positive-ion cross sections and calibrating their sum with the total ionization cross section measurements of Rapp and Englander Golden.[156] Their effective electron energy resolution was between 0.08 and 0.1 eV with an estimated uncertainty of the electron energy scale of ±0.1 eV. Rao and Srivastava[113] measured peak cross section values for SF_4^-, SF_3^-, and SF_2^-, respectively, equal to 4.0×10^{-19}, 8.8×10^{-20}, and 1.3×10^{-20} cm^2. The data of Rao and Srivastava in Fig. 25 were taken off their plots[113] and were put on an absolute scale using these peak cross section values. In Fig. 25 the data of Lehmann were shifted to lower energies by 0.6 eV, as suggested by Kline *et al.*[26]

With the applied shift in the data of Lehmann,[114] the agreement in the magnitude and energy dependence of the cross sections for these three ions as measured by Lehmann[114] and by Rao and Srivastava[113] is reasonable. The energy position of the maxima in the cross sections for each of these ions as determined from the data reported by Lehmann,[114] Kline *et al.*,[26] and Rao and Srivastava[113] are listed in Table 26, along with similar data derived from the relative cross section measurements of Fenzlaff *et al.*[115]

The solid lines shown in the figure for each negative ion fragment represent our respective suggested cross sections. They were obtained by a least squares fit to all three sets of measurements for each ion, except for the case of the SF_3^- ion for which only the data of Refs. 113 and 114 were considered. In Table 27 are listed the suggested values for the cross sections of these three fragment negative ions derived from the solid lines in Fig. 25.

6.1.4. F_2^-

Figure 26 compares the room temperature cross section measurements of Lehmann,[114] Kline *et al.*,[26] and Rao and Srivastava[113] for the production of F_2^-. The F_2^- ion is produced in the energy range from ~1 to ~14 eV, and the cross sections exhibit maxima near 2.2, 4.7 eV, and 11.5 eV (Table 26). The data of Lehmann shown here were again shifted to lower energy by 0.6 eV as discussed previously. Rao and Srivastava[113] gave a value of 2.6×10^{-20} cm^2 for the cross section of this ion at the maximum of the third peak at

TABLE 27. Suggested cross sections for the formation of SF_4^-, SF_3^-, SF_2^-, F_2^-, and F^- by dissociative electron attachment to SF_6 as a function of the electron energy. Note that the cross section units are $10^{-22}\,m^2$

Energy (eV)	Cross section ($10^{-22}\,m^2$)				
	σ_{da,SF_4^-}	σ_{da,SF_3^-}	σ_{da,SF_2^-}	σ_{da,F_2^-}	σ_{da,F^-}
1.50	—	—	—	0.0030	—
2.00	—	—	—	0.0080	0.022
2.25	—	—	—	0.0075	0.075
2.50	—	—	—	0.0060	0.149
2.75	—	—	—	0.0042	0.162
3.00	—	—	—	0.0026	0.098
3.50	0.0084	—	—	0.0026	0.171
4.00	0.0350	—	—	0.0265	0.856
4.50	0.144	—	—	0.0707	2.69
5.00	0.457	—	—	0.0489	4.63
5.50	0.528	—	—	0.0155	4.39
6.00	0.394	—	—	0.0038	2.78
6.50	0.251	—	—	0.0019	1.37
7.00	0.130	—	—	0.0015	0.749
7.50	0.0460	—	—	0.0015	0.615
8.00	0.0084	0.0014	—	0.0018	0.977
8.50	0.0032	0.0046	—	0.0031	1.42
9.00	—	0.0150	—	0.0065	1.57
9.50	—	0.0330	—	0.0104	1.39
10.00	—	0.0510	—	0.0200	1.13
10.25	—	0.0577	0.000 19	0.0308	1.14
10.50	—	0.0640	0.000 37	0.0503	1.31
11.00	—	0.0750	0.001 40	0.0910	2.10
11.50	—	0.0710	0.004 20	0.0954	2.35
12.00	—	0.0490	0.007 60	0.0615	1.95
12.50	—	0.0260	0.010 60	0.0274	1.22
13.00	—	0.0110	0.008 70	0.0111	0.629
13.50	—	0.0031	0.004 40	0.0050	0.400
14.00	—	0.0008	0.001 70	0.0032	0.340
14.50	—	—	0.000 68	0.0018	0.310
15.00	—	—	0.000 28	0.0012	0.300

11.5 eV which is lower than the other two sets of measurements by nearly a factor of 10. The solid line in Fig. 26 is our suggested cross section, $\sigma_{da,F_2^-}(\varepsilon)$, for this ion that was obtained by considering all three sets of experimental data. Values derived from this curve are listed in Table 27.

6.1.5. F^-

The F^- ion is the predominant fragment negative ion produced by dissociative electron attachment to SF_6 at ambient temperature at electron energies above ~3 eV. Cross sections for the formation of this ion are shown in Fig. 27, and these exhibit maxima near 2.8, 5.2, 9.1, and 11.5 eV. Above ~15 eV the data of Rao and Srivastava[113] show formation of F^- possibly via ion-pair processes. The energy positions of the maxima in the F^- cross section function as determined from the various sources and possible reaction mechanisms of formation are given in Table 26. Not included in Table 26 is an early observation by Curran[133] of F^- formation at ~0.0 eV (presumably via the reaction $e+SF_6 \rightarrow F^- + SF_5$). None of the subsequent room temperature investigations identified this resonance, and the observation by Curran[133] has been questioned by Fenzlaff *et al.*[115]

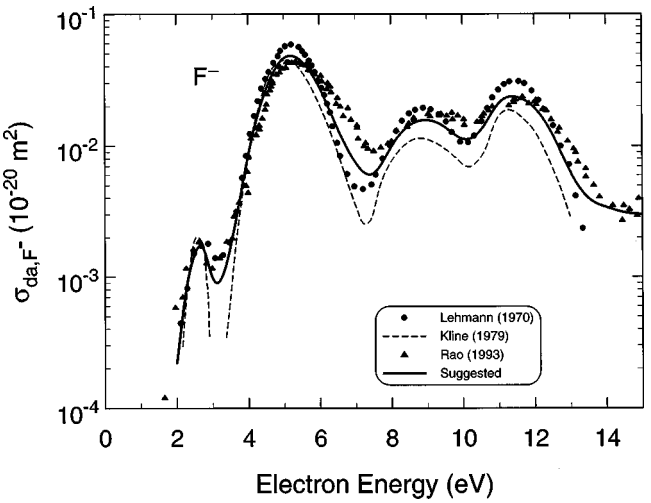

FIG. 27. Cross section for the formation of F^- by dissociative electron attachment to SF_6 as a function of the electron energy: (●) Ref. 114; (- - -) Ref. 26; (▲) data from Ref. 113 adjusted upwards by a factor of 10 as discussed in the text; (—) suggested data.

The original data of Rao and Srivastava[113] for this ion were mistakenly reported at values that were low by a factor of 10.[262] The data plotted in Fig. 27 are the original values corrected upward by a factor of 10. The various cross section measurements along with a least squares fit to the three sets of data (solid line) are shown in Fig. 27. Values obtained from the solid line in Fig. 27 are listed in Table 27 as our suggested data for the $\sigma_{da,F^-}(\varepsilon)$.

6.2. Total Electron Attachment Cross Section, $\sigma_{a,t}(\varepsilon)$, and Total Dissociative Electron Attachment Cross Section, $\sigma_{da,t}(\varepsilon)$

In Fig. 28 are plotted the recommended or suggested cross sections for the various negative ions as determined in the preceding sections, namely, for SF_6^- [Fig. 24(a)], SF_5^- [Fig. 24(b)], SF_4^-, SF_3^-, and SF_2^- (Fig. 25), F_2^- (Fig. 26), and F^- (Fig. 27). The total electron attachment cross section, $\sigma_{a,t}(\varepsilon)$, as represented by the sum of all these recommended or suggested cross sections is shown in Fig. 28 by the dotted line, which overlaps with the solid line for SF_5^- below ~1.5 eV and the solid line for SF_6^- below ~0.2 eV. Data derived from the dotted line are listed in column 2 of Table 28 as our recommended values for the $\sigma_{a,t}(\varepsilon)$ of the SF_6 molecule in the energy range 0.0001–15 eV. The total dissociative electron attachment cross section $\sigma_{da,t}(\varepsilon)$, as represented by the sum of the suggested dissociative electron attachment cross sections for all fragment negative ions, is listed in column 3 of Table 28. The values listed represent our suggested data for the $\sigma_{da,t}(\varepsilon)$ of the SF_6 molecule. It is seen from Fig. 28 that beyond ~0.3 eV, $\sigma_{da,t}(\varepsilon)=\sigma_{a,t}(\varepsilon)$. It is also seen that $\sigma_{da,t}(\varepsilon)$ is dominated by the formation of SF_5^- below ~1.5 eV and by the formation of F^- above this energy.

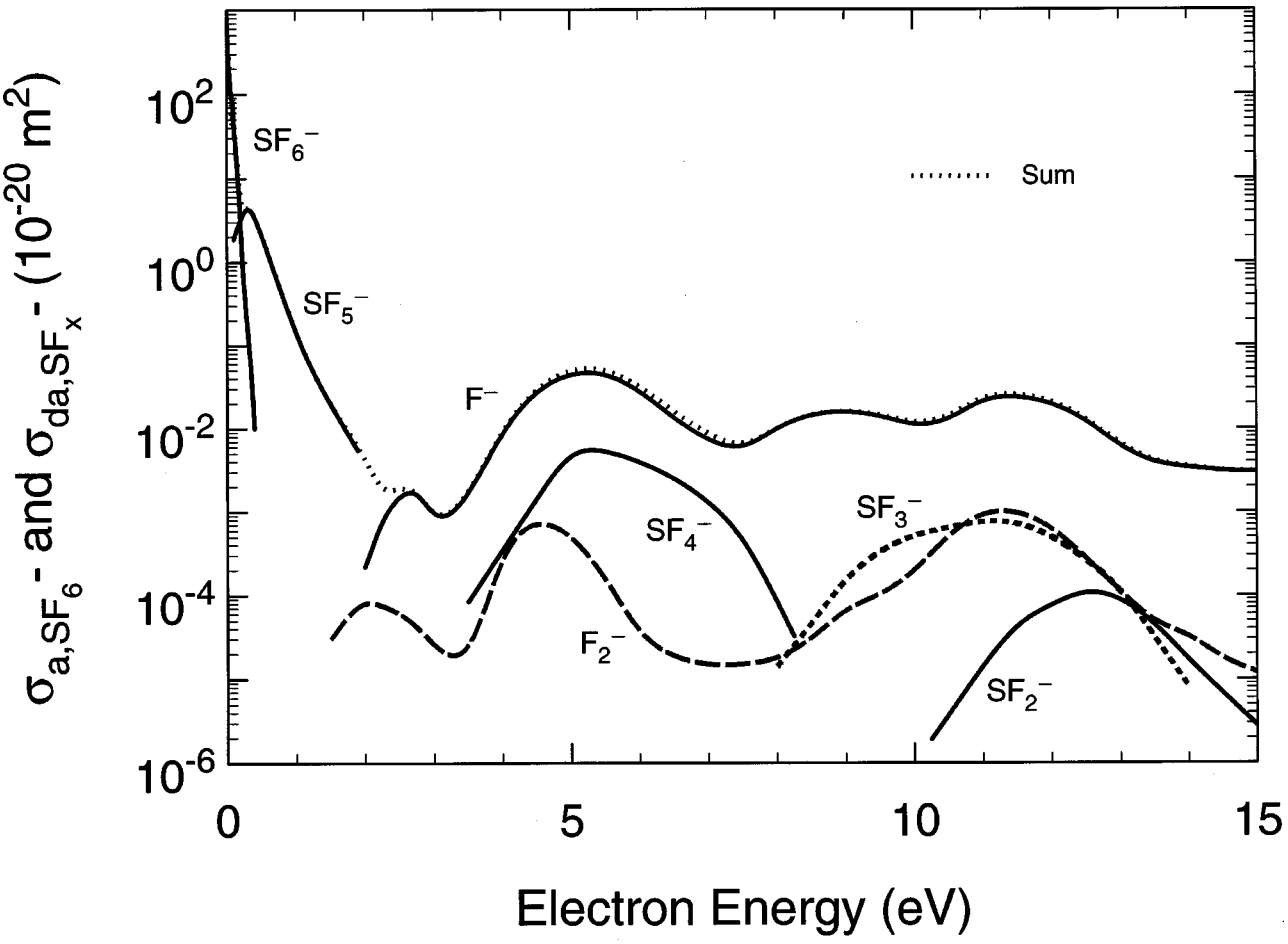

FIG. 28. Recommended and suggested cross sections for the formation of SF_6^- [Fig. 24(a)], SF_5^- [Fig. 24(b)], SF_4^-, SF_3^-, and SF_2^- (Fig. 25), F_2^- (Fig. 26), and F^- (Fig. 27) by electron attachment or dissociative attachment. (···) Suggested $\sigma_{a,t}(\varepsilon)$ (sum of all cross sections in figure).

6.3. Total Electron Attachment Rate Constant, $k_{a,t}$, as a Function of E/N and $\langle\varepsilon\rangle$

6.3.1. $k_{a,t}(E/N)$ in Ar, Xe, and N_2

Hunter *et al.*[228] measured the total electron attachment rate constant $k_{a,t}(E/N)$ near 300 K in mixtures of SF_6 with N_2, Ar, and Xe buffer gases. The E/N range they covered for the three buffer gases corresponds to the mean electron energy range from ~0.04 to ~4.3 eV. The uncertainty in their measurements varies from ±5% to ±15% depending on the value of E/N. Hunter *et al.* obtained values of the rate constants uninfluenced by changes in the electron energy distribution function of the pure buffer gases by using extremely low concentrations of SF_6 (the SF_6 fractional concentrations were as low as 1.3×10^{-9} for N_2, 1.5×10^{-9} for Ar, and 2.2×10^{-10} for Xe). This was achieved by extrapolating the measured electron attachment coefficient, $\eta/N_a(E/N)$, (normalized to the attaching gas number density N_a) at each value of E/N to zero SF_6 concentration and multiplying the extrapolated values of $\eta/N_a(E/N)$ by the electron drift velocity for the pure gas. The data of Hunter *et al.* are shown in Fig. 29. In Table 29 are listed the values of $k_{a,t}(E/N)$ and $\eta/N_a(E/N)$ for mixtures of SF_6 with Ar and Xe, along with the values of the electron drift velocity $w(E/N)$ and the mean electron energy $\langle\varepsilon\rangle(E/N)$ for the Ar and Xe buffer gases given by Hunter *et al.*[228] Similar data are given in Table 30 for the N_2 buffer gas.

Also plotted in Fig. 29 are the earlier measurements of the $k_{a,t}(E/N)$ of SF_6 conducted by Gant[225] in mixtures of SF_6 with N_2 and Ar buffer gases, and by Christophorou *et al.*,[108] Lakdawala and Moruzzi,[263] and Christophorou and Datskos[264] in mixtures of SF_6 with N_2. Christophorou and Datskos[264] reported $k_{a,t}$ only as a function of the mean electron energy $\langle\varepsilon\rangle$. For presentation in Fig. 29, we converted their $k_{a,t}(\langle\varepsilon\rangle)$ data to $k_{a,t}(E/N)$ by using the $\langle\varepsilon\rangle(E/N)$ in Table 30. We deduce the $k_{a,t}(E/N)$ of Lakdawala and Moruzzi[263] from their measurements of $\eta/N_a(E/N)$ in mixtures of SF_6 with N_2. The data in Fig. 2 of their paper represent measurements for a number of SF_6 concentrations in N_2 ranging from 0.03% to 0.6%. We performed a least squares fit to all their $\eta/N_a(E/N)$ data points and values from this fit were converted to $k_{a,t}(E/N)$ using the electron drift velocities in N_2 given by Hunter and Christophorou[265] and Wedding *et al.*[266] The resultant values of $k_{a,t}(E/N)$ are plotted in Fig. 29. It is seen that although the data of Lakdawala and Moruzzi considerably expand the E/N range of the measurements, they are incompatible with the rest of the data in this buffer gas.

TABLE 28. Suggested room temperature values of the total electron attachment cross section $\sigma_{a,t}(\varepsilon)$ and the total dissociative electron attachment $\sigma_{da,t}(\varepsilon)$ for SF_6

Electron energy (eV)	$\sigma_{a,t}(\varepsilon)$ (10^{-20} m^2)	$\sigma_{da,t}(\varepsilon)$ (10^{-20} m^2)	Electron energy (eV)	$\sigma_{a,t}(\varepsilon)$ (10^{-20} m^2)	$\sigma_{da,t}(\varepsilon)$ (10^{-20} m^2)
0.0001	7617	—	0.30	4.40	4.24
0.0002	5283	—	0.35	4.12	4.07
0.0003	4284	—	0.40	3.46	3.45
0.0004	3692	—	0.45	2.75	2.75
0.0005	3280	—	0.50	2.15	2.15
0.0006	2968	—	0.60	1.25	1.25
0.0007	2724	—	0.70	0.722	0.722
0.0008	2529	—	0.80	0.416	0.416
0.0009	2369	—	0.90	0.245	0.245
0.001	2237	—	1.00	0.147	0.147
0.002	1511	—	1.20	0.060	0.060
0.003	1202	—	1.50	0.020	0.020
0.004	993	—	2.00	0.0043	0.0043
0.005	859	—	2.25	0.0020	0.0020
0.006	760	—	2.50	0.0019	0.0019
0.007	683	—	2.75	0.0017	0.0017
0.008	621	—	3.0	0.0010	0.0010
0.009	569	—	3.5	0.0018	0.0018
0.010	526	—	4.0	0.0092	0.0092
0.015	383	—	4.5	0.0290	0.0290
0.020	304	—	5.0	0.0514	0.0514
0.025	257	—	5.5	0.0493	0.0493
0.030	221	—	6.0	0.0317	0.0317
0.035	190	—	6.5	0.0162	0.0162
0.040	171	—	7.0	0.0088	0.0088
0.045	149	—	7.5	0.0066	0.0066
0.050	132	—	8.0	0.0099	0.0099
0.060	109	—	8.5	0.0143	0.0143
0.070	92.7	—	9.0	0.0159	0.0159
0.080	82.9	—	9.5	0.0144	0.0144
0.090	74.3	—	10.0	0.0120	0.0120
0.10	51.4	1.85	10.5	0.0142	0.0142
0.12	32.9	2.09	11.0	0.0227	0.0227
0.14	20.2	2.36	11.5	0.0252	0.0252
0.15	16.7	2.48	12.0	0.0206	0.0206
0.16	13.1	2.61	12.5	0.0128	0.0128
0.18	8.72	2.87	13.0	0.0066	0.0066
0.20	6.01	3.15	13.5	0.0041	0.0041
0.22	4.69	3.45	14.0	0.0035	0.0035
0.25	4.38	3.86	14.5	0.0031	0.0031
0.28	4.40	4.15	15.0	0.0030	0.0030

For an indirect determination of the total electron attachment rate constant $k_{a,t}(E/N)$ in pure SF_6 see Table 37 in Sec. 7.1.

6.3.2. $k_{a,t}(\langle\varepsilon\rangle)$

Since the electron energy distribution can be calculated as a function of E/N for Ar, Xe, and N_2, one can determine the total electron attachment rate constant as a function of the mean electron energy, $k_{a,t}(\langle\varepsilon\rangle)$, from measurements of $k_{a,t}(E/N)$ for SF_6 in low-concentration mixtures of SF_6 with each of these buffer gases. This facilitates a comparison of the measurements made in different buffer gases. In Fig. 30 are plotted the $k_{a,t}(\langle\varepsilon\rangle)$ for SF_6 based on the measurements of $k_{a,t}(E/N)$ made at room temperature in the buffer gases N_2,[108,225,228,264] Ar,[225,228] Xe,[228] and also C_2H_4.[108] The uncertainty in these data is likely to vary from $\pm 5\%$ to $\pm 15\%$ depending on E/N. Differences in the $k_{a,t}(\langle\varepsilon\rangle)$ values measured in the various buffer gases may reflect differences in the electron energy distribution functions $f(\varepsilon,E/N)$ and hence the mean electron energies. This may be especially

TABLE 29. Values of $k_{a,t}(E/N)$, and $\eta/N_a(E/N)$ for SF_6 measured in the buffer gases Ar and Xe by Hunter *et al.* (Ref. 228), and values of $w(E/N)$, and $\langle\varepsilon\rangle(E/N)$ for these buffer gases as reported by Hunter *et al.* (Ref. 228)

	SF_6/Ar				SF_6/Xe			
E/N (10^{-17} V cm^2)	$\langle\varepsilon\rangle$ (eV)	η/N_a (10^{-13} cm^2)	w (10^5 cm s^{-1})	$k_{a,t}$ (10^{-7} cm^3 s^{-1})	$\langle\varepsilon\rangle$ (eV)	η/N_a (10^{-12} cm^2)	w (10^5 cm s^{-1})	$k_{a,t}$ (10^{-7} cm^3 s^{-1})
0.003	0.130	26.8	0.533	1.43	—	—	—	—
0.004	0.178	16.5	0.668	1.10	0.0391	145.8	0.0153	2.23
0.005	0.213	11.4	0.750	0.854	0.0392	118.30	0.0191	2.26
0.006	0.240	8.92	0.803	0.716	0.0393	99.1	0.0230	2.28
0.007	0.260	7.49	0.840	0.629	0.0394	83.9	0.0268	2.25
0.008	0.277	6.19	0.869	0.538	0.0396	73.4	0.0308	2.26
0.010	0.304	4.94	0.915	0.452	0.0401	57.9	0.0387	2.24
0.012	—	—	—	—	0.0406	47.9	0.0469	2.25
0.0125	0.331	3.87	0.962	0.372	—	—	—	—
0.014	—	—	—	—	0.0414	39.4	0.0554	2.18
0.015	0.354	3.28	1.000	0.329	—	—	—	—
0.017	—	—	—	—	0.0432	31.0	0.0691	2.14
0.0175	0.375	2.91	1.040	0.302	—	—	—	—
0.02	0.394	2.66	1.070	0.285	0.0463	24.6	0.0849	2.09
0.03	0.461	1.89	1.190	0.224	0.0801	11.1	0.1690	1.87
0.05	0.570	1.21	1.360	0.165	0.3430	2.00	0.5110	1.02
0.07	0.663	0.904	1.490	0.135	0.5960	0.65	0.7420	0.48
0.10	0.784	0.648	1.650	0.107	0.7770	0.23	0.8610	0.20
0.15	0.956	0.433	1.850	0.080	0.9290	0.111	0.9240	0.1024
0.20	1.10	0.319	1.990	0.0637	1.03	0.0802	0.9820	0.0787
0.30	1.34	0.217	2.210	0.0480	1.18	0.0517	1.0500	0.0543
0.50	1.72	0.133	2.510	0.0335	1.40	0.0359	1.1500	0.0413
0.70	2.02	0.097	2.720	0.0265				
1.00	2.39	0.071	2.960	0.0210				
1.09[a]	2.49	0.0656	3.020	0.0192				
1.24	2.65	0.0581	3.120	0.0176				
1.55	2.95	0.0473	3.290	0.0154				
1.86	3.22	0.0403	3.450	0.0137				
2.17	3.48	0.0354	3.590	0.0125				
2.48	3.72	0.0317	3.720	0.0115				
2.79	3.94	0.0290	3.830	0.0108				
3.11	4.15	0.0263	3.960	0.0102				
3.42	4.33	0.0244	4.100	0.0096				

[a]Data beyond this E/N value were taken with another (higher pressure) electron swarm apparatus. The rest of the measurements were made using a pulsed Townsend technique.

true in the case of the Xe data since the cross sections for this buffer gas are not as well established (see below). The $\langle\varepsilon\rangle(E/N)$ values for the buffer gas ethylene are those determined from $\langle\varepsilon\rangle(E/N)=3/2(eD_T/\mu)(E/N)$, where $D_T/\mu(E/N)$ is the ratio of the lateral electron diffusion coefficient to electron mobility as a function of E/N for this gas.

In Fig. 30 are also plotted the $k_{a,t}(\langle\varepsilon\rangle)$ for SF_6 measured at room temperature in a Xe buffer gas by Shimamori *et al.*[267] using a pulse-radiolysis microwave cavity technique. The calibration of the mean electron energy in this study was made by analyzing the time profile of the microwave conductivity signals for ''thermalized'' electrons produced by pulsed x-rays in gaseous Xe and assuming a Maxwellian form for $f(\varepsilon,E/N)$. The data of Shimamori *et al.* obtained from measurements in a Xe buffer gas disagree with the data of Hunter *et al.*[228] obtained using the same buffer gas, and are not in good overall agreement with the other electron swarm data. This may indicate that the electron energy distribution functions in Xe as assumed by Shimamori *et al.* and as determined by Hunter *et al.* are different, and both are less accurate than those for the N_2 and Ar buffer gases.

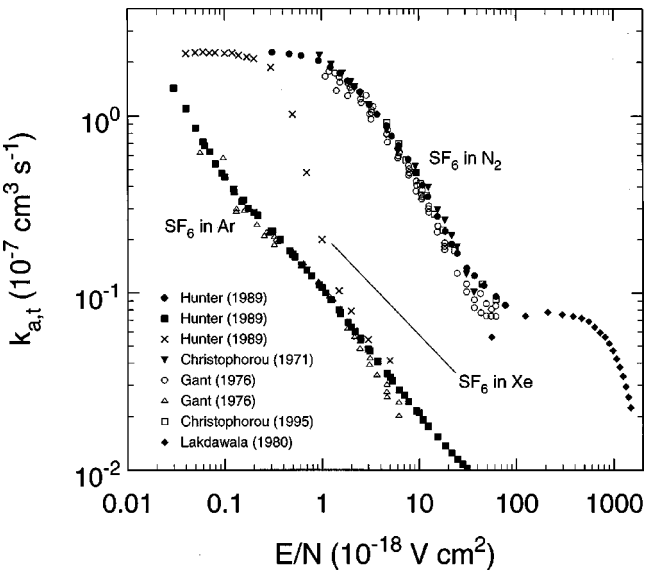

FIG. 29. Total electron attachment rate constant, $k_{a,t}(E/N)$, as a function of E/N for SF_6 measured in mixtures with various buffer gases: N_2 – (●) Ref. 228; (▼) Ref. 108; (○) Ref. 225; (♦) Ref. 263; (□) Ref. 264. Ar – (■) Ref. 228; (△) Ref. 225. Xe – (×) Ref. 228.

TABLE 30. Values of $k_{a,t}(E/N)$ and $\eta/N_a(E/N)$ for SF_6 measured in the buffer gas N_2 by Hunter *et al.* (Ref. 228), and values of $w(E/N)$, and $\langle\varepsilon\rangle(E/N)$ for this buffer gas as reported by Hunter *et al.* (Ref. 228)

	SF_6/N_2			
E/N (10^{-17} V cm^2)	$\langle\varepsilon\rangle$ (eV)	η/N_a (10^{-13} cm^2)	w (10^5 cm s^{-1})	$k_{a,t}$ (10^{-7} cm^3 s^{-1})
0.0311	0.0403	21.2	1.07	2.27
0.0466	0.0433	14.9	1.49	2.22
0.0621	0.0466	11.9	1.83	2.17
0.0932	0.0548	8.88	2.30	2.04
0.124	0.0644	7.27	2.57	1.87
0.155	0.0751	6.34	2.73	1.73
0.186	0.0864	5.55	2.83	1.57
0.217	0.0977	5.02	2.91	1.46
0.249	0.109	4.58	2.97	1.36
0.311	0.130	3.70	3.10	1.15
0.373	0.150	3.16	3.23	1.02
0.466	0.179	2.54	3.45	0.878
0.528	0.199	2.14	3.59	0.769
0.621	0.229	1.79	3.80	0.679
0.777	0.282	1.39	4.09	0.569
0.932	0.335	1.10	4.35	0.479
1.09	0.388	0.885	4.60	0.407
1.24	0.436	0.725	4.82	0.350
1.55	0.514	0.512	5.29	0.271
1.86	0.578	0.387	5.77	0.223
2.17	0.628	0.300	6.26	0.188
2.48	0.668	0.247	6.76	0.167
3.11	0.729	0.177	7.78	0.138
3.73	0.772	0.142	8.79	0.125
4.66	0.817	0.107	10.27	0.110
5.28	0.840	0.0903	11.25	0.102
6.21	0.870	0.0748	12.6	0.095
7.76	0.901	0.0567	15.0	0.085

Also plotted in Fig. 30 is the recommended value (2.25×10^{-7} cm^3 s^{-1}) of the thermal value, $(k_{a,t})_{th}$ ($T\sim300$ K), of the electron attachment rate constant (see Table 32, Sec. 6.3.3).

Besides the measurements of $k_{a,t}(\langle\varepsilon\rangle)$ made using the electron swarm method, there have been a number of other measurements of this quantity using the laser-photoelectron-attachment and the high-Rydberg-atom methods which have extended the values of $k_{a,t}(\langle\varepsilon\rangle)$ for SF_6 down to the μeV range. The results of these methods dealing with the electron attachment cross section for the formation of SF_6^- have been discussed earlier in Sec. 6.1. Most of the rate-constant measurements involving high-Rydberg atoms are normally given in terms of the dependence of the rate constant on the principal quantum number n or the effective principal quantum number n^* of the Rydberg atom involved (see Fig. 23). However, the bound-electron attachment rate constant, $k_{a,be}(\langle\varepsilon\rangle)$, can be expressed as a function of the average kinetic energy of the Rydberg electron which is given by R/n^2 or R/n^{*2}, where R is the Rydberg constant (13.6 eV) (see discussion in Sec. 6.1). In Fig. 30 are plotted the $k_{a,t}(\langle\varepsilon\rangle)$ data of Klar *et al.*[152] using the laser-photoelectron-attachment technique and the data of a number of investigators using the high-Rydberg-atom method. All data on the bound-electron attachment rate constants, $k_{a,be}(\langle\varepsilon\rangle)$, are shown in Fig. 30 by the same symbol (+), although they involve a number of studies and various Rydberg atoms: Xe*(nf) (Refs. 237 and 238), Rb*(ns,nd) (Ref. 241), K*(nd) (Refs. 242 and 245), K*(np) (Ref. 248), Na*(np) (Ref. 244), and Ne*(ns,nd) (Ref. 234). They refer to the production of SF_6^- and are consistent with the electron swarm measurements only for large n values (small values of $\langle\varepsilon\rangle$). The $k_{a,be}(\langle\varepsilon\rangle)$ becomes progressively smaller than $k_{a,t}(\langle\varepsilon\rangle)$ as the value of n decreases, that is, as the energy increases for the reasons discussed in Sec. 6.1.

We performed a least squares fit to only the swarm data in Fig. 30, excluding the measurements in the Xe buffer and also those in C_2H_4, and required the fit to agree with the recommended thermal value (2.25×10^{-7} cm^3 s^{-1}) of $k_{a,t}(\langle\varepsilon\rangle)$. This fit is shown by the solid line in Fig. 30, and recommended values of $k_{a,t}(\langle\varepsilon\rangle)$ in the energy range from 0.038 to 4.0 eV obtained from this fit are listed in Table 31.

6.3.3. Thermal Value, $(k_{a,t})_{th}$, of the Total Electron Attachment Rate Constant

Many measurements have been made of this quantity which vary significantly. They are summarized in Table 32. The most reliable data lie between 2.2×10^{-7} and 2.3

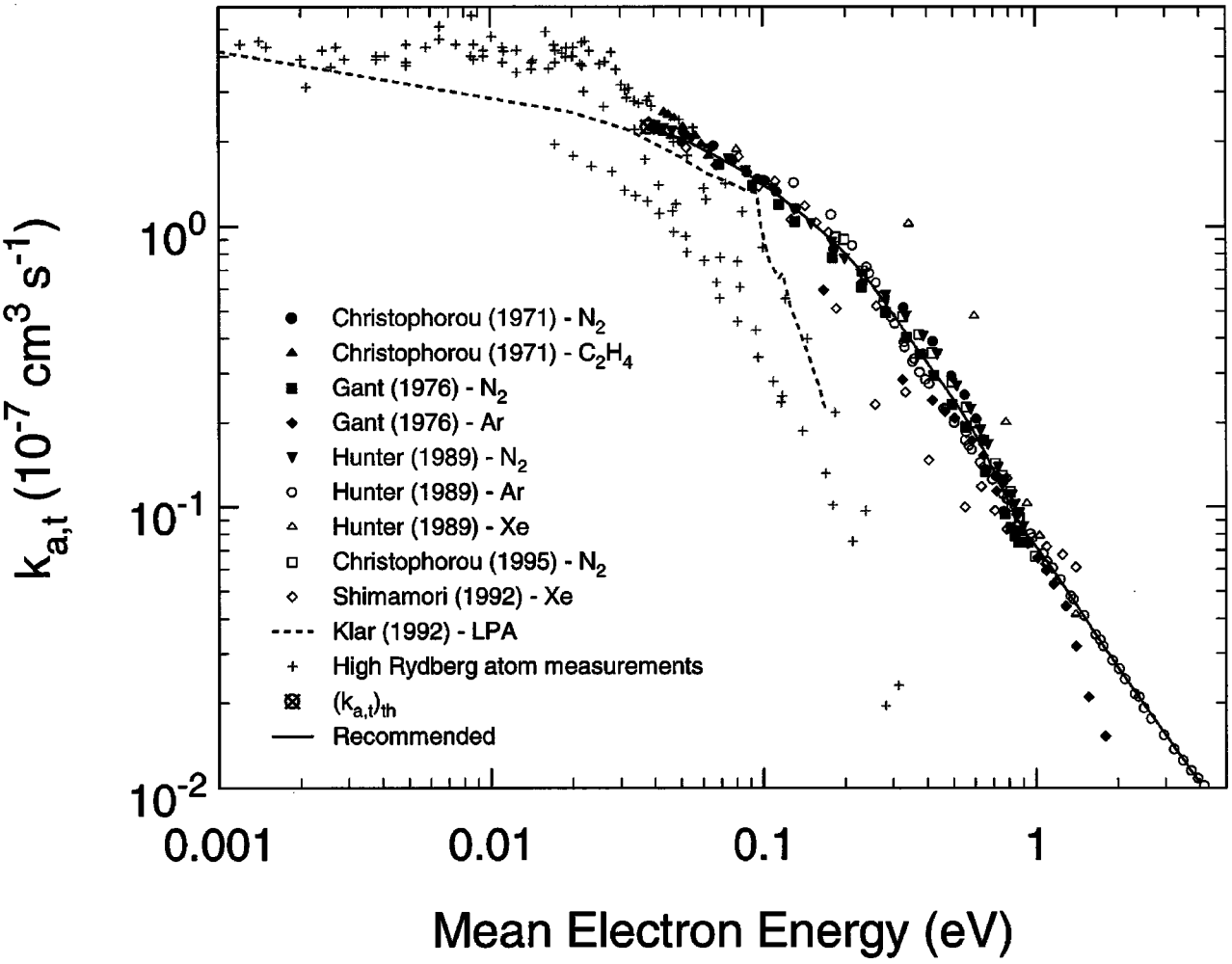

FIG. 30. Total electron attachment rate constant, $k_{a,t}(\langle\varepsilon\rangle)$, for SF_6 as a function of the mean electron energy $\langle\varepsilon\rangle$. For the electron swarm data, measurements were made in the buffer gases indicated in the legend. Electron swarm measurements: (●), (▲) Ref. 108; (■), (◆) Ref. 225; (▼), (○), (△) Ref. 228; (□) Ref. 264; (◇) Ref. 267; (⊗) Recommended value of $(k_{a,t})_{th}$. Laser photoelectron attachment measurements: (- - -) Ref. 152. High-Rydberg-atom measurements: (+), this same symbol was used for data from all of the following sources: West *et al.* in Ref. 237 [Xe*(nf)]; Foltz *et al.* in Ref. 238 [Xe*(nf)]; Zollars *et al.* in Ref. 241 [Rb*(ns,nd)]; Zollars *et al.* in Ref. 242 [K*(nd)]; Beterov *et al.* in Ref. 244 [Na*(np)]; Zheng *et al.* in Ref. 245 [K*(nd)]; Harth *et al.* in Ref. 234 [Ne*(ns,nd)]; and Ling *et al.* in Ref. 248 [K*(np)]. The recommended values of $k_{a,t}(\langle\varepsilon\rangle)$ are shown by the solid line.

$\times 10^{-7}$ cm^3 s^{-1}. The average of the ten values in this range is 2.25×10^{-7} cm^3 s^{-1} which is our recommended value.

6.4. Effect of Temperature on Electron Attachment to SF_6

6.4.1. Effect of Temperature on the Production of SF_5^- from SF_6

In Fig. 31 are shown the relative cross section measurements of Chen and Chantry[110] for the production of SF_5^- from SF_6 at temperatures ranging from 300 to 880 K. Two peaks are seen in the energy dependence of the production of SF_5^-, one at $\sim$0.0 eV and the other at near 0.38 eV. The near-zero-energy peak is very sensitive to temperature, has an activation energy of $\sim$0.2 eV,[110] and is due to dissociative electron attachment to ''hot'' SF_6 molecules, i.e., due to attachment of near-zero-energy electrons to vibrational/rotational states of SF_6 lying at energies 0.2 eV above the molecular ground state

TABLE 31. Recommended values for the total electron attachment rate constant, $k_{a,t}(\langle\varepsilon\rangle)$, of SF_6 as a function of the mean electron energy $\langle\varepsilon\rangle$

$\langle\varepsilon\rangle$ (eV)	$k_{a,t}(\langle\varepsilon\rangle)$ (10^{-7} cm^3 s^{-1})	$\langle\varepsilon\rangle$ (eV)	$k_{a,t}(\langle\varepsilon\rangle)$ (10^{-7} cm^3 s^{-1})
0.038	2.25	0.5	0.241
0.04	2.20	0.6	0.181
0.05	2.05	0.7	0.135
0.06	1.88	0.8	0.103
0.07	1.74	0.9	0.0833
0.08	1.62	1.0	0.0721
0.09	1.51	1.5	0.0406
0.10	1.41	2.0	0.0268
0.15	1.04	2.5	0.0197
0.20	0.801	3.0	0.0154
0.25	0.622	3.5	0.0125
0.30	0.487	4.0	0.0104
0.40	0.327		

TABLE 32. Thermal ($T=295-300$ K) values $(k_{a,t})_{th}$ of the total electron attachment rate constant for SF_6

$(k_{a,t})_{th}$ (10^{-7} cm^3 s^{-1})	Reference
0.385	198
2.06 ± 0.08	268
2.13 ± 0.04	269
2.2	270
2.2 ± 0.1	271
2.20	272
2.27 ± 0.07	254
2.24 ± 0.15	256
2.27 ± 0.09	256
2.3	273
2.3 ± 0.2	267
2.25 ± 0.2	228
2.30 ± 0.1	228
2.41	274
2.5	275
2.6	276
2.70	108
2.78	108
2.77	277
2.8 ± 0.3	278
3.1	279
3.1 ± 0.47	280
2.25×10^{-7} cm^3 s^{-1}	**Recommended value**

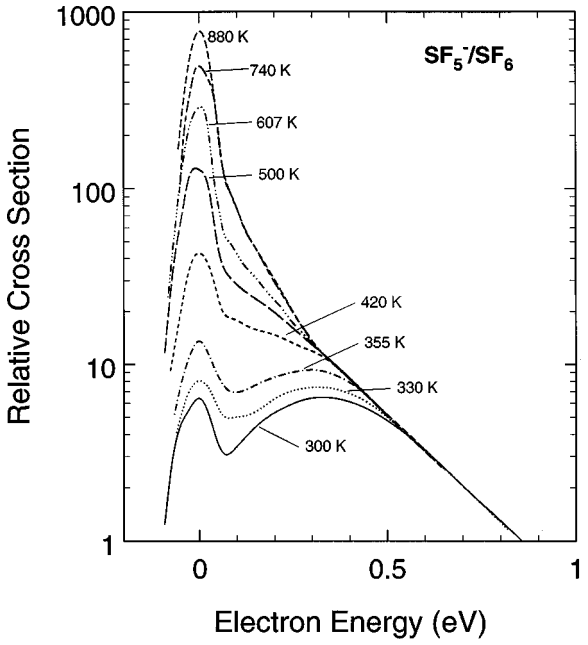

FIG. 31. Temperature dependence of the relative cross section for the formation of SF_5^- by electron impact on SF_6 (data of Chen and Chantry from Ref. 110).

$$SF_6^*(\nu, r \gtrsim 0.2\,\text{eV}) + e(\sim 0\,\text{eV}) \rightarrow SF_5^- + F. \qquad (9)$$

The 0.38 eV peak is broad, insensitive to temperature variation, and results from the capture of ~ 0.38 eV electrons by unexcited SF_6 molecules reaching the lowest repulsive negative ion state of SF_6^-, that is, due to the reaction

$$SF_6(\nu=0) + e(\sim 0.38\,\text{eV}) \rightarrow SF_5^- + F \qquad (10)$$

(see, however, Refs. 259 and 281). It is interesting to observe that in spite of this large increase in the formation of SF_5^- from SF_6 with increasing T, the total electron attachment rate constant and cross section at near-zero-electron energy (Sec. 6.4.2) is independent of T. This may imply that at ~ 0.0 eV, the formation of SF_6^- in electron beam experiments where the $SF_6^-{}^*$ is not stabilized by collision or radiation prior to its detection, decreases with T. Indeed, such a decrease has been observed[219] and would be consistent with the decrease in the autodetachment lifetime of $SF_6^-{}^*$ with increasing internal energy of the transient anion.[201] The data in Fig. 31 can be put on an absolute scale by considering the magnitude of the cross section for the production of SF_5^- at 0.38 eV at room temperature. A value of $\sim 3.8\times10^{-16}$ cm^2 is suggested from Fig. 24(b) and Table 25.

The strong increase of the cross section for the production of SF_5^- from SF_6 with increasing vibrational excitation energy of the SF_6 molecule has led Chen and Chantry[110] to anticipate that the zero-energy peak in Fig. 31 could be photoenhanced. Thus, they used specific lines from a CO_2 laser to produce (via n-photon absorption processes, $n \geq 1$) vibrationally excited SF_6 molecules, SF_6^*, and observed the production of SF_5^- from electron impact on SF_6^* as a function of the electron energy, viz.

$$n(h\nu)_{laser} + SF_6 \rightarrow (SF_6^*)_{laser} \text{ followed by } (SF_6^*)_{laser} + e \rightarrow (SF_5)^-_{laser} + F. \qquad (11)$$

Chen and Chantry found that the production of SF_5^- from electron impact on SF_6^* is enhanced and that this infrared enhancement of SF_5^- production is different for the ^{32}S and ^{34}S isotopes. Thus, the formation of SF_5^- was found to be radiation-wavelength dependent. With the 936.856 cm^{-1} CO_2 line the $^{32}SF_5^-$ enhancement was optimized and the $^{34}SF_5^-$ was unaffected. With the 920.810 cm^{-1} CO_2 laser line the $^{34}SF_5^-$ line was optimized and the $^{32}SF_5^-$ was unaffected. This isotopic specificity is an illustration of possible isotope separation processes using knowledge of low-energy electron–molecule reactions. It is consistent with the earlier observations of Beterov *et al.*[282] and Beterov and Fateyev[283] of optogalvanic effects when they used a CO_2 laser to vibrationally excite SF_6 molecules (see also Avrillier and Schermann[284]).

6.4.2. Effect of Temperature on the Total Electron Attachment Rate Constant, $k_{a,t}(\langle\varepsilon\rangle, T)$

In Table 33 are listed the thermal values, $(k_{a,t})_{th}$, of the total electron attachment rate constant for SF_6 as a function of gas temperature.[108,198,256,272,273,277,280] Although the data listed in Table 33 show $(k_{a,t})_{th}$ to be virtually constant for T between about 300 and 600 K, the more recent measurements of Le Garrec *et al.*[277] below room temperature indicate a small increase with increasing T in the low-temperature range they investigated [see Table 33 and Fig. 32(a)].

TABLE 33. Variation with temperature of the thermal electron attachment rate constant, $(k_{a,t})_{th}$, of SF_6

$(k_{a,t})_{th}$ $(10^{-7}\ cm^3\ s^{-1})$	Temperature (K)	Reference(s)
2.70	298–418	108, 198
2.20	293–523	272
3.10	205	280
3.10	300	
4.50	455	
4.00	590	
2.27	294	256
2.20	500	
2.30	300	273
2.60	329	
2.80	362	
3.10	411	
2.80	449	
2.70	498	
2.20	545	
1.41	49	277
1.44	85	
1.42	126	
1.65	162	
1.73	174	
2.77	304	

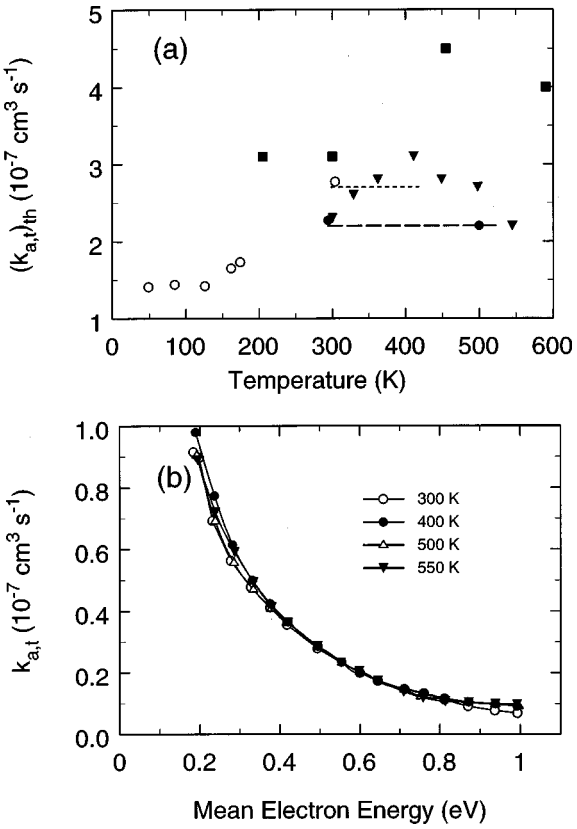

FIG. 32. (a)Variation of the rate constant for electron attachment to SF_6 at thermal electron energies with gas temperature (see Table 33): (- - -) Refs. 108, 198; (– –) Ref. 256; (▼) Ref. 273; (○) Ref. 277; (■) Ref. 280; (●) Ref. 272. (b) Variation of the rate constant for electron attachment to SF_6 as a function of mean electron energies for a range of temperatures. The data are those of Christophorou and Datskos from Ref. 264 taken for mixtures of SF_6 in N_2 buffer gas.

Consistent with the finding that the thermal electron attachment rate constant for SF_6 is independent of T for temperatures a few hundred degrees above ambient, are the results of a beam study[222] which showed the energy-integrated total electron attachment cross section at thermal (and near-thermal) energies to be independent of T in the range from 300 to 1200 K. Interestingly, the temperature independence of the total rate of electron attachment to SF_6 is evident for mean energies up to at least 1 eV as can be seen from the data in Fig. 32(b).[264,285]

6.5. Density-Reduced Electron Attachment Coefficient, $\eta/N(E/N)$

There have been at least 17 room-temperature (293–298 K) measurements of $\eta/N(E/N)$ in pure SF_6,[26,175,177,178,180–186,188,189,286–290] over a period of 40 yr, normally at high E/N to avoid the difficulty arising from the strong electron attachment at low E/N. They mostly employed the steady-state Townsend or the pulsed-Townsend methods. The more recent time-resolved measuring techniques provided an improvement over the traditional avalanche-shape method. All determinations except that of Kline *et al.*[26] assumed that electron detachment is negligible in these measurements and this is a reasonable assumption[26,180,291] (see also Sec. 8).

The experimental results obtained by these methods are shown in Fig. 33. Their quoted uncertainties range from $\pm 5\%$ to $\pm 15\%$, but clearly some of the data diverge considerably more than this. For instance, this is the case for the lowest five data points of McAffee and Edelson[286] [their E/N dependence is inconsistent with the well-established steep rise of the electron attachment rate constant as the E/N (or $\langle\varepsilon\rangle$) decreases toward zero (Figs. 29 and 30)], and for the measurements of Siddagangappa *et al.*[288,289] The solid line in Fig. 33 up to $E/N = 450\times10^{-17}\ V\ cm^2$ is a least squares fit to all the data except those just mentioned. (Aschwanden[186] reported two values of η/N at each value of E/N for which he made measurements below $243\times10^{-17}\ V\ cm^2$. In Fig. 33 are only plotted the lower set of values since these are consistent with the other available measurements.) For E/N values above $450\times10^{-17}\ V\ cm^2$, we prefer the data of Aschwanden,[185,186] as opposed to the other diverging data.[180–182,184,189,290] Aschwanden's data are more consistent with the values (broken line in Fig. 33) of $\eta/N(E/N)$ we obtained from $\alpha/N(E/N)-[(\alpha-\eta)/N(E/N)]$ using our recommended values for $\alpha/N(E/N)$ (Fig. 17) and $(\alpha-\eta)/N(E/N)$ (Fig. 34). Values obtained from the solid line in Fig. 33 are listed in Table 34 as our recommended values for the $\eta/N(E/N)$ of SF_6.

It should be noted that there have been a number of calculations of the $\eta/N(E/N)$ of SF_6 using Boltzmann and Monte Carlo codes (e.g., see Refs. 11, 26–28, 30–34, 38, 40, 41, and 44). These, however, are not discussed here.

Finally, it should be pointed out that one can determine

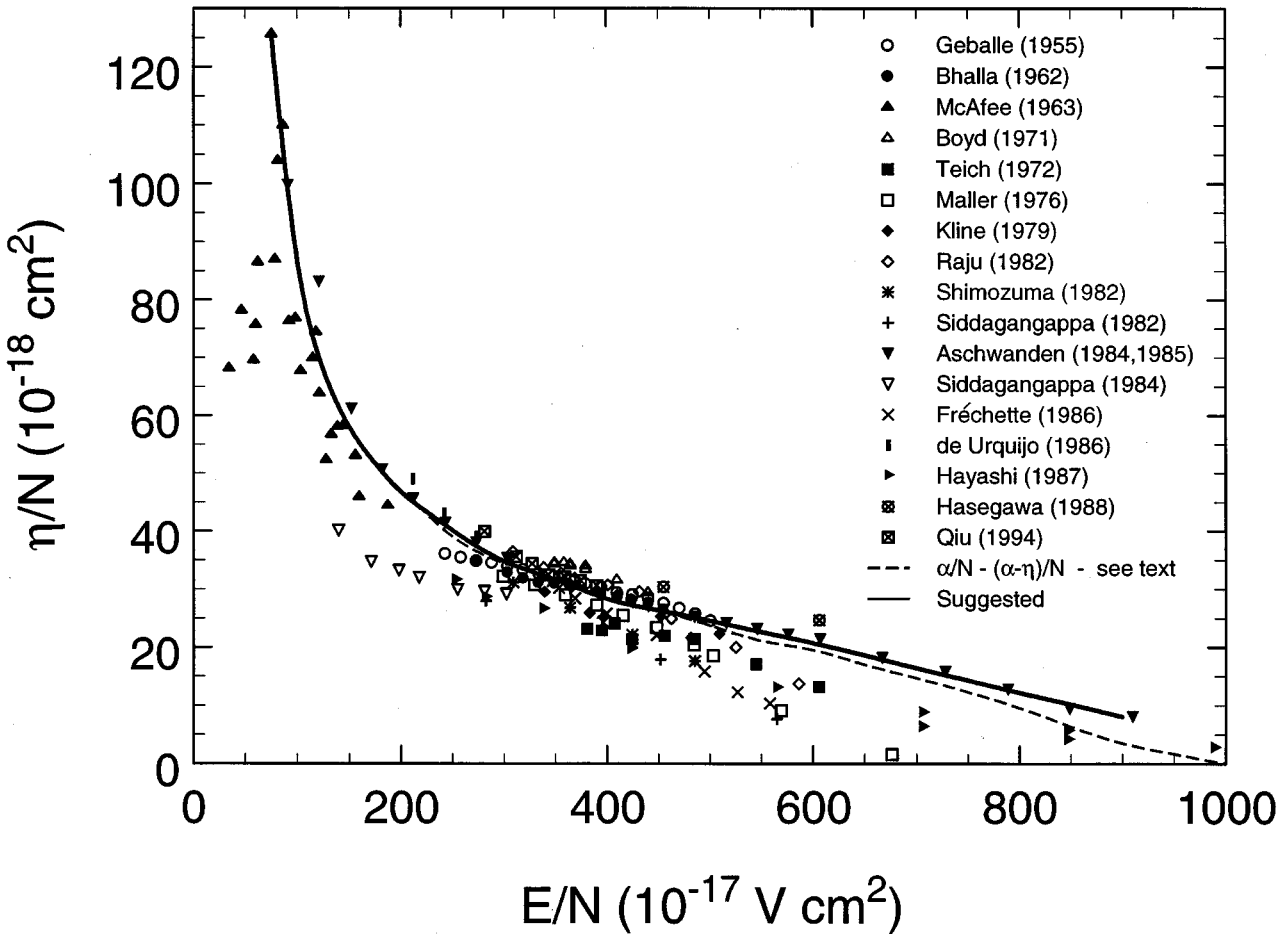

FIG. 33. Measured density-reduced electron attachment coefficient, $\eta/N\,(E/N)$, for SF_6: (○) Ref. 175; (●) Ref. 177; (▲) Ref. 286; (△) Ref. 178; (■) Ref. 184; (□) Ref. 180; (◆) Ref. 26; (◇) Ref. 287; (*) Ref. 181; (+) Ref. 288; (▼) Refs. 185 and 186; (▽) Ref. 289; (×) Ref. 290; (▮) Ref. 188; (▶) Ref. 182; (⊗) Ref. 189; (⊠) Ref. 183; (- - -) $(\alpha/N)-(\alpha-\eta)/N$ (see text); (—) suggested.

values of $\eta/N_a(E/N)$ [where N_a refers to the SF_6 gas number density in a mixture with a buffer gas of density N ($N \gg N$a)] for SF_6 in various buffer gases (N_2, Ar, Xe) from the electron-attachment-rate constant data presented in Sec. 6.3 by making use of the $w(E/N)$ values in the corresponding buffer gases (Tables 29 and 30). Furthermore, if the $\langle\varepsilon\rangle(E/N)$ is known (as in the measurements of $\eta/N_a(E/N)$ for SF_6 in N_2, Ar, and Xe buffer gases by Hunter *et al.*[228]), values of $\eta/N_a(\langle\varepsilon\rangle)$ can be obtained.

6.6. Density-Reduced Effective Ionization Coefficient, $(\alpha-\eta)/N(E/N)$

The data from direct experimental measurements of the density-reduced effective ionization coefficient, $(\alpha-\eta)/N(E/N)$,[26,175,177,178,181,183,185,186,189,287,290,292–295] are compared in Fig. 34 [Fig. 34(b) is an expanded view of a portion of Fig. 34(a)]. The solid line in Fig. 34 represents our recommended data for $(\alpha-\eta)/N(E/N)$ up to an $E/N = 4000\times10^{-17}\,\mathrm{V\,cm^2}$, based upon a fit to all of the available data. Values obtained from this line are listed in Table 35. Analysis of the data in Fig. 34 in the region near where $(\alpha-\eta)/N(E/N)=0$ gives a so-called critical value, $(E/N)_{cr}$, of E/N (the value of E/N at which $\eta/N=\alpha/N$) of $(359.3\pm3)\times10^{-17}\,\mathrm{V\,cm^2}$.

For $E/N > 4000\times10^{-17}\,\mathrm{V\,cm^2}$, there is only one set of measurements, namely, that of Hasegawa *et al.*[189] made using the steady-state Townsend method. As discussed previ-

TABLE 34. Recommended values of the density-reduced electron attachment coefficient $\eta/N\,(E/N)$ for SF_6 as a function of E/N

E/N (10^{-17} V cm^2)	$\eta/N\,(E/N)$ (10^{-18} cm^2)	E/N (10^{-17} V cm^2)	$\eta/N\,(E/N)$ (10^{-18} cm^2)
75	126	450	26.3
100	87	500	24.5
125	68	550	22.6
150	58.0	600	20.7
175	51.7	650	18.6
200	46.8	700	16.4
225	43.3	750	14.3
250	40.1	800	12.2
300	34.8	850	10.2
350	31.6	900	8.06
400	28.3		

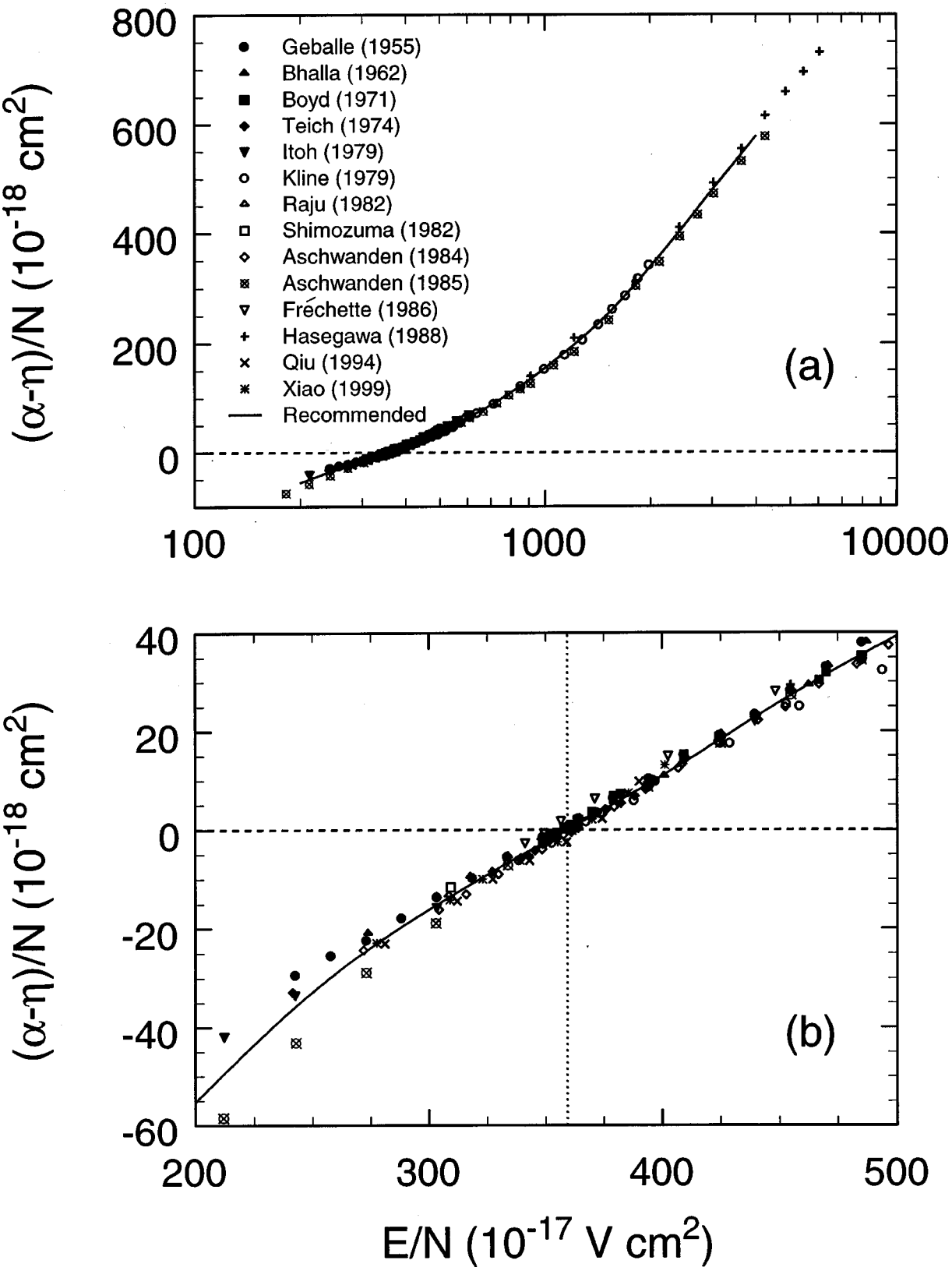

FIG. 34. (a) Measured density-reduced effective ionization coefficient, $(\alpha-\eta)/N\,(E/N)$, for SF_6, (b) an expanded portion of Fig. 34(a): (●) Ref. 175; (▲) Ref. 177; (■) Ref. 178; (♦) Ref. 295; (▼) Ref. 292; (○) Ref. 26; (△) Ref. 287; (□) Ref. 181; (◇) Ref. 185; (⊗) Ref. 186; (▽) Ref. 290; (+) Ref. 189; (×) Ref. 183; (*) Ref. 293; (—) recommended. The dotted vertical line in Fig. 34(b) shows $(E/N)_{cr}=(359.3\pm3)\times10^{-17}$ V cm^2.

TABLE 35. Recommended values of the density-reduced effective ionization coefficient $(\alpha-\eta)/N\,(E/N)$ for SF_6 as a function of E/N

E/N (10^{-17} V cm^2)	$(\alpha-\eta)/N\,(E/N)$ (10^{-18} cm^2)	E/N (10^{-17} V cm^2)	$(\alpha-\eta)/N\,(E/N)$ (10^{-18} cm^2)
200	−55.3	800	110
250	−32.8	850	122
300	−16.1	900	132
350	−2.43	950	143
400	10.9	1000	154
450	25.8	1250	204
500	39.3	1500	250
550	51.9	2000	338
600	63.8	2500	413
650	75.2	3000	478
700	87.0	3500	531
750	98.8	4000	578

ously, the values of Hasegawa *et al.*[189] of $(\alpha-\eta)/N$ for $E/N>4000\times10^{-17}$ V cm^2 agree with the α/N values of Hayashi and Wang.[182]

Finally, it should be noted that measurements of $(\alpha-\eta)/N(E/N)$ in mixtures of SF_6 with Xe have been made by Hilmert *et al.*[296] and Xiao *et al.*[297] Similar measurements have also been made by Qiu and Xiao[183] in mixtures of SF_6 with Ar and Kr, and by Xiao *et al.*[293] in mixtures of SF_6 with Ne.

7. Electron Transport in SF_6

7.1. Electron Drift Velocity, $w(E/N)$

The experimental data[185,186,293,294,298–304] on $w(E/N)$ for SF_6 are plotted in Fig. 35. These measurements were taken at ''room temperature'' (~293–300 K) and generally at high values of E/N. The reported uncertainties range from <1% to 15%, as evidenced by the uncertainty of ±15% reported by Harris and Jones,[298] ±5% claimed by Naidu and Prasad,[300] and the very low uncertainty of ±0.5% quoted by Aschwanden.[185] In general, the lower the E/N, the higher the expected uncertainty.

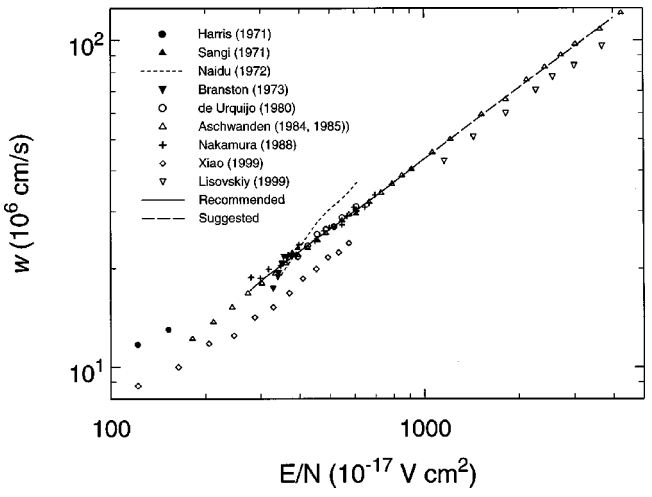

FIG. 35. Electron drift velocity, $w\,(E/N)$, in SF_6: (●) Ref. 298; (▲) Ref. 299; (- - -) Ref. 300; (▼) Ref. 301; (○) Ref. 302; (△) Refs. 185 and 186; (+) Ref. 303; (◇) Ref. 293; (▽) Ref. 304; (—) recommended values.

TABLE 36. Recommended, suggested, and deduced values of the electron drift velocity $w\,(E/N)$ for SF_6 (see text)

E/N (10^{-17} V cm^2)	$w\,(E/N)$ (10^6 cm/s)	E/N (10^{-17} V cm^2)	$w\,(E/N)$ (10^6 cm/s)
0	[0.0][a]	650	31.7
25	[4.1]	700	33.4
50	[6.8]	750	35.1
100	[10.2]	800	36.8
150	[12.1]	850	38.5
200	[13.5]	900	40.1
250	[15.6]	950	41.8
275	17.0[b]	1000	43.4
300	18.3	1500	(58.3)[c]
350	20.5	2000	(71.7)
400	22.6	2500	(83.9)
450	24.6	3000	(95.4)
500	26.4	3500	(106.3)
550	28.2	4000	(116.8)
600	30.0		

[a]Values in square brackets are deduced from available data (see text).
[b]Recommended values.
[c]Values in parenthesis are suggested data based upon the measurements of Aschwanden (Ref. 186).

In the E/N range between $\sim250\times10^{-17}$ and $\sim600\times10^{-17}$ V cm^2, the data are more consistent than in the low E/N region. The solid line in Fig. 35 represents a fit to all measurements in the E/N range of 250×10^{-17}–1000×10^{-17} V cm^2, except those of Branston,[301] Naidu and Prasad,[300] and Xiao *et al.*[293,294] The reason for excluding these three sets of measurements is because the first two do not show the correct dependence of the electron drift velocity on E/N, and the third is consistently ~20% lower in magnitude than the rest of the data. Values from the solid line in Fig. 35 are given in Table 36 as our recommended data for the $w(E/N)$ in SF_6.

Above $E/N=1000\times10^{-17}$ V cm^2, there are only two sets of measurements, namely, those of Aschwanden[186] and those of Lisovskiy and Yegorenkov.[304] The latter lie systematically lower than the former, but the data sets agree within combined uncertainties. Since the measurements of Aschwanden agree well with the other data at lower E/N, we choose his data as our suggested values of $w(E/N)$ for $E/N>1000\times10^{-17}$ V cm^2. These suggested values are shown in Fig. 35 by the broken line and are listed in parenthesis in Table 36.

There are no reliable experimental measurements for the electron drift velocity $w(E/N)$ in SF_6 at low E/N. The data of Harris and Jones[298] are not direct measurements, but rather values based on an empirical formula they deduced from their measurements. The values of w at low E/N are difficult to measure because the strong electron attachment at low E/N depletes the electrons and results in very weak electron currents. This may also prevent the electron swarm from reaching a steady-state condition with regard to electron attachment.[305] Unfortunately, there are no calculated

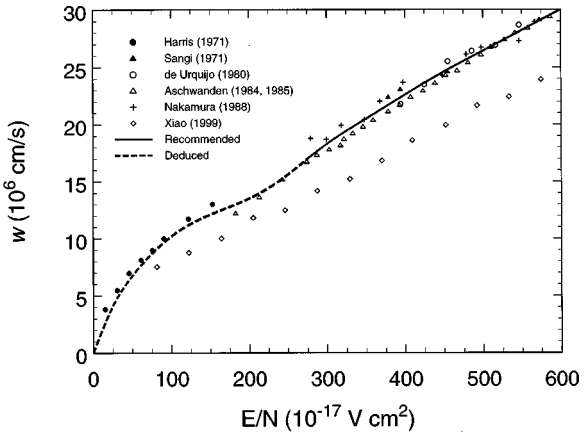

FIG. 36. Electron drift velocity, $w\,(E/N)$, in SF_6 at low E/N (see text): (●) Ref. 298; (▲) Ref. 299; (○) Ref. 302; (△) Refs. 185 and 186; (+) Ref. 303; (◇) Ref. 293; (—) recommended values from Fig. 35; (- - -) deduced values for low E/N.

values of $w(E/N)$ at low E/N either. Calculations using the Boltzmann transport equation or the Monte Carlo method (e.g., Refs. 11, 26, 27, 30–32, 34, 38–41, 44, and 306) do not extend to low E/N. However, in an effort to provide an estimate of the $w(E/N)$ in SF_6 at low E/N, we have fit a curve to the limited data below 300×10^{-17} V cm^2, requiring that the fitted curve goes through the origin since $w(E/N)=0$ at $E/N=0$. This fit is shown by the broken line in Fig. 36, and values from the broken curve are presented (in brackets) in Table 36 as our deduced values for $w(E/N)$ for $E/N\leqslant250\times10^{-17}$ V cm^2 in lieu of direct measurements. It is emphasized that for electronegative gases, such as SF_6 for which the electron attachment cross section is very large at thermal and near thermal electron energies, the definition of electron drift velocity becomes questionable in the E/N region where the majority of electrons are attached prior to reaching a steady-state electron energy distribution.

Now that we have been able to obtain independent values of $\eta/N(E/N)$ and $w(E/N)$, we can determine their product, $\eta/N(E/N)\times w(E/N)$, which represents the total electron attachment rate constant, $k_{a,t}(E/N)$, for SF_6 as a function of E/N in pure SF_6. Values of this quantity are listed in Table 37. Since, moreover, plots of the electron attachment rate constant as a function of the mean electron energy, $k_{a,t}(\langle\varepsilon\rangle)$, in various buffer gases is a unique function of the mean electron energy (see Fig. 30), one may infer that the rate constant $k_{a,t}$ measured in a buffer gas A has the same magnitude as measured in a buffer gas B, when the E/N values in A and B are such that the mean electron energies in the two buffer gases are the same. From such considerations, we infer from the data in Table 37 and Fig. 30, that the mean electron energy in pure SF_6 at $E/N=100\times10^{-17}$ V cm^2 is $\sim$4.5 eV. Unfortunately, the data in Table 37 do not extend to sufficiently low E/N to allow determination of $\langle\varepsilon\rangle$ for SF_6 at $E/N<100\times10^{-17}$ V cm^2. An estimate of the mean electron energies at 350×10^{-17} V cm$^2<E/N<700\times10^{-17}$ V cm^2 can be made by considering the values of the characteristic electron energy $[3/2(eD_T/\mu)]$ inferred from the $D_T/\mu(E/N)$ data in Sec. 7.2 (Fig. 37). From these data, the characteristic energy in SF_6 is estimated to be 7.4 eV at $E/N=400\times10^{-17}$ V cm^2 and 8.6 eV at $E/N=650\times10^{-17}$ V cm^2.

TABLE 37. Assessed values of $\eta/N\,(E/N)$ and $w\,(E/N)$, and their product—total electron attachment rate constant $k_{a,t}\,(E/N)$—for pure SF_6 (see text)

E/N (10^{-17} V cm^2)	$w\,(E/N)$ (10^6 cm s^{-1})	$\eta/N\,(E/N)$ (10^{-18} cm^2)	$k_{a,t}\,(E/N)$ (10^{-12} cm^3 s^{-1})
100	10.2	87.0	887
150	12.1	58.0	702
200	13.5	46.8	632
250	15.6	40.1	626
300	18.3	34.8	637
350	20.5	31.6	648
400	22.6	28.3	440
450	24.6	26.3	647
500	26.4	24.5	647
550	28.2	22.6	637
600	30.0	20.7	621
650	31.7	18.6	590

7.2. Transverse Electron Diffusion Coefficient to Electron Mobility Ratio, $D_T/\mu(E/N)$

In Fig. 37 are plotted the values of $D_T/\mu(E/N)$ as measured by Naidu and Prasad[300] at 293 K. These are the mean values of a number of measurements made at a pressure of 0.27 kPa. Also plotted in Fig. 37 are similar subsequent measurements made by Maller and Naidu[307] along with their indicated errors. The two sets of measurements are consistent with each other. A fit to the most recent data is shown by the solid line in the figure and is listed in Table 38 as our presently suggested values of the $D_T/\mu(E/N)$ for SF_6. They can be used to determine the characteristic energy, $3/2(eD_T/\mu)$, of electrons in SF_6 gas as a function of E/N. Calculated

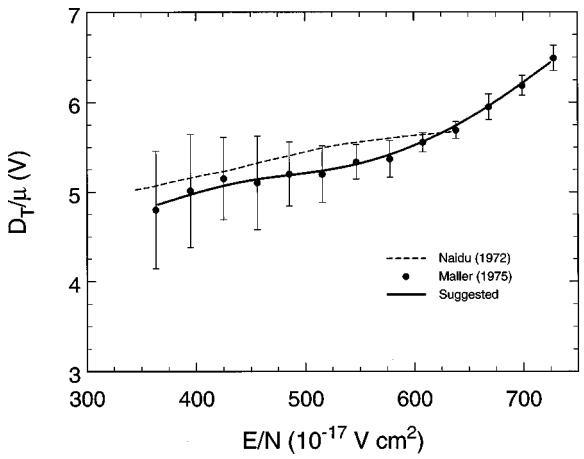

FIG. 37. Transverse electron diffusion coefficient to electron mobility ratio as a function of E/N, $D_T/\mu\,(E/N)$, for SF_6: (- - -) Ref. 300; (●) Ref. 307; (—) suggested values.

TABLE 38. Suggested values of the transverse electron diffusion coefficient to electron mobility ratio $D_T/\mu\,(E/N)$ for SF_6

E/N (10^{-17} V cm^2)	$D_T/\mu\,(E/N)$ (V)	E/N (10^{-17} V cm^2)	$D_T/\mu\,(E/N)$ (V)
365	4.86	600	5.52
400	4.99	650	5.82
450	5.13	700	6.22
500	5.21	725	6.44
550	5.32		

values of $D_T/\mu(E/N)$ for SF_6 using Boltzmann code analysis or the Monte Carlo method can be found in Refs. 11, 26–28, 30–32, 34, 39–41, 43, and 44.

7.3. Product of Gas Number Density and Longitudinal Electron Diffusion Coefficient, $ND_L(E/N)$

There are three sets of measurements[185,186,293] of this quantity which are plotted in Fig. 38. Two of these are by Aschwanden[185,186] and have uncertainties as shown by the error bars in the figure. The other set of mesurements is by Xiao *et al.*[293] who state no uncertainties. The solid line in Fig. 38 represents a fit to the three data sets, and values from this fit are listed in Table 39 as our suggested data for the $ND_L(E/N)$ of SF_6. Calculated values of the longitudinal electron diffusion coefficient D_L (or ND_L or D_L/μ) using a Boltzmann code analysis or the Monte Carlo method can be found in Refs. 27, 39–41, 43, and 44.

8. Autodetachment, Thermally Induced Detachment, Photodetachment, and Collisional Detachment of SF_6^-

Electron detachment from SF_6^- ions is an important process of basic and applied interest. It can be induced via a number of ways, for instance, automatically from unstable

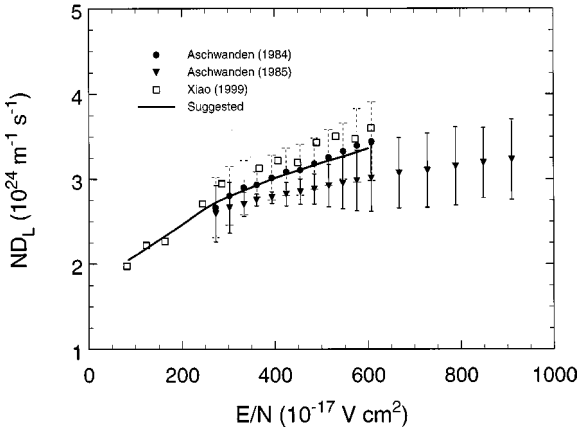

FIG. 38. Measured values of the product, $ND_L(E/N)$, of the gas number density N and the longitudinal electron diffusion coefficient D_L as a function of E/N for SF_6: (●) Ref. 185; (▼) Ref. 186; (□) Ref. 293; (—) suggested values.

TABLE 39. Suggested values of the product of the gas number density and the longitudinal electron diffusion coefficient $ND_L\,(E/N)$ for SF_6

E/N (10^{-17} V cm^2)	$ND_L\,(E/N)$ (10^{24} m^{-1} s^{-1})	E/N (10^{-17} V cm^2)	$ND_L\,(E/N)$ (10^{24} m^{-1} s^{-1})
85	2.05	350	2.90
100	2.10	400	3.01
150	2.28	450	3.10
200	2.46	500	3.19
250	2.65	550	3.27
300	2.79	600	3.36

SF_6^-*, or from SF_6^-* or SF_6^- by an applied electric field, or by heat, or by collision with photons, electrons, or neutral species. In this section we briefly elaborate on the autodetachment of SF_6^-* and summarize pertinent findings on thermally induced detachment, photodetachment, and collisional detachment of SF_6^- (see, also, Refs. 14, 202, 308, and 309).

8.1. Autodetachment

As shown in the previous section, low-energy free electrons attach very efficiently to the SF_6 molecule forming SF_6^-* parent anions. The initially produced isolated SF_6^-* parent ion is long lived, but metastable. Its mean lifetime toward autodetachment, that is, for the process

$$SF_6^-{}^* \rightarrow SF_6^{(*)} + e \tag{12}$$

is $>1\ \mu$s. Process (12) is a function of the internal energy of the unstable SF_6^-*.[202] Alternatively, the unstable SF_6^-* species can be easily stabilized by collision

$$SF_6^-{}^* + \text{collision} \rightarrow SF_6^- + \text{energy} \tag{13}$$

and/or by emission of infrared radiation $h\nu$

$$SF_6^-{}^* \rightarrow SF_6^- + h\nu. \tag{14}$$

8.2. Thermally Induced Detachment

The possible effect of temperature on electron detachment from stabilized SF_6^- ions has recently been investigated by Christophorou and collaborators.[264,285] These studies have shown that when the gas temperature was raised from 300 to $\sim$600 K, thermally enhanced electron detachment is observed for such negative ions as $C_6F_6^-$ and c-$C_4F_6^-$, but not for SF_6^-, that is, not for the reaction

$$SF_6^- + \text{heat} \rightarrow SF_6 + e. \tag{15}$$

This may be related to the relatively larger electron affinity of the SF_6 molecule (1.06 eV, Table 5) compared to those of the other two molecules (<0.5 eV).[264,285,310] Also, the energetically stabilized SF_6^- ion does not detach in collisions with SF_6 for collision energies less than $\sim$90 eV (see Refs. 311 and 312, and Sec. 8.4).

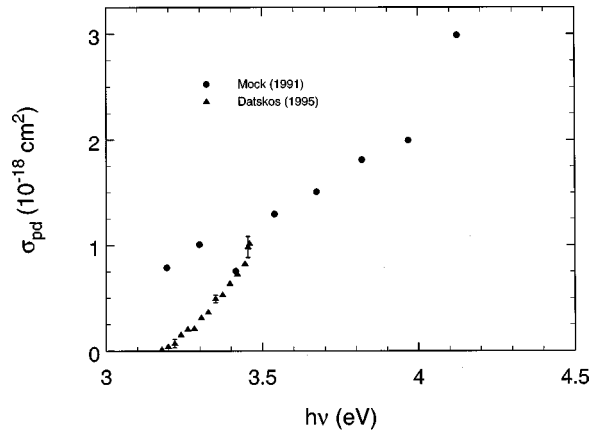

FIG. 39. Photodetachment cross section, $\sigma_{pd}(h\nu)$, for SF_6^- as a function of the photon energy $h\nu$: (●) Ref. 314; (▲) Ref. 318.

TABLE 40. Suggested values of the photodetachment cross section $\sigma_{pd}(h\nu)$ of SF_6^- as a function of photon energy (data of Datskos *et al.* obtained by digitizing Fig. 4 of Ref. 318)

Photon energy (eV)	$\sigma_{pd}(h\nu)$ (10^{-18} cm^2)	Photon energy (eV)	$\sigma_{pd}(h\nu)$ (10^{-18} cm^2)
3.18	0.013	3.35	0.492
3.20	0.042	3.37	0.530
3.22	0.070	3.40	0.638
3.24	0.152	3.42	0.725
3.26	0.205	3.44	0.825
3.28	0.211	3.45	0.983
3.30	0.313	3.46	1.02
3.33	0.366		

8.3. Photodetachment

The first attempt to investigate the photodetachment process in SF_6^- was made by Drzaic and Brauman[98,99] who reported observation of electron detachment from gas-phase SF_6^- induced by IR multiphoton absorption. However, they did not observe photodetachment of SF_6^- with ''visible light.'' According to Hay,[94] Freiser and Beauchamp[313] observed a monotonically increasing photodetachment signal at wavelengths shorter than 350 nm (3.55 eV), but were unable to detect photodetachment from SF_6^- below 370–380 nm (3.25–3.35 eV). Following these initial investigations, new photodetachment methods[314–318] enabled a quantitative measurement of the photodetachment cross section and energetics of the SF_6^- ion. Thus, Mock and Grimsrud[314] observed photodetachment from SF_6^- (in a mixture of SF_6 with nitrogen at 1 atm and 423 K) over a portion of the wavelength range between 300 and 450 nm and estimated a photodetachment onset of 387 nm (3.2 eV). No photodetachment was detectable in the spectral range from 450 to 1200 nm. Mock and Grimsrud[314] were able to determine absolute values of the photodetachment cross section $\sigma_{pd}(\lambda)$ in the wavelength range between 300 and 400 nm, and these are shown in Fig. 39 [the data plotted were taken from Fig. 1(a) of their paper].

A more detailed set of measurements was made by Datskos *et al.*[318] using a more sensitive method,[315,316] which allowed accurate determination of the absolute photodetachment cross section, $\sigma_{pd}(h\nu)$, of SF_6^- as a function of photon energy $h\nu$. In this method the photodetachment cross section and the photodetachment threshold E_{th} are determined using a two-laser arrangement.[315,316] Photoelectrons generated by one laser pulse attach to SF_6 forming SF_6^-. Another tunable laser pulse, delayed with respect to the first, photodetaches the electrons from the SF_6^- ions when $h\nu > E_{th}$. The photodetached electrons, being more mobile than the SF_6^- ions, induce a detectable transient voltage signal while drifting as free electrons prior to being again attached to SF_6. The size of this transient signal due to the photodetached electrons is measured and used to determine the cross section $\sigma_{pd}(h\nu)$ (see Refs. 315, 316, and 318 for details).

In Fig. 39 are shown the data for the photodetachment cross section $\sigma_{pd}(h\nu)$ for the reaction

$$SF_6^- + h\nu \rightarrow SF_6 + e, \tag{16}$$

obtained by Datskos *et al.*[318] using this technique, along with typical associated errors. They show that the photodetachment cross section has a threshold (i.e., a vertical detachment energy) at 3.16 eV which is about three times the size of the electron affinity of the SF_6 molecule. The cross section increases from a zero value at the threshold to $\sim 1.0 \times 10^{-18}$ cm^2 at a photon energy of 3.46 eV. The small size of the measured cross section $\sigma_{pd}(h\nu)$ has been attributed to the large relaxation in the equilibrium internuclear positions of SF_6^- compared to SF_6.[94,231,318] With the exception of the lowest two data points of Mock and Grimsrud (which are considered uncertain due to the low sensitivity of the experiment at these wavelengths), the measurements of Mock and Grimsrud are in agreement with those of Datskos *et al.* in the small wavelength range in which they overlap. Since the measurements of $\sigma_{pd}(h\nu)$ for SF_6^- by Datskos *et al.*[318] are more extensive and their uncertainty indicated, they are listed in Table 40 as our suggested data.

Ingólfsson *et al.*[317] employed a somewhat similar technique to that of Christophorou and co-workers,[315,316,318] but used only a fixed wavelength (337 nm) from a pulsed nitrogen laser. At this wavelength (which corresponds to a photon energy of 3.68 eV) they observed photodetachment from SF_6^- with an estimated cross section of $\sim 10^{-18}$ cm^2. This value is not inconsistent with the data in Fig. 39.

The cross section data in Fig. 39 should be valuable to investigations attempting to measure the SF_6^- ion densities in various types of gas discharges (e.g., see Ishikawa *et al.*[319] and Kono *et al.*[320]). The small measured cross section for photodetachment of SF_6^- would also indicate that this electron detachment mechanism is of minor significance compared to collisional detachment in gas discharges and gas-insulated high-voltage equipment using SF_6 gas.[321–324]

Finally, it should be noted that no photodetachment cross sections appear to have been published for the other negative ions produced by dissociative electron attachment to SF_6, except for F^-.[309]

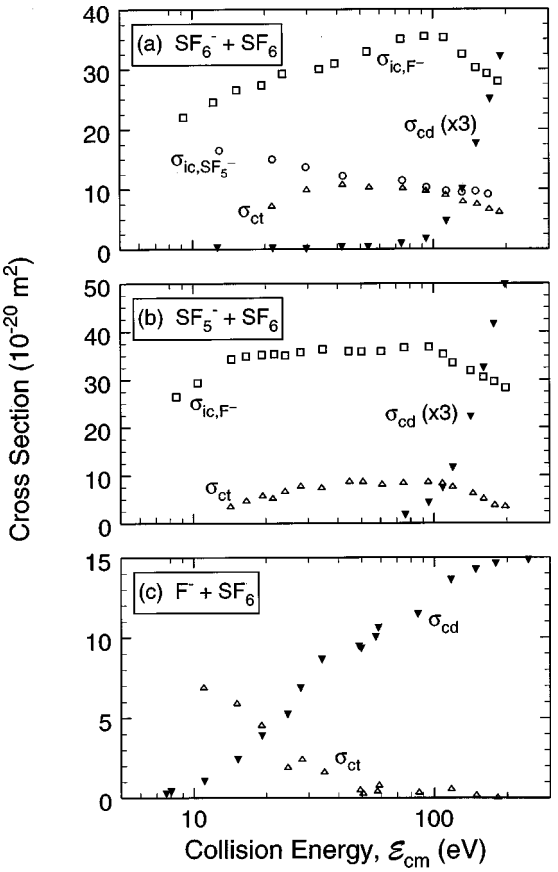

FIG. 40. (a) Measured cross sections for collisions of (a) SF_6^-, (b) SF_5^-, and (c) F^- on SF_6 for the following processes: (▼) collisional detachment, $\sigma_{cd}(\mathcal{E}_{cm})$; (□) collisional production of F^-, $\sigma_{ic,F^-}(\mathcal{E}_{cm})$; (○) collisional production of SF_5^-, $\sigma_{ic,SF_5^-}(\mathcal{E}_{cm})$; and (△) charge transfer processes, $\sigma_{ct}(\mathcal{E}_{cm})$. All data in this figure are those of Wang *et al.* from Ref. 325. Note that in Figs. 40(a) and 40(b) the cross section values for $\sigma_{cd}(\mathcal{E}_{cm})$ have been multiplied by a factor of 3 for the convenience of display.

8.4. Collisional Detachment

Collisional detachment studies involving the three major negative ions (SF_6^-, SF_5^-, and F^-) formed by electron attachment to SF_6 have been performed by Champion and collaborators.[311,312,325] Collisional detachment from SF_6^- and SF_5^- in SF_6 was found to have anomalously high energy thresholds [see Figs. 40(a) and 40(b)]. The thresholds for electron release in the reactions

$$SF_6^- + SF_6 \rightarrow SF_6 + SF_6 + e \tag{17}$$

and

$$SF_5^- + SF_6 \rightarrow SF_5 + SF_6 + e \tag{18}$$

are ~90 eV in the center-of-mass (cm) system. These values are much larger in comparison with the respective electron affinities of SF_6 (1.06 eV, Table 5) and SF_5 (2.7 eV–3.7 eV, Ref. 103). The anomalously high energy threshold for the collisional detachment reaction (17) has been attributed[311,312,325] to the competing ion-conversion and charge-transfer reactions at cm energies below ~100 eV, viz.

$$SF_6^- + SF_6 \rightarrow F^- + SF_5 + SF_6, \tag{19}$$

$$SF_6^- + SF_6 \rightarrow SF_5^- + F + SF_6, \tag{20}$$

and

$$SF_6^- + SF_6 \rightarrow \text{charge transfer products} + SF_6. \tag{21}$$

As can be seen from Fig. 40(a), the cross sections, $\sigma_{ic,F^-}(\mathcal{E}_{cm})$, $\sigma_{ic,SF_5^-}(\mathcal{E}_{cm})$, and $\sigma_{ct}(\mathcal{E}_{cm})$, for reactions (19), (20), and (21) respectively, are much larger than the cross section, $\sigma_{cd}(\mathcal{E}_{cm})$, for the collisional detachment reaction (17), and their thresholds lie at much lower collision energies $\mathcal{E}_{cm}$ (collision energy in the cm system). The energetic thresholds for collisionally decomposing ground-state SF_6^- via the reactions (17), (19), and (20) are, respectively, 1.06 eV [$=EA(SF_6)$, Table 5], 1.61 eV [$=D(SF_5–F)+EA(SF_6)–EA(F)$, with $D(SF_5–F)=3.95$ eV (Table 8), $EA(SF_6)=1.06$ eV, and $EA(F)=3.40$ eV[103]], and 1.34 eV [$=D(SF_5–F)+EA(SF_6)–EA(SF_5)$, with $D(SF_5–F)=3.95$ eV (Table 8), $EA(SF_6)=1.06$ eV, and $EA(SF_5)=3.66$ eV (average of the two highest values listed in Ref. 103)]. Clearly, the data in Fig. 40(a) show that electron detachment from SF_6^- by SF_6 has a very small probability of occurrence for collision energies $\mathcal{E}_{cm}<60$ eV, and that the dominant collisional decomposition mechanism of SF_6^- is dissociation. It is interesting to note also that studies of reactions of the form $A^-+B\rightarrow A+B^-$, with A^- being SF_6^-, have shown[326] that the large geometrical change between SF_6^- and SF_6 introduces an internal barrier in the reaction coordinates and hence such reactions proceed with a low reaction rate constant.

Similarly, the measurements of Wang *et al.*[325] shown in Fig. 40(b) for SF_5^-, indicate that the cross sections for the reactions

$$SF_5^- + SF_6 \rightarrow F^- + SF_4 + SF_6 \tag{22}$$

and

$$SF_5^- + SF_6 \rightarrow \text{charge transfer products} + SF_6 \tag{23}$$

have much lower energy thresholds than that for the electron detachment reaction (18). The cross sections for reactions (22) and (23) far exceed that for reaction (18) below ~100 eV.

In contrast to the above findings on the collisional detachment in SF_6 of the SF_6^- and SF_5^- ions, the measurements of Wang *et al.* shown in Fig. 40(c) for the collisional detachment of F^- in SF_6, viz.,

$$F^- + SF_6 \rightarrow F + SF_6 + e \tag{24}$$

indicate a rather low energy threshold (~8.0 eV). Additionally, the cross-section values for reaction (24) progressively exceed those of the charge-transfer reactions as the reaction energy increases above ~20 eV. It is clear then that charge transfer and collision-induced dissociation processes are the dominant inelastic channels in SF_6 involving the destruction of SF_6^-, SF_5^-, and F^- at low collision energies. These find-

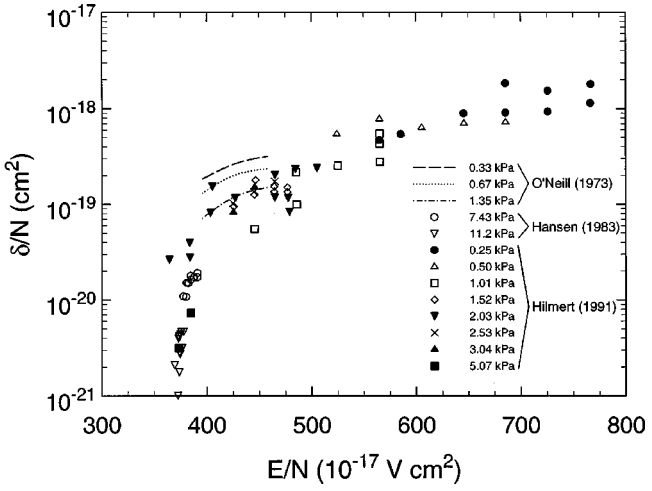

FIG. 41. Density-reduced electron detachment coefficient $\delta/N\,(E/N)$ as a function of E/N for SF_6 ($T=293-296$ K) at the pressures indicated in the legend: (– –, ···, – · –) Ref. 291; (○), (▽) Ref. 329; (●), (△), (□), (◇), (▼), (×), (▲), (■) Ref. 330.

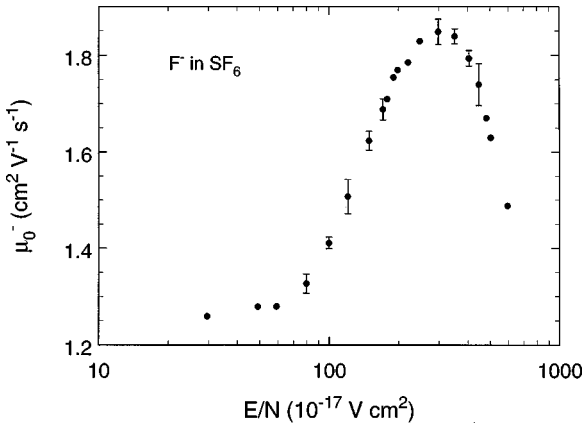

FIG. 43. Measured reduced mobilities $\mu_0^-\,(E/N)$ for the fastest ion in the study of Nakamura in Ref. 303, presumed to be F^- in SF_6.

ings are also consistent with the results of Wang *et al.*[325] on the destruction of SF_6^-, SF_5^-, and F^- in rare gases.

Interestingly, evidence has been obtained[311,325] that long-lived energetically unstable states of SF_6^- can contribute to collisional detachment. Also, experimental evidence has been provided[327–330] that negative-ion clusters such as $(SF_6^-)SF_6$ (and also clusters involving F^-) can form in parent SF_6 gas and can contribute to the pressure dependence[329] of the measured density-normalized electron detachment coefficient δ/N in SF_6 (the gas pressure in these experiments was 7.4 and 11.1 kPa).

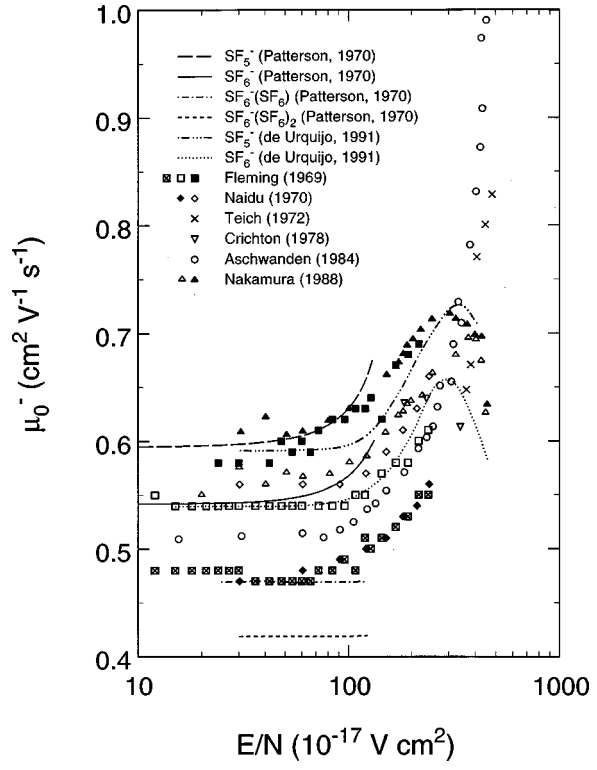

FIG. 42. Measured reduced mobilities $\mu_0^-\,(E/N)$ for negative ions in SF_6. Mass identified data of Patterson from Ref. 327: (– –) SF_5^-; (—) SF_6^-; (– · –) $SF_6^-(SF_6)$; (- - -) $SF_6^-(SF_6^-)_2$. Mass identified data of de Urquijo *et al.* from Ref. 340: (– ··· –) SF_5^-; (···) SF_6^-. Measurements without mass analysis: (⊠), (□), (■) Ref. 336; (◆), (◇) Ref. 337; (×) Ref. 184; (▽) Ref. 338; (○) Ref. 339; (△), (▲) Ref. 303.

Figure 41 shows the measurements of the density-reduced electron detachment coefficient, $\delta/N(E/N)$, measured in SF_6 by O'Neill and Craggs,[291] Hansen *et al.*,[329] and Hilmert and Schmidt.[330] The density dependence of $\delta/N(E/N)$ observed by O'Neill and Craggs (at pressures between 0.33 and 1.35 kPa) is seen to continue up to the higher pressures (7.43 and 11.15 kPa) employed by Hansen *et al.*[329] The coefficient $\delta/N(E/N)$ decreases with increasing N. They attributed this decrease to a three-body process $SF_6^-+SF_6+SF_6 \rightarrow (SF_6^-)SF_6+SF_6$, which leads to the formation of a stable complex $(SF_6^-)SF_6$ in which the electron is more tightly bound than in SF_6^-. This process then competes with the two-body detachment reaction which is pressure independent. The data shown in Fig. 41 were obtained using swarm techniques. Data obtained by time-lag to breakdown experiments[323,324,331] are not plotted since they gave very different and less accurate values because of the way the coefficient was evaluated in these experiments (see discussion in Hilmert and Schmidt[330]).

The high-energy collisional detachment thresholds of the SF_6 negative ions in SF_6 gas accounts for the observed small values of the collisional detachment coefficient compared to the values of the coefficients of other negative ion–molecule reactions in SF_6.[311] As a consequence, collisional detachment in SF_6, and electrical properties of SF_6 such as discharge initiation probabilities that depend on electron detachment, are sensitive to the presence of impurities, such as water and air, that may form clusters with SF_6-originated negative ions for which collisional detachment may be more probable.[332–334]

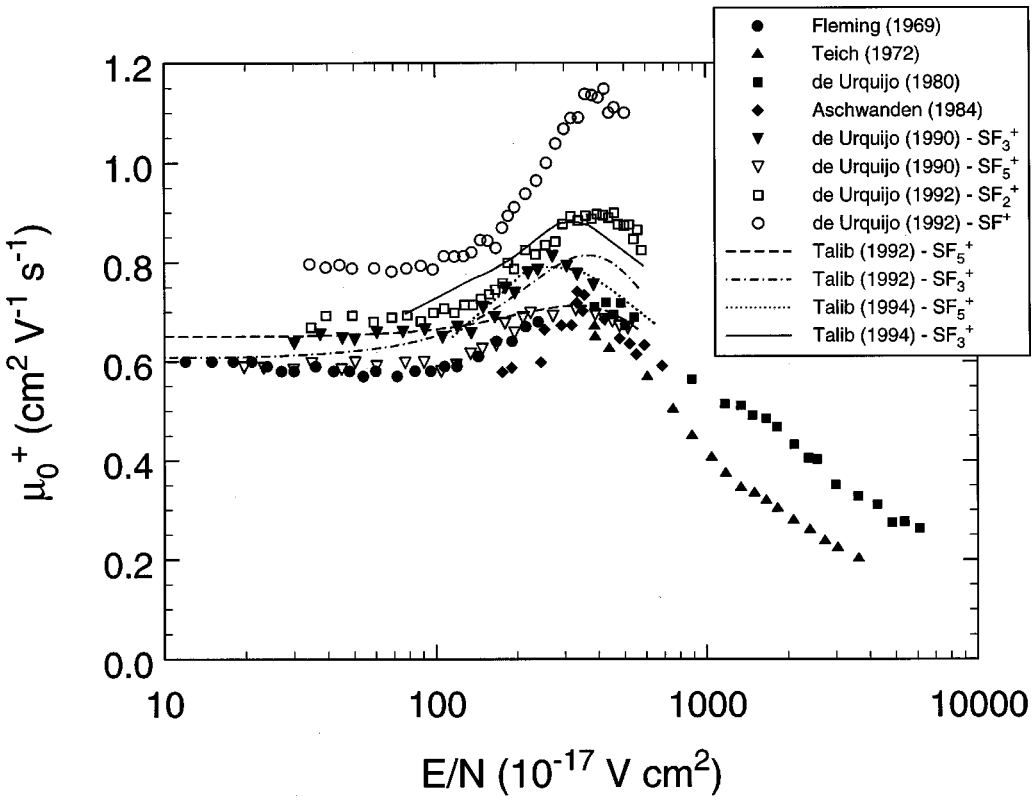

FIG. 44. Measured reduced mobilities, $\mu_0^+(E/N)$, for SF_5^+ and SF_3^+ in parent SF_6 gas ($T=290-300$ K): (●) Ref. 336; (▲) Ref. 184; (■) Ref. 341; (♦) Ref. 339; (▼) SF_3^+ from Ref. 342; (▽) SF_5^+ from Ref. 342; (- - -) SF_5^+ from Ref. 344; (— · —) SF_3^+ from Ref. 344; (—) SF_3^+ from Ref. 345; (· · ·) SF_5^+ from Ref. 345. Also shown are the reduced mobilities of (○) SF^+ and (□) SF_2^+ from Ref. 343.

9. Ion Transport in SF_6

The motion of ions through SF_6 gas is an important aspect of modeling many systems utilizing SF_6. While no direct cross sections are available for these processes, some ion transport data are available. We briefly summarize the available data here.

A number of studies have attempted to quantify the motion of negative ions[184,303,327,335–340] and positive ions[184,336,339,341–345] formed by electron impact on SF_6 in parent SF_6 gas. These studies include measurements of ion mobilities[184,303,327,336–345] and ion diffusion.[303,337,340,342,343] They are not only limited in number, but the interpretation of the measurements is often hindered by the absence of mass spectrometric identification of the ions present in the system and also by the absence of reliable information on the pertinent ion-transformation processes under varied experimental conditions. Only the work of Patterson[327] and de Urquijo *et al.*[340] on negative ions and the work of de Urquijo *et al.*[342] on positive ions included mass analysis. The rest of the studies inferred the nature of the ions by reference to the mass spectrometric data of these three studies. The early data on the mobilities of positive ions, negative ions, and ion clusters in the parent SF_6 gas have been summarized and discussed by Brand and Jungblut[328] and by Morrow.[12]

In Fig. 42 are plotted the reduced mobilities [that is, mobilities referred to standard pressure (101.325 kPa) and temperature (277.16 K)], $\mu_0^-(E/N)$, for the negative ions SF_5^-, SF_6^-, $SF_6^-(SF_6)$, and $SF_6^-(SF_6)_2$ in SF_6. As mentioned in the preceding paragraph, only Patterson[327] and de Urquijo[340] identified the ions by mass spectrometry. The identification of the ionic mobilities with the anionic species by other researchers was made primarily by virtue of their agreement with the $\mu_0^-(E/N)$ data of Patterson for the corresponding negative-ion species. According to Brand and Jungblut,[328] all measured negative ion mobilities can be assigned to one or more of the following ions: SF_5^-, SF_6^-, $SF_6^-(SF_6)$, and $SF_6^-(SF_6)_2$.

In Fig. 43 are shown the $\mu_0^-(E/N)$ measurements of Nakamura[303] for the fastest negative ion observed in parent SF_6 gas in his study, which he presumed to be F^-.

Similar measurements of the reduced mobilities, $\mu_0^+(E/N)$, of positive ions in parent SF_6 gas are shown in Fig. 44. Along with the early data[184,336,339,341] plotted in Fig. 44 are shown the more recent mass-identified measurements of Talib and Saporoschenko[344,345] and de Urquijo *et al.*[342,343]

In Fig. 45(a) are shown the $ND_L^-(E/N)$ measurements of Nakamura[303] for negative ions in SF_6 (closed symbols). Although in the experiments of Nakamura there was no mass analysis of the negative ions present in the system, he ascribed his mobility measurements to the SF_6^-, SF_5^-, and F^- ions as shown in the figure. More recent mass-identified measurements of $ND_L^-(E/N)$ for SF_6^- and SF_5^- in SF_6 by de

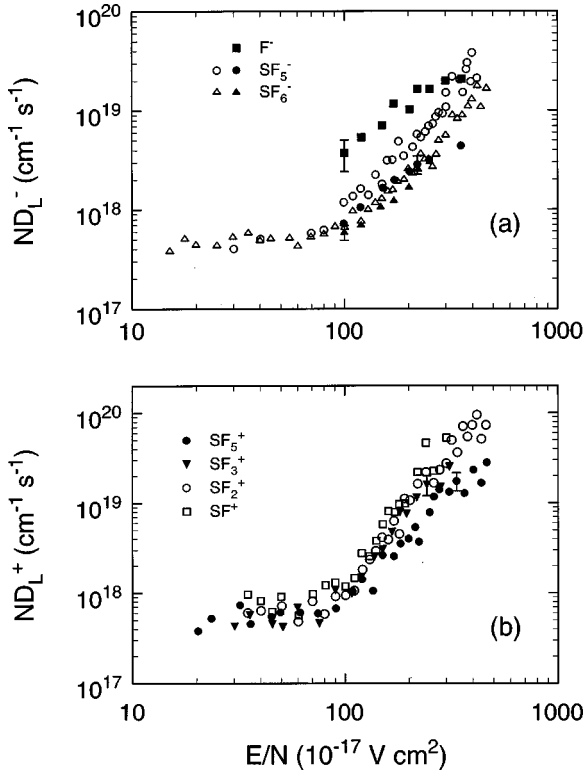

FIG. 45. (a) $ND_L^-(E/N)$ for the negative ions SF_6^-, SF_5^- and F^- in SF_6 (closed symbols, data of Nakamura from Ref. 303; open symbols, data of de Urquijo *et al.* from Ref. 340). (b) $ND_L^+(E/N)$ for the positive ions SF_5^+, SF_3^+, SF_2^+, and SF^+ in SF_6 (data of de Urquijo *et al.* from Refs. 342 and 343).

Urquijo *et al.*[340] are also shown. De Urquijo *et al.*[342,343] also measured $ND_L^+(E/N)$ for the positive ions SF_5^+, SF_3^+, SF_2^+, and SF^+ in SF_6, and these results are shown in Fig. 45(b).

There seem to be no measurements of $D_T^-/\mu(E/N)$ for negative ions in SF_6. However, Naidu and Prasad[337] measured the so-called Townsend energy factor k_T (ratio of the mean ion energy to the mean energy of the gas molecules) as a function E/N at $T=293$ K for pressures equal to 0.16 and 0.32 kPa. Table 41 lists the measurements of Naidu and Prasad[337] for $k_T^-(E/N)$ and the $D_T^-/\mu(E/N)$ values we calculated from these using the equation $k_T^-(E/N)=39.6D_T^-/\mu(E/N)$ (for $T=293$ K and a Maxwell distribution function for the ion kinetic energies). The quantity $D_T^-/\mu(E/N)$ is seen to increase from a value of 0.025 V at $E/N=30.3\times10^{-17}$ V cm^2 to a value of 0.149 V at $E/N=212.2\times10^{-17}$ V cm^2.

TABLE 41. $k_T^-(E/N)$ and $D_T^-/\mu(E/N)$ for negative ions in SF_6 ($T=293$ K) (data of Naidu and Prasad in Ref. 337)

E/N (10^{-17} V cm^2)	$k_T^-(E/N)$	$D_T^-/\mu(E/N)$ (V)
30.3	1.0	0.025
60.6	1.2	0.030
91.0	1.7	0.043
121.3	2.6	0.066
151.6	3.5	0.088
181.9	4.6	0.116
212.2	5.9	0.149

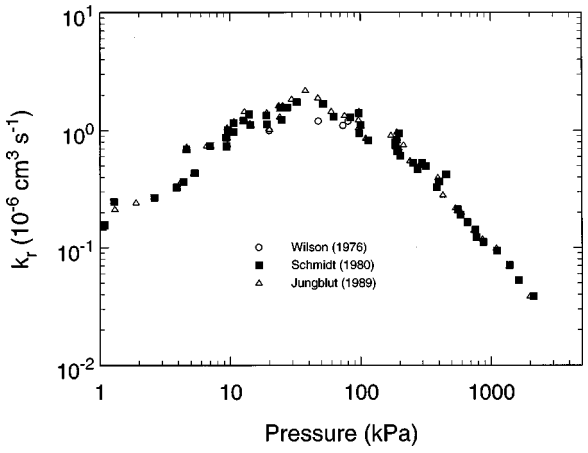

FIG. 46. Volume (ion–ion) recombination rate coefficient k_r in SF_6 as a function of gas pressure: (○) Ref. 346 ($T=298$ K); (■) Ref. 347 ($T=296$ K); (△) Ref. 348 ($T=296$ K).

Finally, in Fig. 46 are shown the measurements of Wilson *et al.*[346] and Schmidt and collaborators[347,348] of the volume (ion–ion) recombination rate coefficient k_r for SF_6 as a function of gas pressure ($T=296$–298 K).

10. Recommended or Suggested Electron Collision Cross Sections and Electron Transport Coefficients for SF_6

In Fig. 47 are plotted the recommended or suggested cross sections for SF_6 discussed in this paper:

(i) $\sigma_{sc,t}(\varepsilon)$–Table 9, Fig. 5;
(ii) $\sigma_{e,int}(\varepsilon)$–Table 13, Fig. 7;
(iii) $\sigma_m(\varepsilon)$–Table 14, Fig. 8;
(iv) $\sigma_{vib,t}(\varepsilon)$–Table 15, Fig. 12;
(v) $\sigma_{i,t}(\varepsilon)$–Table 17, Fig. 14;
(vi) $\sigma_{dis,neut,t}(\varepsilon)$–Table 20; Fig. 18;
(vii) $\sigma_{a,SF_6^-}(\varepsilon)$–Table 28, Figs. 24(a) and 28; and
(viii) $\sigma_{da,t}(\varepsilon)$–Table 28, Fig. 28.

A number of additional electron collision cross sections have been discussed in the paper and data on these can be found as follows:

(i) $\sigma_{e,diff}(\varepsilon)$–Tables 10, 11, and 12, Fig. 6;
(ii) $\sigma_{i,partial}(\varepsilon)$–Fig. 15;
(iii) $\sigma_{a,t}(\varepsilon)$–Table 28, Fig. 22;
(iv) $\sigma_{a,SF_5^-}(\varepsilon)$–Table 25, Fig. 24(b);
(v) $\sigma_{a,SF_4^-}(\varepsilon)$, $\sigma_{a,SF_3^-}(\varepsilon)$, and $\sigma_{a,SF_2^-}(\varepsilon)$–Table 27, Figs. 25 and 28;
(vi) $\sigma_{a,F_2^-}(\varepsilon)$–Table 27, Figs. 26 and 28; and
(vii) $\sigma_{a,F^-}(\varepsilon)$–Table 27, Figs. 27 and 28.

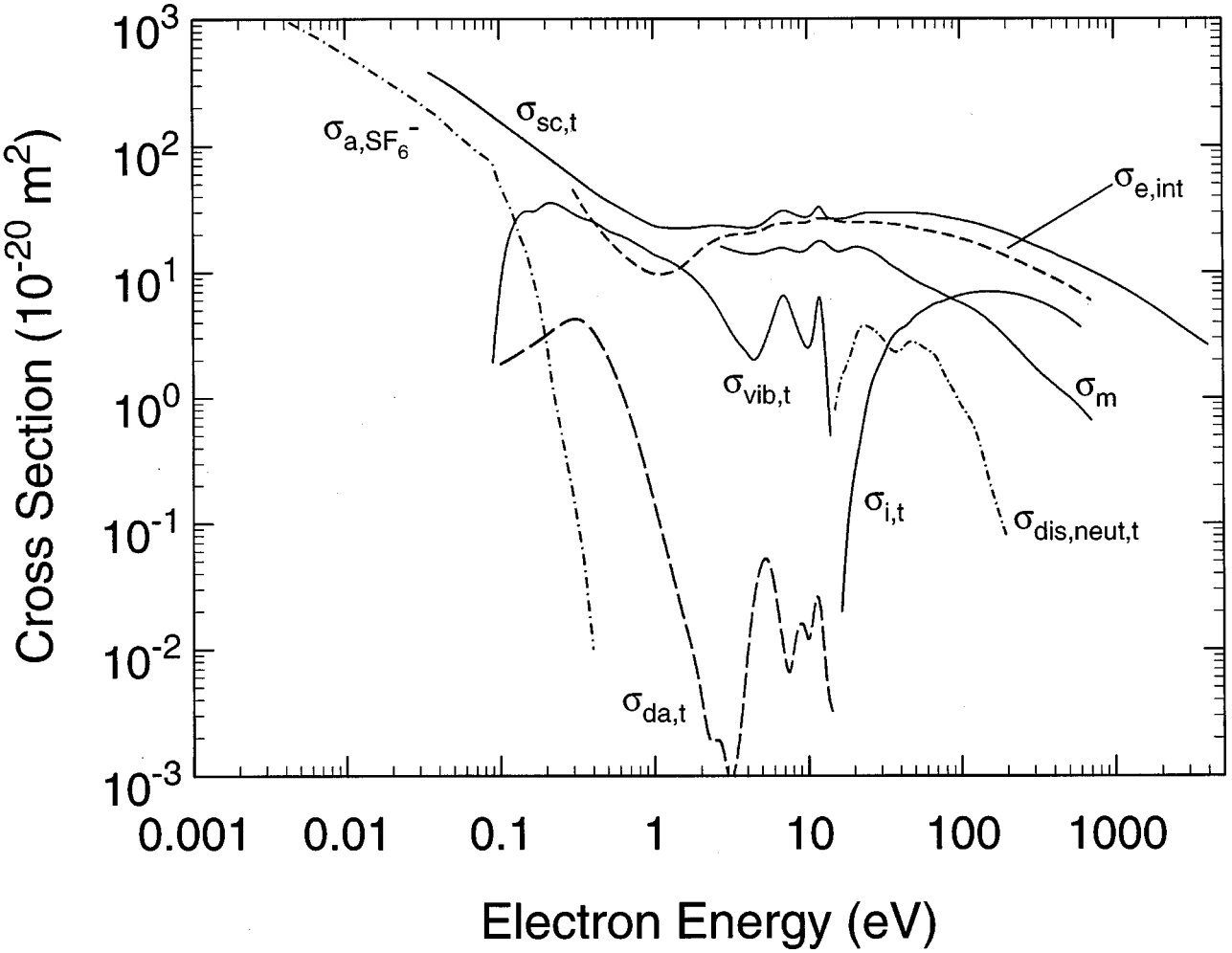

FIG. 47. Recommended and suggested electron collision cross sections for SF_6.

Based on the discussions in the paper, recommended or suggested data for the electron transport coefficients, density-reduced electron attachment and ionization coefficients, and electron attachment rate constants have been presented as follows:

(i) $\alpha/N(E/N)$–Table 19, Fig. 17;
(ii) $\eta/N(E/N)$–Table 34, Fig. 33;
(iii) $\eta/N_a(\langle\varepsilon\rangle)$–Tables 29 and 30;
(iv) $(\alpha-\eta)/N(E/N)$–Table 35, Fig. 34;
(v) $k_{a,t}(E/N)$ in Ar, Xe, or N_2–Tables 29 and 30, Fig. 29;
(vi) $k_{a,t}(\langle\varepsilon\rangle)$–Table 31, Fig. 30;
(vii) $w(E/N)$–Table 36, Figs. 35 and 36;
(viii) $D_T/\mu(E/N)$–Table 38, Fig. 37; and
(ix) $ND_L(E/N)$,–Table 39, Fig. 38.

Tables of the recommended and suggested data can be found at *http://www.eeel.nist.gov/811/refdata* on the World Wide Web.

11. Data Needs for SF_6

In spite of the many studies on electron interactions with the SF_6 molecule there still exist distinct gaps in the available data. The most significant data need is for direct measurements of cross sections for vibrational excitation and for electron-impact dissociation into neutral fragments. Additionally, a determination of the momentum transfer cross section at energies below 2.5 eV is needed. These data are necessary to extend the recommended and suggested data in the present work, and hence provide a reliable source of electron–SF_6 interaction data for use in computer modeling codes.

12. Acknowledgments

We wish to thank Professor M. Hayashi of the Gaseous Electronics Institute, Nagoya, Japan, for providing to us his list of references on SF_6 and for valuable comments, Professor S. J. Buckman of the Australian National University, Canberra, Australia for his unpublished measurements on differential electron scattering cross sections, and Professor H. Hotop of Universität Kaiserslautern for information on their electron attachment data in SF_6 at low electron energies. We are also grateful to Robin J. Martucci of the Electricity Division of the National Institute of Standards and Technology for her assistance with the literature.

13. References

[1] L. G. Christophorou and S. R. Hunter, in *Electron-Molecule Interactions and Their Applications*, edited by L. G. Christophorou (Academic, Orlando, FL, 1984), Vol. 2, Chap. 5.

[2] L. G. Christophorou, J. K. Olthoff, and D. S. Green, ''Gases for Electrical Insulation and Arc Interruption: Possible Present and Future Alternatives to Pure SF_6,'' National Institute of Standards and Technology (NIST), NIST Technical Note 1425 (1997).

[3] Intergovernmental Panel on Climate Change (IPCC), *Climate Change 1995*, edited by J. T. Houghton, L. G. M. Filho, B. A. Callander, N. Harris, A. Kattenberg, and K. Maskell (Cambridge University Press, Cambridge, New York, 1996), p. 22.

[4] M. K. W. Ko, N. D. Sze, W.-C. Wang, G. Shia, A. Goldman, F. J. Murcray, D. G. Murcray, and C. P. Rins, J. Geophys. Res. **98**, 10 499 (1993).

[5] R. A. Morris, T. M. Miller, A. A. Viggiano, J. F. Paulson, S. Solomon, and G. Reid, J. Geophys. Res. **100**, 1287 (1995).

[6] D. J. Wuebbles and A. K. Jain, in ''Electrical Transmission and Distribution Systems, Sulfur Hexafluoride, and Atmospheric Effects of Greenhouse Gas Emissions Conference,'' U.S. Environmental Protection Agency Conference Proceedings Report (August 1995), p. 8.

[7] L. S. Geller, J. W. Elkins, J. M. Lobert, A. D. Clarke, D. F. Hurst, J. H. Butler, and R. C. Myers, Geophys. Res. Lett. **24**, 675 (1997).

[8] T. H. Teich, in *Electron and Ion Swarms*, edited by L. G. Christophorou (Pergamon, New York, 1981), p. 241.

[9] J. W. Gallagher, E. C. Beaty, J. Dutton, and L. C. Pitchford, J. Phys. Chem. Ref. Data **12**, 109 (1983).

[10] S. Trajmar, D. F. Register, and A. Chutjian, Phys. Rep. **97**, 219 (1983).

[11] J. P. Novak and M. F. Fréchette, J. Appl. Phys. **55**, 107 (1984).

[12] R. Morrow, IEEE Trans. Plasma Science **PS-14**, 234 (1986).

[13] E. Weigold, Y. Zheng, and W. von Niessen, Chem. Phys. **150**, 405 (1991).

[14] L. G. Christophorou and R. J. Van Brunt, IEEE Trans. Dielect. Electr. Insul. **2**, 952 (1995).

[15] G. Herzberg, *Molecular Spectra and Molecular Structure III. Electronic Spectra and Electronic Structure of Polyatomic Molecules* (D. Van Nostrand Company, Inc., Princeton, NJ, 1966).

[16] J. Berkowitz, *Photoabsorption, Photoionization, and Photoelectron Spectroscopy* (Academic, New York, 1979).

[17] M. B. Robin, *Higher Excited States of Polyatomic Molecules* (Academic, Orlando, FL, 1985), Vol. III.

[18] J. W. Gallagher, C. E. Brion, J. A. R. Samson, and P. W. Langhoff, J. Phys. Chem. Ref. Data **17**, 9 (1988).

[19] L. G. Christophorou, J. K. Olthoff, and M. V. V. S. Rao, J. Phys. Chem. Ref. Data **25**, 1341 (1996).

[20] L. G. Christophorou, J. K. Olthoff, and M. V. V. S. Rao, J. Phys. Chem. Ref. Data **26**, 1 (1997).

[21] L. G. Christophorou, J. K. Olthoff, and Y. Wang, J. Phys. Chem. Ref. Data **26**, 1205 (1997).

[22] L. G. Christophorou and J. K. Olthoff, J. Phys. Chem. Ref. Data **27**, 1 (1998).

[23] L. G. Christophorou and J. K. Olthoff, J. Phys. Chem. Ref. Data **27**, 889 (1998).

[24] L. G. Christophorou and J. K. Olthoff, J. Phys. Chem. Ref. Data **28**, 131 (1999).

[25] L. G. Christophorou and J. K. Olthoff, J. Phys. Chem. Ref. Data **28**, 967 (1999).

[26] L. E. Kline, D. K. Davies, C. L. Chen, and P. J. Chantry, J. Appl. Phys. **50**, 6789 (1979).

[27] T. Yoshizawa, Y. Saki, H. Tagashira, and S. Sakamoto, J. Phys. D **12**, 1839 (1979).

[28] H. Itoh, M. Shimozuma, and H. Tagashira, J. Phys. D **13**, 1201 (1980).

[29] G. R. Govinda Raju and R. Hackam, J. Appl. Phys. **52**, 3912 (1981).

[30] J. P. Novak and M. F. Fréchette, J. Phys. D **15**, L105 (1982).

[31] M. S. Dincer and G. R. Govinda Raju, J. Appl. Phys. **54**, 6311 (1983).

[32] J. P. Novak and M. F. Fréchette, in *Gaseous Dielectrics IV*, edited by L. G. Christophorou and M. O. Pace (Pergamon, New York, 1984), p. 34.

[33] M. Hayashi and T. Nimura, J. Phys. D **17**, 2215 (1984).

[34] I. M. Bortnik, A. N. Kushko, and A. N. Lobanov, Sov. Phys. Tech. Phys. **30**, 1015 (1985).

[35] M. F. Fréchette and J. P. Novak, J. Phys. D **20**, 438 (1987).

[36] M. Yousfi and A. Chatwiti, J. Phys. D **20**, 1457 (1987).

[37] A. V. Phelps, in *Gaseous Dielectrics V*, edited by L. G. Christophorou and D. W. Bouldin (Pergamon, New York, 1987), p. 1.

[38] H. Itoh, Y. Miura, N. Ikuta, Y. Nakao, and H. Tagashira, J. Appl. Phys. **21**, 922 (1988).

[39] K. Satoh, H. Itoh, Y. Nakao, and H. Tagashira, J. Phys. D **21**, 931 (1988).

[40] A. V. Phelps and R. J. Van Brunt, J. Appl. Phys. **64**, 4269 (1988).

[41] H. Itoh, M. Kawaguchi, K. Satoh, Y. Miura, Y. Nakao, and H. Tagashira, J. Phys. D **23**, 299 (1990).

[42] M. Hayashi and S. Hara, Proceedings of Joint Symposium on Electron and Ion Swarms and Low-Energy Electron Scattering, Gold Coast, Australia, 18–20 July 1991, p. 109.

[43] H. Itoh, T. Miyachi, M. Kawaguchi, Y. Nakao, and H. Tagashira, J. Phys. D **24**, 277 (1991).

[44] H. Itoh, T. Matsumura, K. Satoh, H. Date, Y. Nakao, and H. Tagashira, J. Phys. D **26**, 1975 (1993).

[45] M. Hayashi, K. Nakamura, L. G. Christophorou, and J. K. Olthoff (unpublished).

[46] J. L. Dehmer, A. C. Parr, S. Wallace, and D. Dill, Phys. Rev. A **26**, 3283 (1982).

[47] B. M. Addison-Jones, K. H. Tan, B. W. Yates, J. N. Cutler, G. M. Bancroft, and J. S. Tse, J. Electron Spectrosc. Relat. Phenom. **48**, 155 (1989).

[48] D. M. P. Holland, D. A. Shaw, A. Hopkirk, M. A. MacDonald, and S. M. McSweeney, J. Phys. B **25**, 4823 (1992).

[49] D. M. P. Holland, M. A. MacDonald, P. Baltzer, L. Karlsson, M. Lundqvist, B. Wannberg, and W. von Niessen, Chem. Phys. **192**, 333 (1995).

[50] A. J. Yencha, D. B. Thompson, A. J. Cormack, D. R. Cooper, M. Zubek, P. Bolognesi, and G. C. King, Chem. Phys. **216**, 227 (1997).

[51] E. Fainelli, F. Maracci, R. Platania, and L. Avaldi, J. Electron Spectrosc. Relat. Phenom. **87**, 169 (1998).

[52] K. H. Sze and C. E. Brion, Chem. Phys. **140**, 439 (1990).

[53] L. C. Lee, E. Phillips, and D. L. Judge, J. Chem. Phys. **67**, 1237 (1977).

[54] J. Gustafsson, Phys. Rev. A **18**, 1481 (1978).

[55] G. Bieri, L. Åsbrink, and W. von Niessen, J. Electron Spectrosc. Relat. Phenom. **27**, 129 (1982).

[56] F. A. Gianturco and A. Jain, Phys. Rep. **143**, 347 (1986).

[57] V. I. Nefedov, J. Struct. Chem. **11**, 272 (1970).

[58] J. L. Dehmer, J. Chem. Phys. **56**, 4496 (1972).

[59] A. P. Hitchcock and M. J. Van der Wiel, J. Phys. B **12**, 2153 (1979).

[60] K. Codling, J. Chem. Phys. **44**, 4401 (1966).

[61] D. Blechschmidt, R. Haensel, E. E. Koch, U. Nielsen, and T. Sagawa, Chem. Phys. Lett. **14**, 33 (1972).

[62] M. Sasanuma, E. Ishiguro, H. Masuko, Y. Morioka, and M. Nakamura, J. Phys. B **11**, 3655 (1978).

[63] K. Mitsuke, S. Suzuki, T. Imamura, and I. Koyano, J. Chem. Phys. **93**, 8717 (1990).

[64] J. A. Simpson, C. E. Kuyatt, and S. R. Mielczarek, J. Chem. Phys. **44**, 4403 (1966).

[65] J. F. Ying, T. A. Daniels, C. P. Mathers, H. Zhu, and K. T. Leung, J. Chem. Phys. **99**, 3390 (1993).

[66] T. M. Zimkina and V. A. Fomichev, Sov. Phys.-Dokl. **11**, 726 (1967).

[67] A. S. Vinogradov and T. M. Zimkina, Opt. Spectrosc. **32**, 17 (1972).

[68] E. S. Gluskin, A. A. Krasnoperova, and L. N. Mazalov, J. Struct. Chem. **18**, 156 (1977).

[69] Y. Sato, K. Ueda, H. Chiba, E. Shigemasa, and A. Yagishita, Chem. Phys. Lett. **196**, 475 (1991).

[70] K. Mochiji, K. Lee, C.-I. Ma, D. Y. Kim, M. Mahalingam, and D. M. Hanson, J. Vac. Sci. Technol. A **12**, 216 (1994).

[71] T. Masuoka and J. A. R. Samson, J. Chem. Phys. **75**, 4946 (1981).

[72] J. C. Creasey, I. R. Lambert, R. P. Tuckett, K. Codling, L. J. Frasinski, P. A. Hatherly, and M. Stankiewicz, J. Chem. Soc. Faraday Trans. **87**, 1287 (1991).

[73] D. S. Peterka, M. Ahmed, C.-Y. Ng, and A. G. Suits, Chem. Phys. Lett. **312**, 108 (1999).

[74] V. H. Dibeler and F. L. Mohler, J. Res. Natl. Bur. Stand. **40**, 25 (1948).

[75] D. M. Curtis and J. H. D. Eland, Int. J. Mass Spectrom. Ion Phys. **63**, 241 (1985).

[76] L. J. Frasinski, M. Stankiewicz, K. J. Randall, P. A. Hatherly, and K. Codling, J. Phys. B **19**, L819 (1986).

[77] J. H. D. Eland, F. S. Wort, P. Lablanquie, and I. Nenner, Z. Phys. D **4**, 31 (1986).

[78] V. H. Dibeler and J. A. Walker, J. Chem. Phys. **44**, 4405 (1966).

[79] M. Sasanuma, E. Ishiguro, T. Hayaisha, H. Masuko, Y. Morioka, T. Na-

kajima, and M. Nakamura, J. Phys. B **12**, 4057 (1979).
[80] L. Karlsson, L. Mattsson, R. Jadrny, T. Bergmark, and K. Siegbahn, Phys. Scr. **14**, 230 (1976).
[81] A. W. Potts, H. J. Lempka, D. G. Streets, and W. C. Price, Philos. Trans. R. Soc. London, Ser. A **268**, 59 (1970).
[82] R. K. Asundi and J. D. Craggs, Proc. Phys. Soc. **83**, 611 (1964).
[83] S. Trajmar and A. Chutjian, J. Phys. B **10**, 2943 (1977).
[84] E. D. Nostrand and A. B. F. Duncan, J. Am. Chem. Soc. **76**, 3377 (1954).
[85] T.-K. Liu, G. Moe, and A. B. F. Duncan, J. Chem. Phys. **19**, 71 (1951).
[86] A. Chutjian, S. K. Srivastava, and S. Trajmar, Ninth International Conference on the Physics of Electronic and Atomic Collisions, Seattle, WA, 1975, Vol. 1, p. 137.
[87] C. C. Turci, J. T. Francis, T. Tyliszczak, G. G. B. de Souza, and A. P. Hitchcock, Phys. Rev. A **52**, 4678 (1995).
[88] J. T. Francis, C. C. Turci, T. Tyliszczak, G. G. B. de Souza, N. Kosugi, and A. P. Hitchcock, Phys. Rev. A **52**, 4665 (1995).
[89] I. W. Fomunung, Z. Chen, and A. Z. Msezane, Phys. Rev. A **53**, 806 (1996).
[90] Z. Felfli, I. Fomunung, D. Bessis, and A. Z. Msezane, Chem. Phys. **211**, 325 (1996).
[91] K. Rohr, J. Phys. B **10**, 1175 (1977).
[92] J. Randell, D. Field, S. L. Lunt, G. Mrotzek, and J. P. Ziesel, J. Phys. B **25**, 2899 (1992).
[93] P. J. Hay, J. Am. Chem. Soc. **99**, 1013 (1977).
[94] P. J. Hay, J. Chem. Phys. **76**, 502 (1982).
[95] R. Tang and J. Callaway, J. Chem. Phys. **84**, 6854 (1986).
[96] M. Klobukowski, Z. Barandiaran, L. Seijo, and S. Huzinaga, J. Chem. Phys. **86**, 1637 (1987).
[97] J. A. D. Stockdale, R. N. Compton, and H. C. Schweinler, J. Chem. Phys. **53**, 1502 (1969).
[98] P. S. Drzaic and J. I. Brauman, Chem. Phys. Lett. **83**, 508 (1981).
[99] P. S. Drzaic and J. I. Brauman, J. Am. Chem. Soc. **104**, 13 (1982).
[100] G. L. Gutsev (Plenum, New York, 1992), p. 504 [translated from Izv. Ak. Nauk, Se. Khimi. No. **3**, 641 (1992)].
[101] G. L. Gutsev, Int. J. Mass Spectrom. Ion Processes **115**, 185 (1992).
[102] K. W. Richman and A. Banerjee, Int. J. Quantum Chem.: Quantum Chem. Symp. **27**, 759 (1993).
[103] A. A. Christodoulides, D. L. McCorkle, and L. G. Christophorou, in *Electron-Molecule Interactions and Their Applications*, edited by L. G. Christophorou (Academic, New York, 1984), Vol. 2, Chap. 6.
[104] E. P. Grimsrud, S. Chowdhury, and P. Kebarle, J. Chem. Phys. **83**, 1059 (1985).
[105] E. C. M. Chen, L.-R. Shuie, E. D. D'sa, C. F. Batten, and W. E. Wentworth, J. Chem. Phys. **88**, 4711 (1988).
[106] E. C. M. Chen, J. R. Wiley, C. F. Batten, and W. E. Wentworth, J. Phys. Chem. **98**, 88 (1994).
[107] E. Miyoshi, Y. Sakai, and S. Miyoshi, J. Chem. Phys. **88**, 1470 (1988).
[108] L. G. Christophorou, D. L. McCorkle, and J. G. Carter, J. Chem. Phys. **54**, 253 (1971); **57**, 2228E (1972).
[109] L. G. Christophorou, D. L. McCorkle, and J. G. Carter, J. Chem. Phys. **57**, 2228 (1972).
[110] C. L. Chen and P. J. Chantry, J. Chem. Phys. **71**, 3897 (1979).
[111] P. W. Harland and J. C. J. Thynne, J. Phys. Chem. **73**, 4031 (1969).
[112] J. L. Dehmer, J. Siegel, and D. Dill, J. Chem. Phys. **69**, 5205 (1978).
[113] M. V. V. S. Rao and S. K. Srivastava, Proceedings of the XVIIIth International Conference on the Physics of Electronic and Atomic Collisions, Aarhus, Denmark, July 21–27, 1993; Abstracts of Contributed Papers, edited by T. Andersen, B. Fastrup, F. Folkmann, and H. Knudsen, p. 345.
[114] B. Lehmann, Z. Naturforsch. **25A**, 1755 (1970).
[115] M. Fenzlaff, R. Gerhard, and E. Illenberger, J. Chem. Phys. **88**, 149 (1988).
[116] M. S. Dababneh, Y.-F. Hsieh, W. E. Kauppila, C. K. Kwan, S. J. Smith, T. S. Stein, and M. N. Uddin, Phys. Rev. A **38**, 1207 (1988).
[117] G. Kasperski, P. Mozejko, and C. Szmytkowski, Z. Phys. D **42**, 187 (1997).
[118] N. I. Romanyuk, I. V. Chernyshova, and O. B. Shpenik, Sov. Phys. Tech. Phys. **29**, 1204 (1984).
[119] R. E. Kennerly, R. A. Bonham, and M. McMillan, J. Chem. Phys. **70**, 2039 (1979).
[120] K. Rohr, J. Phys. B **12**, L185 (1979).
[121] F. A. Gianturco, R. R. Lucchese, and N. Sanna, J. Chem. Phys. **102**, 5743 (1995).
[122] W. M. Johnstone and W. R. Newell, J. Phys. B **24**, 473 (1991).
[123] I. Gyemant, Zs. Varga, and M. G. Benedict, Int. J. Quantum Chem. **XVII**, 255 (1980).
[124] M. G. Benedict and I. Gyemant, Int. J. Quantum Chem. **XIII**, 597 (1978).
[125] D. Edelson and K. B. McAffe, J. Chem. Phys. **19**, 1311 (1951).
[126] H. H. Claassen, G. L. Goodman, J. H. Holloway, and H. Selig, J. Chem. Phys. **53**, 341 (1970).
[127] H. Brunet, IEEE J. Quantum Electron. **QE-6**, 678 (1970).
[128] K. Kim, R. S. McDowell, and W. T. King, J. Chem. Phys. **73**, 36 (1980).
[129] M. W. Chase, Jr., C. A. Davis, J. R. Downey, Jr., D. J. Frurip, R. A. McDonald, and A. N. Syverud, J. Phys. Chem. Ref. Data **14**, 1163 (1985).
[130] C. Chapados and G. Birnbaum, J. Mol. Spectrosc. **132**, 323 (1988).
[131] M. M. Hubers and J. Los, Chem. Phys. **10**, 235 (1975).
[132] D. L. Hildenbrand, J. Phys. Chem. **77**, 897 (1973).
[133] R. K. Curran, J. Chem. Phys. **34**, 1069 (1961).
[134] T. Kiang, R. C. Estler, and R. N. Zare, J. Chem. Phys. **70**, 5925 (1979).
[135] L. M. Babcock and G. E. Streit, J. Chem. Phys. **74**, 5700 (1981).
[136] A. A. Ischenko, J. D. Ewbank, and L. Schäfer, J. Phys. Chem. **98**, 4287 (1994).
[137] J. Ferch, W. Raith, and K. Schröder, J. Phys. B **15**, L175 (1982).
[138] A. Zecca, G. Karwasz, and R. S. Brusa, Chem. Phys. Lett. **199**, 423 (1992).
[139] H.-X. Wan, J. H. Moore, J. K. Olthoff, and R. J. Van Brunt, Plasma Chem. Plasma Process. **13**, 1 (1993).
[140] S. K. Srivastava, S. Trajmar, A. Chutjian, and W. Williams, J. Chem. Phys. **64**, 2767 (1976).
[141] Y. Jiang, J. Sun, and L. Wan, Phys. Rev. A **52**, 398 (1995).
[142] T. Sakae, S. Sumiyoshi, E. Murakami, Y. Matsumoto, K. Ishibashi, and A. Katase, J. Phys. B **22**, 1385 (1989).
[143] H. Cho, R. J. Gulley, and S. J. Buckman, J. Phys. B **33**, L309 (2000).
[144] S. J. Buckman (private communication, February 2000).
[145] Y. Jiang, J. Sun, and L. Wan, Phys. Lett. A **231**, 231 (1997).
[146] J. A. Rees, in *Gaseous Dielectrics III*, edited by L. G. Christophorou (Pergamon, New York, 1982), p. 1.
[147] D. F. Register, S. Trajmar, and S. K. Srivastava, Phys. Rev. A **21**, 1134 (1980).
[148] R. K. Nesbet, Phys. Rev. A **20**, 58 (1979).
[149] R. H. J. Jansen, F. J. de Heer, H. J. Luyken, B. van Wingerden, and H. J. Blaauw, J. Phys. B **9**, 185 (1976).
[150] J. C. Gibson, M. A. Green, K. W. Trantham, S. J. Buckman, P. J. O. Teubner, and M. J. Brunger, J. Phys. B **32**, 213 (1999).
[151] F. H. Read and J. M. Channing, Rev. Sci. Instrum. **67**, 2372 (1996).
[152] D. Klar, M.-W. Ruf, and H. Hotop, Aust. J. Phys. **45**, 263 (1992).
[153] D. Klar, M.-W. Ruf, and H. Hotop, Meas. Sci. Technol. **5**, 1248 (1994).
[154] J. L. Forand, K. Becker, and J. W. McConkey, Can. J. Phys. **64**, 269 (1986).
[155] K. A. Blanks, A. E. Tabor, and K. Becker, J. Chem. Phys. **86**, 4871 (1987).
[156] D. Rapp and P. Englander-Golden, J. Chem. Phys. **43**, 1464 (1965).
[157] T. Stanski and B. Adamczyk, Int. J. Mass Spectrom. Ion Phys. **46**, 31 (1983).
[158] D. Margreiter, G. Walder, H. Deutsch, H. U. Poll, C. Winkler, K. Stephan, and T. D. Märk, Int. J. Mass Spectrom. Ion Processes **100**, 143 (1990).
[159] M. V. V. S. Rao and S. K. Srivastava, XX International Conference on the Physics of Electronic and Atomic Collisions, Scientific Program and Abstracts of Contributed Papers, Vol. II, Vienna, Austria, 23–29 July, 1997, Paper MO 151.
[160] A. H. Al-Nasir, M. A. Chaudhry, A. J. Duncan, R. Hippler, D. M. Campbell, and H. Kleinpoppen, J. Phys. B. **29**, 1849 (1996).
[161] B. P. Pullen and J. A. D. Stockdale, Int. J. Mass Spectrom. Ion Phys. **19**, 35 (1976).
[162] H. Shibata, T. Tonuma, T. Matsuo, H. Kumagai, and H. Tawara, in *VIth International Conference on the Physics of Highly Charged Ions* (Manhattan, KS, 1992), edited by P. Richard, M. Stöckli, C. L. Cocke, and C. D. Lin, AIP Conf. Proc. **274**, 335 (1993).
[163] D. Margreiter, H. Deutsch, M. Schmidt, and T. D. Märk, Int. J. Mass Spectrom. Ion Processes **100**, 157 (1990).
[164] W. Hwang, Y.-K. Kim, and M. E. Rudd, J. Chem. Phys. **104**, 2956 (1996).
[165] V. Tarnovsky, H. Deutsch, S. Matt, T. D. Märk, R. Basner, M. Schmidt,

and K. Becker, in *Gaseous Dielectrics VIII*, edited by L. G. Christophorou and J. K. Olthoff (Plenum, New York, 1998), p. 3.
[166] V. Tarnovsky, H. Deutsch, K. E. Martus, and K. Becker, J. Chem. Phys. **109**, 6596 (1998).
[167] Y.-K. Kim and M. E. Rudd, Comments At. Mol. Phys. **34**, 309 (1999).
[168] H. Deutsch, P. Scheier, and T. D. Märk, Int. J. Mass Spectrom. Ion Processes **74**, 81 (1986).
[169] Y. H. Hilal and L. G. Christophorou, J. Phys. D **20**, 975 (1987).
[170] I. Lopes, H. Hilmert, and W. F. Schmidt, J. Phys. D **19**, L107 (1986).
[171] L. G. Christophorou, *Atomic and Molecular Radiation Physics* (Wiley, New York, 1971), Chap. 2.
[172] M. A. Ali, K. K. Irikura, and Y.-K. Kim, Int. J. Mass Spectrom. (in press).
[173] M. Ito, M. Goto, H. Toyoda, and H. Sugai, Contrib. Plasma Phys. **35**, 405 (1995).
[174] S. G. Lias, J. E. Bartmess, J. F. Liebman, J. L. Holmes, R. D. Levin, and W. G. Mallard, J. Phys. Chem. Ref. Data **17**, 1 (1988).
[175] R. Geballe and M. A. Harrison, as reported by L. B. Loeb, *Basic Processes of Gaseous Electronics* (University of California Press, Berkeley, Los Angeles, 1955), Chap. 5, p. 415.
[176] M. A. Harrison and R. Geballe, Phys. Rev. **91**, 1 (1953).
[177] M. S. Bhalla and J. D. Craggs, Proc. Phys. Soc. (London) **80**, 151 (1962).
[178] H. A. Boyd and G. C. Crichton, Proc. IEE **118**, 1872 (1971).
[179] I. M. Bortnik and A. A. Panov, Sov. Phys.-Tech. Phys. **16**, 571 (1971).
[180] V. N. Maller and M. S. Naidu, Proc. IEE **123**, 107 (1976).
[181] M. Shimozuma, H. Itoh, and H. Tagashira, J. Phys. D **15**, 2443 (1982).
[182] M. Hayashi and G. Wang (unpublished results, 1987); M. Hayashi (private communication, 1999).
[183] Y. Qiu and D. M. Xiao, J. Phys. D **27**, 2663 (1994).
[184] T. H. Teich and R. Sangi, Proceedings First International Symposium on High Voltage Technology, Munich, 1972, edited by F. Heidbromer, 1972, Vol. 1, p. 391.
[185] Th. Aschwanden, in *Gaseous Dielectrics IV*, edited by L. G. Christophorou and M. O. Pace (Pergamom, New York, 1984), p. 24.
[186] Th. Aschwanden, Ph.D. thesis, ETH, Zürich, 1985.
[187] J. de Urquijo-Carmona, C. Cisneros, and I. Alvarez, J. Phys. D **18**, 2017 (1985).
[188] J. de Urquijo-Carmona, I. Alvarez, and C. Cisneros, J. Phys. D **19**, L207 (1986).
[189] H. Hasegawa, A. Taneda, K. Murai, M. Shimozuma, and H. Tagashira, J. Phys. D **21**, 1745 (1988).
[190] H. Toyoda (private communication, 2000).
[191] J. J. Corr, M. A. Khakoo, and J. W. McConkey, J. Phys. B **20**, 2597 (1987).
[192] K. A. Blanks and K. Becker, J. Phys. B **20**, 6157 (1987).
[193] T. Field and J. H. D. Eland, Chem. Phys. Lett. **197**, 542 (1992).
[194] T. H. Teich and R. Bräunlich, in *Gaseous Dielectrics IV*, edited by L. G. Christophorou and M. O. Pace (Pergamon, New York, 1984), p. 71.
[195] K. Masek, L. Laska, V. Perina, and J. Krasa, Acta Phys. Slovaca **33**, 145 (1983).
[196] R. J. Van Brunt and J. T. Herron, IEEE Trans. Electr. Insul. **25**, 55 (1990).
[197] D. Edelson, J. E. Griffiths, and K. B. McAfee, Jr., J. Chem. Phys. **37**, 917 (1962).
[198] R. N. Compton, L. G. Christophorou, G. S. Hurst, and P. W. Reinhardt, J. Chem. Phys. **45**, 4634 (1966).
[199] P. W. Harland and J. C. J. Thynne, J. Phys. Chem. **75**, 3517 (1971).
[200] L. G. Christophorou, *Atomic and Molecular Radiation Physics* (Wiley, New York, 1971), Chap. 6.
[201] L. G. Christophorou, Adv. Electron. Electron Phys. **46**, 55 (1978).
[202] L. G. Christophorou, D. L. McCorkle, and A. A. Christodoulides, in *Electron-Molecule Interactions and Their Applications*, edited by L. G. Christophorou (Academic, New York, 1984), Vol. 1, Chap. 6.
[203] J. M. S. Henis and C. A. Mabie, J. Chem. Phys. **53**, 2999 (1970).
[204] R. W. Odom, D. L. Smith, and J. H. Futrell, J. Phys. B **8**, 1349 (1975).
[205] M. S. Foster and J. L. Beauchamp, Chem. Phys. Lett. **31**, 482 (1975).
[206] C. E. Klots, J. Chem. Phys. **46**, 1197 (1967).
[207] P. M. Collins, L. G. Christophorou, E. L. Chaney, and J. G. Carter, Chem. Phys. Lett. **4**, 646 (1970).
[208] L. G. Christophorou, A. Hadjiantoniou, and J. G. Carter, J. Chem. Soc., Faraday Trans. 2 **69**, 1713 (1975).
[209] C. D. Cooper and R. N. Compton, J. Chem. Phys. **59**, 3550 (1973).
[210] J. P. Johnson, D. L. McCorkle, L. G. Christophorou, and J. G. Carter, J. Chem. Soc., Faraday Trans. 2 **71**, 1742 (1975).
[211] S. M. Spyrou, I. Sauers, and L. G. Christophorou, J. Chem. Phys. **78**, 7200 (1983).
[212] J. E. Delmore and A. D. Appelhans, J. Chem. Phys. **84**, 6238 (1986).
[213] S. P. Heneghan and S. W. Benson, Int. J. Chem. Kinet. **15**, 109 (1983).
[214] R. K. Curran, J. Chem. Phys. **38**, 780 (1963).
[215] R. N. Compton, L. G. Christophorou, and R. H. Huebner, Phys. Lett. **23**, 656 (1966).
[216] R. N. Compton, R. H. Huebner, P. W. Reinhardt, and L. G. Christophorou, J. Chem. Phys. **48**, 901 (1968).
[217] L. G. Christophorou, D. L. McCorkle, and J. G. Carter, J. Chem. Phys. **60**, 3779 (1974).
[218] W. M. Hickam and R. E. Fox, J. Chem. Phys. **25**, 642 (1956).
[219] W. M. Hickam and D. Berg, J. Chem. Phys. **29**, 517 (1958).
[220] I. S. Buchel'nikova, Sov. Phys. JETP **35**, 783 (1959).
[221] D. Rapp and D. D. Briglia, J. Chem. Phys. **43**, 1480 (1965).
[222] D. Spence and G. J. Schulz, J. Chem. Phys. **58**, 1800 (1973).
[223] J. K. Olthoff, R. J. Van Brunt, H.-X. Wan, J. H. Moore, and J. A. Tossell, in *Gaseous Dielectrics VI*, edited by L. G. Christophorou and I. Sauers (Plenum, New York, 1991), p. 19.
[224] K. S. Gant and L. G. Christophorou, J. Chem. Phys. **65**, 2977 (1976).
[225] K. S. Gant, Ph.D. dissertation, University of Tennessee, 1976.
[226] R. Y. Pai, L. G. Christophorou, and A. A. Christodoulides, J. Chem. Phys. **70**, 1169 (1979).
[227] D. L. McCorkle, A. A. Christodoulides, L. G. Christophorou, and I. Szamrej, J. Chem. Phys. **72**, 4049 (1980); **76**, 753E (1982).
[228] S. R. Hunter, J. G. Carter, and L. G. Christophorou, J. Chem. Phys. **90**, 4879 (1989).
[229] J. M. Ajello and A. Chutjian, J. Chem. Phys. **65**, 5524 (1976).
[230] A. Chutjian, Phys. Rev. Lett. **46**, 1511 (1981); **48**, 289E (1982).
[231] A. J. Chutjian, J. Phys. Chem. **86**, 3518 (1982).
[232] A. Chutjian, S. H. Alajajian, and O. J. Orient, in *Gaseous Dielectrics IV*, edited by L. G. Christophorou and M. O. Pace (Pergamon, New York, 1984), p. 42.
[233] A. Chutjian and S. H. Alajajian, Phys. Rev. A **31**, 2885 (1985).
[234] K. Harth, M.-W. Ruf, and H. Hotop, Z. Phys. D **14**, 149 (1989).
[235] D. Klar, M.-W. Ruf, and H. Hotop, Chem. Phys. Lett. **189**, 448 (1992).
[236] A. Schramm, J. M. Weber, J. Kreil, D. Klar, H.-W. Ruf, and H. Hotop, Phys. Rev. Lett. **81**, 778 (1998).
[237] W. P. West, G. W. Foltz, F. B. Dunning, C. J. Latimer, and R. F. Stebbings, Phys. Rev. Lett. **36**, 854 (1976).
[238] G. W. Foltz, C. J. Latimer, G. F. Hildebrandt, F. G. Kellert, K. A. Smith, W. P. West, F. B. Dunning, and R. F. Stebbings, J. Chem. Phys. **67**, 1352 (1977).
[239] J. P. Astruc, R. Barbé, and J. P. Schermann, J. Phys. B **12**, L377 (1979).
[240] B. G. Zollars, K. A. Smith, and F. B. Dunning, J. Chem. Phys. **81**, 3158 (1984).
[241] B. G. Zollars, C. Higgs, F. Lu, C. W. Walter, L. G. Gray, K. A. Smith, F. B. Dunning, and R. F. Stebbings, Phys. Rev. A **32**, 3330 (1985).
[242] B. G. Zollars, C. W. Walter, F. Lu, C. B. Johnson, K. A. Smith, and F. B. Dunning, J. Chem. Phys. **84**, 5589 (1986).
[243] F. B. Dunning, J. Phys. Chem. **91**, 2244 (1987).
[244] I. M. Beterov, G. L. Vasilenko, I. I. Riabtsev, B. M. Smirnov, and N. V. Fatayev, Z. Phys. D **6**, 55 (1987).
[245] Z. Zheng, K. A. Smith, and F. B. Dunning, J. Chem. Phys. **89**, 6295 (1988).
[246] H. S. Carman, Jr., C. E. Klots, and R. N. Compton, J. Chem. Phys. **90**, 2580 (1989).
[247] A. Pesnelle, C. Ronge, M. Perdrix, and G. Watel, Phys. Rev. A **42**, 273 (1990).
[248] X. Ling, B. G. Lindsay, K. A. Smith, and F. B. Dunning, Phys. Rev. A **45**, 242 (1992).
[249] R. A. Popple, M. A. Durham, R. W. Marawar, B. G. Lindsay, K. A. Smith, and F. B. Dunning, Phys. Rev. A **45**, 247 (1992).
[250] A. Pesnelle, M. Perdrix, and G. Watel, J. Chem. Phys. **96**, 4303 (1992).
[251] D. Klar, B. Mirbach, H. J. Korsch, M.-W. Ruf, and H. Hotop, Z. Phys. D **31**, 235 (1994).
[252] M. T. Frey, S. B. Hill, K. A. Smith, F. B. Dunning, and I. I. Fabrikant, Phys. Rev. Lett. **75**, 810 (1995).
[253] F. B. Dunning, J. Phys. B **28**, 1645 (1995).
[254] R. W. Crompton and G. N. Haddad, Aust. J. Phys. **36**, 15 (1983).

[255] H. Hotop, D. Klar, J. Kreil, M.-W. Ruf, A. Schramm, and J. M. Weber, in *The Physics of Electronic and Atomic Collisions*, edited by L. J. Dubé, J. B. A. Mitchell, J. W. McConkey, and C. E. Brion (AIP Press, Woodbury, NY) [AIP Conf. Proc. **360**, 267 (1995)].
[256] Z. Lj. Petrovic and R. W. Crompton, J. Phys. B **18**, 2777 (1985).
[257] E. P. Wigner, Phys. Rev. **73**, 1002 (1948).
[258] A. Chutjian (private communication, 1999).
[259] S. Matejcik, P. Eichberger, B. Plunger, A. Kiendler, A. Stamatovic, and T. D. Märk, Int. J. Mass Spectrom. Ion Processes **144**, L13 (1995).
[260] A. Schramm, dissertation, University of Kaiserslautern, 1998.
[261] H. Hotop (private communication, March 2000).
[262] M. V. V. S. Rao (private communication, 1999).
[263] V. K. Lakdawala and J. L. Moruzzi, J. Phys. D **13**, 1439 (1980).
[264] L. G. Christophorou and P. G. Datskos, Int. J. Mass Spectrom. Ion Processes **149/150**, 59 (1995).
[265] S. R. Hunter and L. G. Christophorou, in *Electron-Molecule Interactions and Their Applications* (Academic, New York, 1984), Vol. 2, Chap. 3.
[266] A. B. Wedding, H. A. Blevin, and J. Fletcher, J. Phys. D **18**, 2361 (1985).
[267] H. Shimamori, Y. Tatsumi, Y. Ogawa, and T. Sunagawa, J. Chem. Phys. **97**, 6335 (1992).
[268] J. Sherwell, R. Cooper, D. C. Nguyen, and S. P. Mezyk, Aust. J. Chem. **41**, 1491 (1988).
[269] F. J. Davis and D. R. Nelson, Chem. Phys. Lett. **6**, 277 (1970).
[270] K. M. Bansal and R. W. Fessenden, J. Chem. Phys. **59**, 1760 (1973).
[271] H. Shimamori and R. W. Fessenden, J. Chem. Phys. **71**, 3009 (1979).
[272] F. C. Fehsenfeld, J. Chem. Phys. **53**, 2000 (1970).
[273] T. M. Miller, A. E. S. Miller, J. F. Paulson, and X. Liu, J. Chem. Phys. **100**, 8841 (1994).
[274] E. C. M. Chen, R. D. George, and W. E. Wentworth, J. Chem. Phys. **49**, 1973 (1968).
[275] I. Szamrej and M. Forys, in *Gaseous Dielectrics VI*, edited by L. G. Christophorou and I. Sauers (Plenum, New York, 1991), p. 43.
[276] K. G. Mothes and R. N. Schindler, Ber. Bunsen-Ges. **75**, 938 (1971).
[277] J. L. Le Garrec, O. Sidko, J. L. Queffelec, S. Hamon, J. B. A. Mitchell, and B. R. Rowe, J. Chem. Phys. **107**, 54 (1997).
[278] J. A. Ayala, W. E. Wentworth, and E. C. M. Chen, J. Phys. Chem. **85**, 3989 (1981).
[279] B. H. Mahan and C. E. Young, J. Chem. Phys. **44**, 2192 (1966).
[280] D. Smith, N. G. Adams, and E. Alge, J. Phys. B **17**, 461 (1984).
[281] D. Smith, P. Španěl, S. Matejcik, A. Stamatovic, T. D. Märk, T. Jaffke, and E. Illenberger, Chem. Phys. Lett. **240**, 481 (1995).
[282] I. M. Beterov, V. P. Chebotaev, N. V. Fateev, and D. V. Yakovin, Sov. J. Quantum Electron. **8**, 533 (1978).
[283] I. M. Beterov and N. V. Fateyev, J. Phys. Colloq. **44**, C7–447 (1983).
[284] S. Avrillier and J.-P. Schermann, Opt. Commun **19**, 87 (1976).
[285] P. G. Datskos, L. G. Christophorou, and J. G. Carter, J. Chem. Phys. **99**, 8607 (1993).
[286] K. B. McAfee, Jr. and D. Edelson, Proc. Phys. Soc. London **81**, 382 (1963).
[287] G. R. G. Raju and M. S. Dincer, J. Appl. Phys. **53**, 8562 (1982).
[288] M. C. Siddagangappa, C. S. Lakshminarasimha, and M. S. Naidu, J. Phys. D **15**, L83 (1982).
[289] M. C. Siddagangappa, C. S. Lakshminarasimha, and M. S. Naidu, in *Gaseous Dielectrics IV*, edited by L. G. Christophorou and M. O. Pace (Pergamon, New York, 1984), p. 49.
[290] M. F. Fréchette, J. Appl. Phys. **59**, 3684 (1986).
[291] B. C. O'Neill and J. D. Craggs, J. Phys. B **6**, 2634 (1973).
[292] H. Itoh, M. Shimozuma, H. Tagashira, and S. Sakamoto, J. Phys. D **12**, 2167 (1979).
[293] D. M. Xiao, H. L. Liu, and Y. Z. Chen, J. Appl. Phys. **86**, 6611 (1999).
[294] D. M. Xiao, L. L. Zhu, and Y. Z. Chen, J. Phys. D: Appl. Phys. **32**, L18 (1999).
[295] T. H. Teich and D. W. Branston, *Third International Conference on Gas Discharges*, IEE Conf. Publ. **118**, 109 (1974).
[296] H. Hilmert, W. F. Schmidt, Y. Sakai, and S. Sawada, Jpn. J. Appl. Phys., **30**, 1487 (1991).
[297] D. M. Xiao, H. L. Liu, and L. Qin, Jpn. J. Appl. Phys., Part 2 **38**, L875 (1999).
[298] F. M. Harris and G. J. Jones, J. Phys. B **4**, 1536 (1971).
[299] B. Sangi, Ph.D. thesis, University of Manchester, 1971, as quoted in Ref. 8.
[300] M. S. Naidu and A. N. Prasad, J. Phys. D **5**, 1090 (1972).
[301] D. W. Branston, Ph.D. thesis, University of Manchester, 1973, as quoted in Ref. 8.
[302] J. de Urquijo-Carmona, Ph.D. thesis, University of Manchester, 1980, as quoted in Ref. 8.
[303] Y. Nakamura, J. Phys. D **21**, 67 (1988).
[304] V. A. Lisovskiy and V. D. Yegorenkov, Proceedings of the International Symposium on Electron-Molecule Collisions and Swarms, edited by Y. Hatano, H. Tanaka, and N. Kouchi, Tokyo, Japan, 18–20 July, 1999, p. 156; J. Phys. D **32**, 2645 (1999).
[305] B. Shizgal, J. Phys. B **21**, 1699 (1988).
[306] M. S. Dincer, J. Phys. D **23**, 622 (1990).
[307] V. N. Maller and M. S. Naidu, IEEE Trans. Plasma Sci. **3**, 205 (1975).
[308] R. L. Champion and L. D. Doverspike, in *Electron-Molecule Interactions and Their Applications*, edited by L. G. Christophorou (Academic, New York, 1984), Vol. 1, Chap. 7.
[309] L. G. Christophorou, Contrib. Plasma Phys. **27**, 237 (1987).
[310] S. Chowdhury, E. P. Grimsrud, T. Heinis, and P. Kebarle, J. Am. Chem. Soc. **108**, 3630 (1986).
[311] J. K. Olthoff, R. J. Van Brunt, Y. Wang, R. L. Champion, and L. D. Doverspike, J. Chem. Phys. **91**, 2261 (1989).
[312] R. L. Champion, in *Gaseous Dielectrics VI*, edited by L. G. Christophorou and I. Sauers (Plenum, New York, 1991), p. 1.
[313] B. Freiser and J. L. Beauchamp, quoted in Ref. 94.
[314] R. S. Mock and E. P. Grimsrud, Chem. Phys. Lett. **184**, 99 (1991).
[315] H. Faidas, L. G. Christophorou, and D. L. McCorkle, Chem. Phys. Lett. **193**, 487 (1992).
[316] L. G. Christophorou, P. G. Datskos, and H. Faidas, J. Chem. Phys. **101**, 6728 (1994).
[317] O. Ingólfsson, E. Illenberger, and W. F. Schmidt, Int. J. Mass Spectrom. Ion Processes **139**, 103 (1994).
[318] P. G. Datskos, J. G. Carter, and L. G. Christophorou, Chem. Phys. Lett. **239**, 38 (1995).
[319] I. Ishikawa, K. Koike, T. Akitsu, S. Suganomata, and H. Matsuzawa, Jpn. J. Appl. Phys., **29**, 767 (1990).
[320] A. Kono, M. Endo, K. Ohata, S. Kishimoto, and T. Goto, J. Appl. Phys. **76**, 7221 (1994).
[321] W. F. Schmidt and R. J. Van Brunt, in *Gaseous Dielectrics III*, edited by L. G. Christophorou (Pergamon, New York, 1982), p. 561.
[322] R. J. Van Brunt and M. Misakian, J. Appl. Phys. **54**, 3074 (1983).
[323] N. Wiegart, IEEE Trans. Electr. Insul. **EI-20**, 587 (1985).
[324] J. Kindersberger, *Proceedings VIIIth International Conference on Gas Discharges and Their Applications*, September 16–20, 1985, Oxford, U.K. (University of Leeds Press, Leeds, 1985), p. 263.
[325] Y. Wang, R. L. Champion, L. D. Doverspike, J. K. Olthoff, and R. J. Van Brunt, J. Chem. Phys. **91**, 2254 (1989).
[326] S. Chowdhury and P. Kebarle, J. Chem. Phys. **85**, 4989 (1986).
[327] P. L. Patterson, J. Chem. Phys. **53**, 696 (1970).
[328] K. P. Brand and H. Jungblut, J. Chem. Phys. **78**, 1999 (1983).
[329] D. Hansen, H. Jungblut, and W. F. Schmidt, J. Phys. D **16**, 1623 (1983).
[330] H. Hilmert and W. F. Schmidt, J. Phys. D **24**, 915 (1991).
[331] N. Wiegart, L. Niemeyer, F. Pinnekamp, W. Boeck, J. Kindersberger, R. Morrow, W. Zaengl, M. Zwicky, I. Galimberti, and S. A. Boggs, IEEE Trans. Power Del. **3**, 923, (1988); **3**, 931 (1988); **3**, 939 (1988).
[332] R. J. Van Brunt, J. Appl. Phys. **59**, 2314 (1986).
[333] G. Berger and B. Senouci, J. Phys. D **19**, 2337 (1986).
[334] A. Gilbert, J. Dupuy, P. Domens, G. Riquel, and B. Hutzler, J. Phys. D **26**, 773 (1993).
[335] H. Schlumbohm, Z. Phys. **166**, 192 (1962).
[336] I. A. Fleming and J. A. Rees, J. Phys. B **2**, 777 (1969).
[337] M. S. Naidu and A. N. Prasad, J. Phys. D **3**, 951 (1970).
[338] B. H. Crichton and D.-i. Lee, Proceedings 5th International Conference on Gas Discharges, Liverpool, England, 1978, p. 254.
[339] Th. Aschwanden (private communication, 1984), as quoted in Morrow (Ref. 12).
[340] J. de Urquijo-Carmona, I. Alvarez, H. Martinez, and C. Cisneros, J. Phys. D **24**, 664 (1991).
[341] J. de Urquijo-Carmona, Ph.D. thesis, University of Manchester, 1980, as quoted in Morrow (Ref. 12).
[342] J. de Urquijo-Carmona, I. Alvarez, C. Cisneros, and H. Martinez, J. Phys. D **23**, 778 (1990).
[343] J. de Urquijo-Carmona, C. Cisneros, H. Martinez, and I. Alvarez, J. Phys. D **25**, 1277 (1992).

[344] Z. A. Talib and M. Saporoschenko, Int. J. Mass Spectrom Ion Processes **116**, 1 (1992).
[345] Z. A. Talib and M. Saporoschenko, J. Phys. D **27**, 2307 (1994).
[346] D. E. Wilson, W. J. Quiring, and D. A. Armstrong, J. Appl. Phys. **47**, 1194 (1976).
[347] W. F. Schmidt, H. Jungblut, D. Hansen, and H. Tagashira, in *Gaseous Dielectrics II*, edited by L. G. Christophorou (Pergamon, New York, 1980), p. 1.
[348] H. Jungblut, D. Hansen, and W. F. Schmidt, IEEE Trans. Electr. Insul. **24**, 343 (1989).